Gyrokinetic Theory for Peripheral Plasmas and its Application to Plasma Sheath

KAWAMURA Gakushi

2008

Contents

Chapter 1

Introduction

1.1 Fusion energy

The development of an alterative energy resource is a inevitable issue in 21st century. If the dependence on the fossil energy is kept at the present level, the shortage of the fossil fuels will happen in the late of this century and then the economic activities will receive critical damages. The air pollution caused by the exhaust gas from power plants and automobiles also becomes a critical issue in developing countries. In order to have the sustainable development of the world, the alternative energy resources should satisfy the following requirements at least. Firstly the new energy resource should be easily obtainable almost everywhere on the earth. Secondly a large amount of energy should be available to replace the present supply of the fossil fuels. Thirdly toxic waste should not be emitted to the air or the sea. Lastly the safety of the power plant should be assured.

A number of candidates are being studied and developed; solar power, wind power, biofuel, nuclear energy, *etc.* The combined use of these energy resources may be desirable, but from the view point of the cost and the amount of the power we can utilize, the nuclear energy is the most realistic choice as the main energy resource. There are two kinds of nuclear reactions which can be utilized for the power generator. The nuclear fission is already utilized as a major electric power resource and its ratio to the all power production may increase to the large extent. It will be the most realistic choice of the alternative energy for the moment. However, the producing nations of the fuel, or uranium, are restricted. The spreading of the technology required to develop the power plants potentially raises the risk of the diffusion of nuclear weapons.

The other option is the nuclear fusion. It can solve the problems above. The fuel of the fusion is deuterium and tritium in case of the D-T reaction, D + T $\rightarrow$ ^{4}He + n, which has larger nuclear cross section than others such as D-D and D-^{3}He. Although the amount of the tritium is small on earth because of its short radioactive half-life of 12 years, it

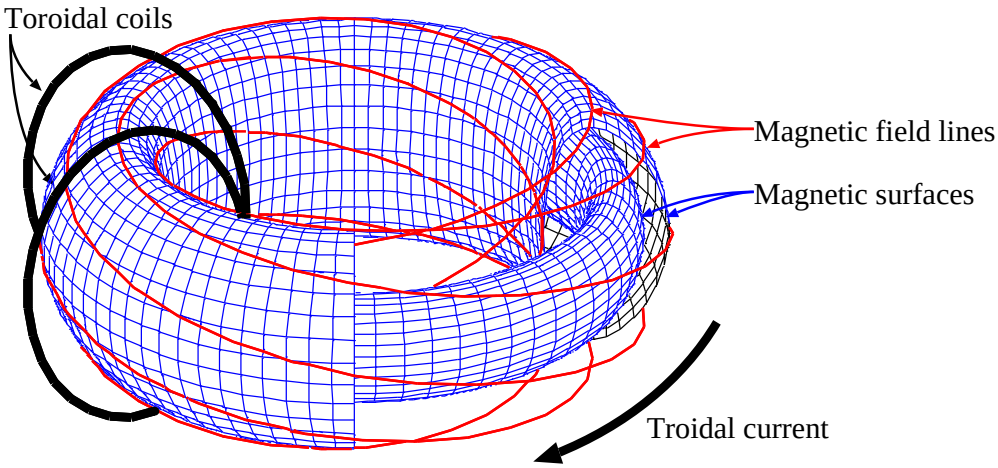

Figure 1.1: Schematic diagram of the torus plasma in a simple tokamak device.

can be bred from the lithium through the following reactions; n + ^{6}Li $\rightarrow$ T + ^{4}He and n + ^{7}Li $\rightarrow$ T + ^{4}He + n. The neutron in these reactions can be supplied from that of the D-T reaction. The deuterium and the lithium can be extracted from the sea water. The absence of the high activity wastes which require the isolation for tens of centuries is also an advantage over the nuclear fission.

1.2 Confinement of the plasma

For the fusion reactions to take place, the nuclei, i.e. D and T, must have high energy to overcome the Coulomb barrier and approach each other within a small distance where the nuclear force dominates. In order to obtain a sufficient reaction rate, the mixing gas of deuterium and tritium have to be kept in high temperature, typically 10keV. In this condition, electrons of the atoms are unbounded from the nuclei and thus the gas is in the plasma state. Since the electrons and ions, or nuclei, can rapidly escape because of their high temperature, e.g. approximately 10^6 m/s for the 10keV ion, magnetic fields are employed to confine the plasma. The Lorentz force acting on the particles restricts their perpendicular motion to magnetic fields. Since magnetic fields do not interfere with the parallel motion, closed magnetic fields are employed to avoid the particle losses from open ends.

A concept of the confinement device, tokamak is illustrated in Fig. 1.1. The magnetic fields are generated by the external toroidal coils and the internal plasma currents. They form nested magnetic surfaces with torus geometry. A magnetic surface is a closed surface filled with a certain magnetic field line when it is followed from a point on the surface along the magnetic line. Since the magnetic fields are tangential to the magnetic

surface they belong to, charged particles do not transported across the surface in the ideal condition. The perpendicular transport, however, exists because of disturbances such as Coulomb collisions and plasma waves, or oscillatory electriomagnetic fields.

The rate of the energy loss is measured by the energy confinement time τ_e. This factor represents the characteristic time for the energy generated in the plasma to escape from it and corresponds to the decay time, i.e. (energy) $\propto \exp(-t/\tau_e)$ if there is no energy input. A small confinement time corresponds to a large energy transport and then a large additional heating is required to maintain the plasma temperature. Since the energy inevitably escapes from the plasma to a greater or lesser extent, the heating is essential factor in the present confinement devices, but small heating power is desirable from the view point of capital costs and energy gain. The performance of the fusion reactor is measured by the Q value, which is defined by $Q = (P_o - P_h)/P_h$. The heating power to maintain the stationary plasma and the thermal output are denoted by P_h and P_o, respectively. If the Q value is unity, the heating power and the fusion power, $P_o - P_h$, are balanced. Obtaining higher Q value in long-time discharges is the goal of the fusion studies. In order to reduce the heating power and obtain the large Q value, a long energy confinement time is required. To this end, understanding of the transport mechanism in the plasma is a essential issue in the fusion studies.

1.3 Transport in magnetically confined plasmas

There are three types of microscopic transport mechanisms in the torus plasma; classical, neoclassical and anomalous transports. The classical transport is caused by Coulomb collisions in the magnetized plasma. When a charged particle experiences a collision with another particle, the velocity is deflected through the momentum exchange and that causes a jump of the guiding-center. A guiding-center is a center position of the cyclotron orbit and given by $\mathbf{X} = \mathbf{x} - \mathbf{B} \times \mathbf{v}/B\Omega$, where the particle position and the cyclotron frequency are denoted by $\mathbf{x}$ and $\Omega = qB/m$. The statistical average over the series of the collisions yields the diffusion which is characterized by the diffusion coefficient $D_c \sim \nu\rho_t^2$, where the collision frequency and the thermal Larmor radius are denoted by ν and $\rho_t = mv_t/qB$, respectively. Here we use the following notations; particle mass m, charge q, temperature T, thermal velocity $v_t = \sqrt{T/m}$ and magnetic field B.

The neoclassical transport is also collisional but caused by different dynamics of particle associated with the toroidicity. In the toroidal magnetic fields, a guiding-center travels around the toroidal and poloidal directions. Since the magnetic field strength is inversely proportional to the major radius, a particle with a small parallel velocity is repelled at a certain poloidal position by the magnetic mirror effect. Such particles are called trapped

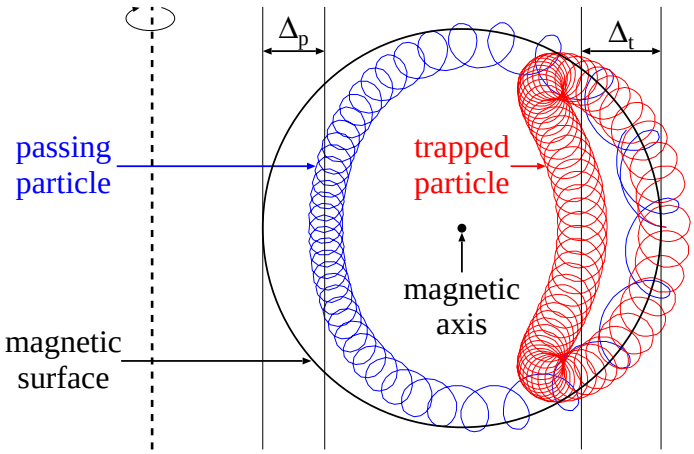

Figure 1.2: The projection of the trajectories of particles in toroidal magnetic fields on a poloidal plane. The passing and trapped particles are denoted by the solid and dashed curves. The dotted circle represents the magnetic surface where the particles started.

particles and the others are called passing particles. An example of each trajectory is illustrated in Fig. 1.2. When a particle travels in toroidal magnetic fields, perpendicular drifts associated with the geometry of the magnetic fields, i.e. grad B and curvature drift, causes a deviation from the magnetic surface where the particle originally located. The deviation for the passing and trapped particle is denoted by Δ_p and Δ_t in the figure. As shown there, the deviation for the passing particle is smaller than that of the trapped particle, or $\Delta_p < \Delta_t$. Since the former, Δ_p, is still larger than the Larmor radius, they act as longer step-lengths in the random walk and yield about one order of magnitude larger transport than the classical one.

The third microscopic transport is the anomalous transport. The origin of its name is its anomalously large transport coefficient observed in experiments. Since the cause of the enhanced transport was not identified, it was named anomalous transport. At present it is widely recognized that turbulence driven by micro-instabilities causes the anomalous transport. Therefore, it is also called a turbulence transport. Especially drift wave type micro-instabilities are the most possible candidates for the turbulence transport. The drift wave is a wave induced in the plasma by gradients of the density and temperature. The time and spatial scales of the drift wave are characterized by the drift frequency $\omega_* \sim \kappa c_s$ and the most unstable wave length $\lambda_* \sim \rho_{ti}$. Here we denote the inverse scale length, the cold ion sound speed and the ion thermal Larmor radius as $\kappa = |\nabla \ln n|$, $c_s = \sqrt{T_i/m_i}$ and $\rho_{ti} = v_{ti}/\Omega_i = \sqrt{m_i T_i}/qB$, respectively. Since the driving force of the turbulence, or micro-instabilities, exists even in the collisionless plasma, the turbulence transport also exists in low collisional regime. This is the most prominent difference of the turbulence transport from the classical and neoclassical ones.

Another difference is the dependence on the structure or state of the plasma. Since the growth rate of the drift wave is roughly proportional to the gradients, the dependence on the plasma profiles is a natural consequence. The dependence on the dynamical structure, i.e. global modes or flows, is one of the key issues in the transport study. As mentioned above, the wave length of the most unstable mode is of the same order as the ion thermal Larmor radius and is much shorter than the system length characterized by the minor radius, or the distance from the magnetic axis to the plasma surface. The existence of nonlinear couplings can, however, excites even the stable modes which has shorter or longer wave length. These processes are called a cascade (toward modes with shorter wave length) and an inverse cascade (longer). One of the nonlinearities comes from the polarization drift, which has been modeled by Hasegawa and Mima [1]. The polarization drift is a perpendicular drift caused by the variation of the electric field in time and has a reducing effect of the electric field. From studies using their single field model, namely the Hasegawa-Mima equation or Charney-Hasegawa-Mima equation, or more generalized models, the importance of the nonlinear couplings are revealed. One of its characteristic roles is structure formation such as a zonal flow and convection cells which are linearly stable. The zonal flow is a poloidal flow generated by a nonlinear stress tensor. The self-suppression effect of the global flow, or structure, has been found through these studies and has a large impact on the transport study.

1.4 Simulation in the turbulence transport study

In turbulence studies, simulations have played a significant role in elucidating the nonlinear characteristics existing in the plasma dynamics associated with the micro-instabilities. A simulation provides physical insights on a complicated system such as the plasma in turbulent or highly structured state and promote the modeling of the turbulence transport. With regard to the rigorousness and the extent of reductions, there are several set of equations employed in the turbulence simulations. The most fundamental one is a kinetic simulation solving the Newton's equations,

$$\frac{d\mathbf{x}}{dt} = \mathbf{v}, \quad m\frac{d\mathbf{v}}{dt} = q\mathbf{v} \times \mathbf{B} + q\mathbf{E}, \tag{1.1}$$

or its continuum expression known as the Vlasov equation,

$$\frac{df}{dt} = \frac{\partial f}{\partial t} + \mathbf{v} \cdot \frac{\partial f}{\partial \mathbf{x}} + (q\mathbf{v} \times \mathbf{B} + q\mathbf{E}) \cdot \frac{\partial f}{\partial \mathbf{v}} = 0, \tag{1.2}$$

where the distribution function f represents the number density in the six dimensional phase space $(\mathbf{x}, \mathbf{v})$ at time t. The simulation using the equations of motion to calculate

the motion of individual particles is called a particle simulation. The force acting on each particle is calculated from the velocities and positions of the other particles. A more simplified simulation using Maxwell's equation is called a particle-in-cell (PIC) simulation and frequently used for plasma simulations. Another commonly used one is called a Vlasov simulation or an Eulerian simulation, which solves the Vlasov equation and Maxwell's equations self-consistently. Maxwell's equations are given by

$$\nabla \cdot \mathbf{E} = \frac{\rho}{\epsilon_0}, \quad \nabla \times \mathbf{E} = -\frac{\partial \mathbf{B}}{\partial t}, \quad \nabla \cdot \mathbf{B} = 0, \quad \nabla \times \mathbf{B} = \mu_0 \mathbf{j} + \frac{1}{c^2}\frac{\partial \mathbf{E}}{\partial t}, \tag{1.3}$$

where the charge and current density, ρ and $\mathbf{j}$, are calculated from the distribution function as

$$\rho(\mathbf{x}) = \sum_{\text{species}} \int q_s f_s(\mathbf{x}, \mathbf{v}) d^3 v, \quad \mathbf{j}(\mathbf{x}) = \sum_{\text{species}} \int q_s \mathbf{v} f_s(\mathbf{x}, \mathbf{v}) d^3 v. \tag{1.4}$$

The simplified expressions of Maxwell's equations are usually employed in the plasma simulations;

$$\left(\nabla^2 - \frac{1}{c^2}\frac{\partial^2}{\partial t^2}\right)\phi = -\frac{\rho}{\epsilon_0}, \quad \left(\nabla^2 - \frac{1}{c^2}\frac{\partial^2}{\partial t^2}\right)\mathbf{A} = -\mu_0 \mathbf{j}, \tag{1.5}$$

where the scalar potential ϕ and the vector potential $\mathbf{A}$ are related to the electromagnetic fields as

$$\mathbf{E} = -\nabla\phi - \frac{\partial \mathbf{A}}{\partial t}, \quad \mathbf{B} = \nabla \times \mathbf{A}. \tag{1.6}$$

Here the potentials *phi* and $\mathbf{A}$ have to satisfy the Lorentz condition,

$$\nabla \cdot \mathbf{A} + \frac{1}{c^2}\frac{\partial \phi}{\partial t} = 0. \tag{1.7}$$

Another type of simulation employs fluid equations. They are derived from the kinetic equation by taking the velocity moments. The zeroth order moment yields the continuity equation, or conservation of the density. The first, second and third moments yield balance equations with respect to the momentum, the pressure and the thermal flux, respectively. Since the Vlasov equation includes the velocity in the form $\mathbf{v} \cdot \nabla f$, the equation for a certain moment contains one order higher moment. The fluid equations are, therefore, composed of the infinite series of hierarchy equations. In order to obtain equations using only the finite number of moments, the hierarchy is usually truncated at a certain order moment by introducing an appropriate closure model. If the second moment is truncated, for instance, the pressure in the equation of state is substituted into the equation of the momentum balance. Therefore, the fluid equations discard the detailed information of the distribution function. Paying the cost of the truncation and the approximation model of higher moment, they have a great advantage in its moderate requirements for the computational resources, especially the memory consumption, because they do not need the

velocity space, while the kinetic equation needs a number of particles for the particle simulations and a number of grids in velocity space for the Vlasov simulations. The fluid model is, therefore, employed for global simulations and the long-time simulations such as an equilibrium, a transport calculation for given or modeled diffusion coefficients, and magnetohydrodynamics phenomena.

In the turbulence simulations related to the anomalous transport, however, the simulations are mostly based on the kinetic equation because the kinetic effects such as the Landau damping, the finite-Larmor-radius (FLR) effects and the particle trapping strongly affect the growth rate of the micro-instabilities and also the turbulence. Some advanced fluid models have been constructed to include the kinetic effects but the calculation based on the first principle is widely recognized as an essential element for the quantitative prediction of the anomalous transport coefficient. As mentioned above, the kinetic equation, or Vlasov equation, involves all the particle dynamics except the Coulomb collision, which can be included as additional terms in the Vlasov equation. Although the kinetic equation can describe the accurate dynamics of the plasma, it requires a vast amount of computational resources and may be an unrealistic choice of a method for the global turbulent simulations. In order to overcomes the difficulty, a reduced but still accurate kinetic equation, namely the gyrokinetics, has been developed.

1.5 Gyrokinetics in the turbulence simulation

The gyrokinetic equations is simplified equations under the condition that the gyration due to the Lorentz force is the fast and dominant motion of charged particles in the plasma. While the kinetic equations, which are now called full-kinetic equations to be distinguished from the gyrokinetic equations, follow the trajectory of a particle, the gyrokinetic equations follow that of the gyrocenter, which is a generalized or 'optimized' position of the guiding-center given by $\mathbf{X} = \mathbf{x} - \mathbf{B} \times \mathbf{v}/B\Omega$. The fundamental concept of the gyrokinetics is the determination of the gyrocenter coordinate system where the equations of motion are reduced to simple equations without gyration. This idea resembles the introduction of an amplitude and a phase into the harmonic oscillator given by $\ddot{x} + \omega^2 x = 0$. It can be reduced to $\dot{A} = 0$ and $\dot{\theta} = \omega$ through the coordinate transformation $x = A\cos(\theta)$. The amplitude and the phase correspond to the magnetic moment given by $mv_\perp^2/2B$ and the phase of the cyclotron motion.

Since the gyration and other motions such as the drift and the parallel motion are completely decoupled in the gyrokinetic equations, one can reduce the dimension of the velocity space to two, i.e. the parallel and perpendicular velocities. In other words, the phase of the gyration can be discarded. It contributes to the large reduction of the com-

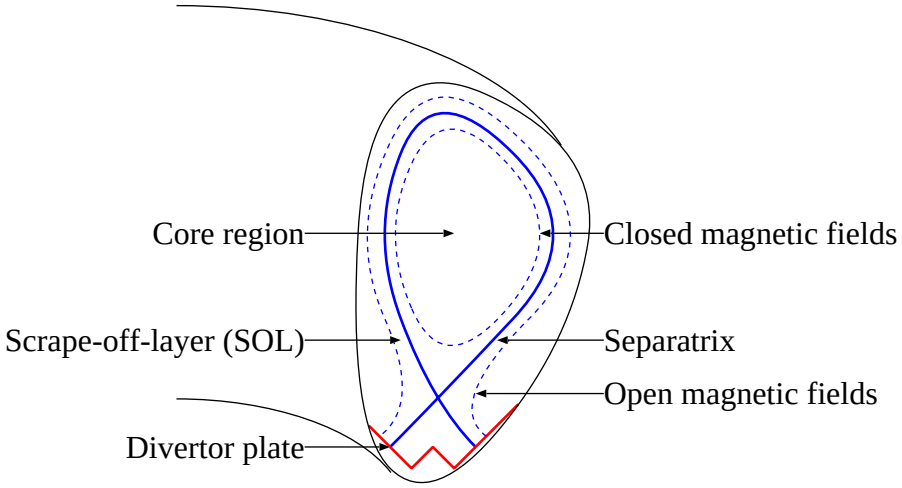

Figure 1.3: Schematic diagram of the poloidal cross section of a tokamak device.

putational resources because the elimination of the gyrating motion enables one to use larger time-steps than the gyration period and also to ignore the velocity space variable corresponding to the phase of the gyration. Another advantage is reduction of the numerical noise in the simulation. The particle is treated as an imaginary ring instead of a point, or the particle itself. The force acting on the particle is calculated from the potential averaged over the ring, or the trajectory of the gyration. Short-scale noise characterized by the Larmor radius and the cyclotron frequency is much reduced compared with the full-kinetic calculation.

The gyrokinetics was first developed for theoretical modelings of the micro-instabilities in the late 1960s [2, 3] and its application to simulation started in the early 1980s [4, 5]. The basis of the modern gyrokinetic equation widely used at present appeared around 1980 [6, 7]. The simulation studies requiring more general and accurate reduced equations of motion has motivated the development of the modern derivation employing analytical mechanics. The establishment of the mathematically unambiguous and rigorous gyrokinetic equation and the rapid progress of high performance computing made the kinetic simulation a realistic choice for the global turbulence study and indeed global, or toroidal, simulations using the gyrokinetic equations has started in the late 1990s [8–10]. The gyrokinetic simulation is now believed to be an essential tool for the study of the turbulent transport driven by the micro-instabilities.

1.6 Peripheral plasmas

We described the plasma confinement and the transport study in the preceding sections. In addition to the core plasma which is confined in the magnetic surfaces, the external, surrounding region also has important role in the fusion devices. A poloidal magnetic configuration of a standard tokamak device is illustrated in Fig. 1.3. In the core region, the magnetic fields are closed and the hot and dense plasma is confined. In the outer region called scrape-off-layer (SOL), the magnetic fields are open to the divertor plate and a relatively cold and thin plasma exists. The boundary between the closed and open magnetic fields is called separatrix. The objectives of separatrix and open magnetic field are the determination of the hot plasma surface and exhaustion of the heat and the alpha particles generated by the fusion reactions. The plasma expelled from the core region is subjected to rapid parallel transport and the main part of the energy flux flows into the the divertor plate.

On the surface contacting with a plasma, various phenomena are observed; large potential formation called sheath, generation of neutral atoms, formation of small particles called dust, secondary electron emission, sputtering of the surface, *etc*. The sheath is a boundary layer formed in front of a surface and has a large electric field. The cause of the electric field is a difference of the thermal velocity between ions and electrons. For instance, a deuterium is approximately sixty times faster than a electron if they have the same energy. Since a particle flux is roughly a product of the density and thermal velocity, an imbalance of the fluxes, or electric current, occurs if a return flux from the surface does not exist. To compensate it, a large electric field is formed in front of the wall surface and the electron return flux is generated.

The behavior of impurity atoms and particles are important issues for the plasma confinement because they may penetrate into the hot plasma. The impurity atoms are excited and cause a considerable energy loss through radiations, especially in case of high atomic number. In order to predict their generation rate and their behavior, the state of the plasma such as the potential profile, energy flux and velocity distribution near the wall are required. Therefore, understanding of the plasma in the divertor region is an essential and fundamental issues in fusion research.

1.7 Outline of this thesis

One of the objectives of this thesis is a new formulation of the gyrokinetic equations applicable to the plasma with strong electric field and the numerical verification. The equation derived here aims at being applied mainly to gyrokinetic simulations of the fusion plasma

in the turbulent state accompanied with global and fast flows. The other objective is to understand the physics of sheath formation in a magnetic field. To this end, a kinetic modeling of the sheath plasma in magnetic fields is provided by using the gyrokinetic equations derived here.

In Chap. 2, a general derivation of the gyrokinetic equation is presented. Comparing previous works, a straightforward way to derive the equation is adopted. After obtaining the general forms, the specific set of gyrokinetic equations are formulated on the assumptions usually employed in the analysis of the micro-instabilities. In Chap. 3, introducing a reference frame in the formulation procedure, improved gyrokinetic equation still valid for large equilibrium electric fields is presented. The criterion for the appropriate choice of the reference frame is discussed and a practically most suitable one is obtained. The validity of the resulting equations is confirmed by numerical comparisons with the full-kinetic equations of motion, or the original Newton's equations.

In Chap. 4, a kinetic model of the magnetized sheath plasma formed in front of a wall is presented. The gyrokinetic equations obtained in Chap. 3 is employed here and modified expressions for the sheath plasma are used. A criterion for the stable formation of the sheath in magnetic fields is derived. The validity of the model is investigated by numerical comparisons with the results of a full-kinetic particle-in-cell simulation. The parameter dependences of the electric field at the wall surface is studied by using numerical solutions of the present sheath model. In Chap. 5, parameter dependences of the incident angle of ions to the wall is studied by using the numerical codes developed in Chap. 4.

In Chap. 6, the summary of this thesis and future works are presented.

Chapter 2

Derivation of the gyrokinetic equations

2.1 Introduction

The concept of the gyrophase-averaging is introduced at the first time by Rutherford and Frieman [2], and Taylor and Hastie [3]. They apply the gyrophase-averaging technique to the WKB expression of the perturbation potential and distribution function and obtain the reduced kinetic equation decoupled from the fast gyrating motion. The procedure in their derivations is called a recursive method and employed in many gyrokinetic analyses [4, 11–13]. One of the advantages of the gyrokinetics is separation of the time scale which enables one to solve only the slow dynamics. The dominant motion of a particle in most of the fusion plasmas is the cyclotron motion characterized by the gyrofrequency $\Omega = qB/m$ and the gyroradius $\rho = v_\perp/\Omega$. In the case of the micro-instabilities such as ion-temperature-gradient (ITG) modes, which are believed to be a essential cause of the anomalous transport in the magnetically confined plasmas, the characteristic frequency is usually much smaller than the gyrofrequency. The separation and averaging of the fast gyration provides the slow dynamics of the plasma such as drift motions in physically clear form in the resulting kinetic equation. The gyrophase-averaging procedure in the recursive formulation also reduces the dimensions of the distribution function, i.e. the gyrophase dependence is eliminated. This is another advantage of the gyrokinetics especially for the simulation studies. The reduction of the computational cost is quite important issue in simulation studies because the statistical accuracy can be improved by using larger number of particles in the particle simulations and the spatial resolution can be improved also in the Vlasov simulations. The recursive formulation is used for the analytical and simulation studies mainly in the 1970s and 1980s.

In 1979, Littlejohn introduced a new approach [16, 17] in the plasma physics, which enables one to treat the particle dynamics rigorously and to decouple the drift motions with the aid of the the differential geometry. The advantage over the previous formulation

is the completeness and unambiguous in the derivation of the higher order nonlinear terms. The derivation starts from a Hamiltonian representation of a particle dynamics, and then the gyrophase and the magnetic moment are determined to be canonical conjugate through the Darboux transformation, and finally the gyrokinetic Hamiltonian is determined to be independent of the gyrophase through the Lie transformation. Since his formulation was for only the equilibrium potentials, the generalization for the perturbation potentials was made by Dubin [14] and Hahm [15].

In 1982, Littlejohn introduced another formulation method [6,7] using the phase space Lagrangian, or 1-form, instead of the Hamiltonian. The efficiency of this representation in the Lie perturbation analysis [21] took the place of the Hamiltonian formulation. The generalization for the perturbation potentials was made by Hahm [15] and Brizard [18]. A closed set of gyrokinetic equations, i.e. equations of motion and the Maxwell's equations, was systematically derived by Brizard [18] and Qin [19, 20] with the aid of the pullback transformation. A brief description of the fundamental concept in the modern derivation, especially the Lagrangian formulation, is presented below.

The basic idea of the modern gyrokinetic theory is that if one chooses an appropriate coordinate system, the equations of motion can be reduced. The coordinate systems used in the gyrokinetic theory are shown in Fig. 2.1. The dashed curve represents the trajectory of a charged particle in a given electromagnetic fields; $\mathbf{B} \propto \hat{\mathbf{z}}$ and $\mathbf{E} \propto (x\hat{\mathbf{x}} + y\hat{\mathbf{y}})/\sqrt{x^2+y^2}$. The dotted and solid curves correspond to those of the guiding-center and the gyrocenter. The trajectory of the guiding-center does not include the gyration due to the Lorentz force. A small oscillatory component, however, remains in the dynamics of the guiding-center. On the other hand, the motion of the gyrocenter is reduced to a simple $\mathbf{E}\times\mathbf{B}$ drift motion along the contour of the electric potential. The goal of the gyrokinetic theory is to determine the most appropriate coordinate system, i.e. gyrocenter coordinate, with the aid of mathematics and the analytic mechanics such as differential geometry, 1-form representations of the particle dynamics, the Lie perturbation analysis and pullback transformation. Before dealing with the particle motion in electromagnetic fields, we discuss a simple dynamics related with a harmonic oscillator. Observing a simple example of determining a suitable coordinate system will be helpful in the later discussion of the gyrokinetic theory.

The dynamics of a harmonic oscillator is described by the 1-form, $\gamma = v\,dx - (v^2/2 + \omega^2 x^2/2)\,dt$, where the position and velocity of a particle are denoted by x and v. The equations of motion are derived by the Euler-Lagrange equation as $\dot{x} = v$ and $\dot{v} = -\omega^2 x$. This simultaneous differential equation can be easily solved and yield sinusoidal solutions. We can, however, obtain more straightforward equations where the two coordinate variables evolves independently each other through a coordinate transformation; $x = \sqrt{2\mu/\omega}\sin\theta$ and $v = \sqrt{2\omega\mu}\cos\theta$. This transformation yields a new expression of the

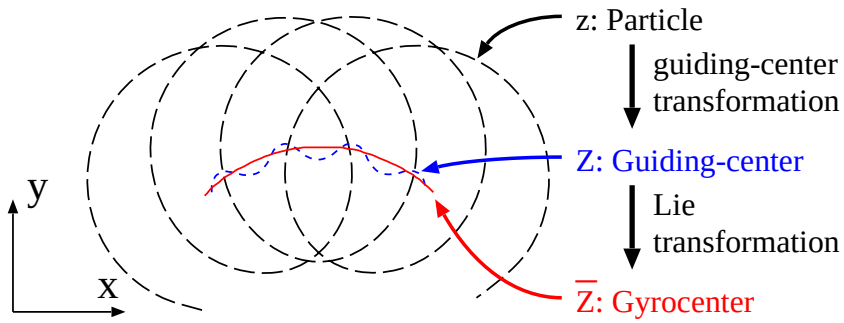

Figure 2.1: Schematic diagram of three coordinate systems; particle (dashed curve), guiding-center (dotted curve) and gyrocenter (solid curve). The coordinate transformations from the particle to the guiding-center and from the guiding-center to the gyrocenter are called guiding-center transformation and Lie transformation, respectively.

1-form $\gamma = \mu\, d\theta - \omega\mu\, dt + d(\mu \sin 2\theta/2)$. Since the exterior derivative of a scalar field does not affect the dynamics, the 1-form is reduced to $\gamma = \mu\, d\theta - \omega\mu\, dt$, i.e. gauge transformation. The new 1-form yields quite simple equations of motion; $\dot{\mu} = 0$ and $\dot{\theta} = \omega$. Since the 1-form does not include θ dependence, each coordinate variables evolve independently. This fact represents the advantage of the new coordinate system (μ, θ) over the original one. The present coordinate system correspond to the guiding-center coordinate system in the gyrokinetic theory. Although it is sufficient for the constant ω, or uniform fields in the gyrokinetic theory, it is not the best in more general cases as is shown in the Fig. 2.1.

We consider another example of more general one. If the Hamiltonian of the harmonic oscillator acquires a perturbation proportional to a small parameter ϵ, an example of such 1-forms is given by $\gamma = \mu\theta - \omega(\mu - \epsilon\cos\theta)\, dt$. In this case, the coordinate transformation, $\bar{\mu} = \mu - \epsilon\cos\theta$, can eliminate the θ dependence in the 1-form; $\gamma = (\bar{\mu} - \epsilon\cos\theta)\, d\theta - \omega\bar{\mu}\, dt = \bar{\mu}\, d\theta - \omega\bar{\mu}\, dt + d(\epsilon\sin\theta)$. The new coordinate system $(\bar{\mu}, \theta)$ corresponds to the gyrocenter coordinate. Although in this simple example the θ dependence is completely eliminated through the coordinate transformation, the dynamics of a charged particle in nonuniform fields involves more complicated coupling between the gyration and potential variation, and thus the determination of the appropriate coordinate system requires a more elegant mathematical technique. In gyrokinetic theory, the Lie transformation technique [18, 21] is employed because of its useful feature as a near-identity transformation. A Lie transformation represents a transport along a flow generated from a vector field g and is usually written as an exponential map, $\exp(\epsilon\mathcal{L}_g)$, with the Lie derivative operator $\mathcal{L}_g = i_g(df) - d(i_g f)$. The generating vector field g is called a Lie generator. In the example of the perturbed harmonic oscillator, the corresponding Lie generator is given by $g = -\cos\theta\,\partial_\theta$. Using the Lie transformation, the new coordinate $\bar{\mu}$ and 1-form are

written as $\bar{\mu} = \exp(\epsilon\mathcal{L})\mu = \mu - \epsilon\cos\theta$ and $\bar{\gamma} = \exp(-\epsilon\mathcal{L})\gamma = \bar{\mu}\,d\theta - \omega\bar{\mu}\,dt + dS$, where the gauge function is denoted by S. In the gyrokinetic theory, the 1-form of a charged particle, the Lie generator and the gauge function are expanded in power series of a small parameter ϵ. Using the Taylor expanded expression of the Lie transform operator, the Lie generator and the new coordinate system are determined order by order to eliminate gyrophase dependences in the original 1-form.

The detailed discussions of the derivation is presented here. In Sec. 2.2, the guiding-center coordinate is introduced in the 1-form of a charged particle. The preliminary calculation for the Lie perturbation analysis is carried out and the zeroth order drift-kinetic equations are presented. The differences in the previous derivations by Littlejohn, Brizard and Qin are also described. In Sec. 2.3, the Lie generator and the gyrocenter coordinate are determined and the first order gyrokinetic equations are presented. The charge and current densities written by the gyrocenter distribution function are also obtained. Finally, conclusions are presented in Sec. 2.4.

2.2 Guiding-center transformation

2.2.1 Guiding-center coordinate

The fist step in the derivation of the gyrokinetic equations is coordinate transformation to the guiding-center system $Z = (Z^0, Z^1, \ldots, Z^6) = (t, \mathbf{X}, \Theta', v_\perp, v_\parallel)$. Definitions introduced by Littlejohn [6, 7] and Qin [19, 22, 28] and by Brizard [18] differs. In the former definition the position of the guiding-center is explicitly defined, while in the latter only the velocity space variables, Θ, $v_\perp$ and $v_\parallel$ are defined and the guiding-center position is recovered through the Lie transformation. Although Brizard use the Lie transformation for the guiding-center transformation to obtain the higher order drift-kinetic equations, it can be omitted and a simple expression can be used for the guiding-center position. We define the guiding-center coordinate variables as inverse transformations;

$$\mathbf{x} \equiv \mathbf{X} + \frac{m v_\perp}{qB(\mathbf{X})}\hat{\mathbf{a}}'(\mathbf{X}, \Theta'), \tag{2.1}$$

$$\mathbf{v} \equiv v_\parallel \hat{\mathbf{b}}(\mathbf{X}) + v_\perp \hat{\mathbf{c}}'(\mathbf{X}, \Theta'). \tag{2.2}$$

Each quantity in the right hand side is a function of the new coordinate variables $(t, \mathbf{X}, \Theta', v_\perp, v_\parallel)$. The meaning of the superscript ' ' ' in these equations is clarified in Sec. 2.2.2. The parallel and perpendicular velocities are given by $v_\parallel \equiv \mathbf{v}\cdot\hat{\mathbf{b}}$ and $v_\perp \equiv \left|\hat{\mathbf{b}}\times\mathbf{v}\times\hat{\mathbf{b}}\right|$, respectively. A set of the orthonormal vectors $\hat{\mathbf{a}}'$, $\hat{\mathbf{b}}$ and $\hat{\mathbf{c}}'$ is introduced to define the gyrophase Θ'

$$\hat{\mathbf{b}} \equiv \frac{\mathbf{B}}{B}, \tag{2.3}$$

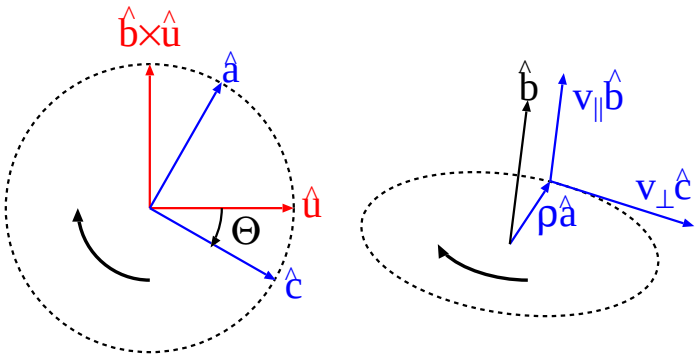

Figure 2.2: Definition of the gyrophase. An unit vector $\hat{\mathbf{u}}$ is used as the base direction.

$$\hat{\mathbf{c}}' \equiv \hat{\mathbf{u}}' \cos\Theta' - \left(\hat{\mathbf{b}} \times \hat{\mathbf{u}}'\right) \sin\Theta', \tag{2.4}$$

$$\hat{\mathbf{a}}' \equiv \hat{\mathbf{u}}' \sin\Theta' + \left(\hat{\mathbf{b}} \times \hat{\mathbf{u}}'\right) \cos\Theta', \tag{2.5}$$

where the magnetic field $\mathbf{B}$ is equilibrium one. These vectors satisfy the relation $\hat{\mathbf{b}} = \hat{\mathbf{c}}' \times \hat{\mathbf{a}}'$ and thus $\hat{\mathbf{c}}'$ and $\hat{\mathbf{a}}'$ makes the perpendicular plane to the magnetic field. The unit vector $\hat{\mathbf{u}}'$ is normal to the magnetic field and represents the base direction for the gyrophase, i.e. $\hat{\mathbf{c}}'|_{\Theta'=0} = \hat{\mathbf{u}}'$. The vector $\hat{\mathbf{c}}'$ and $\hat{\mathbf{a}}'$ are utilized as the direction of the perpendicular velocity and the gyroradius vector. These newly introduced vectors are illustrated in Fig. 2.2. In most of the gyrokinetic study, the base direction vectors are denoted by $\hat{\mathbf{e}}_1$ and $\hat{\mathbf{e}}_2$, but we use $\hat{\mathbf{u}}'$ here to emphasize the role as the base direction of the gyrophase. One can replace $\hat{\mathbf{u}}'$ and $\hat{\mathbf{b}} \times \hat{\mathbf{u}}'$ with $\hat{\mathbf{e}}_1$ and $\hat{\mathbf{e}}_2$.

2.2.2 Gyrogauge transformation

The exterior derivative of the vector $\hat{\mathbf{a}}'$, $\hat{\mathbf{b}}$ and $\hat{\mathbf{c}}'$ are calculated as

$$d\hat{\mathbf{b}} = d\mathbf{X} \cdot \nabla\hat{\mathbf{b}} + dt\frac{\partial\hat{\mathbf{b}}}{\partial t}, \tag{2.6}$$

$$d\hat{\mathbf{c}}' = -\left[d\Theta' - d\hat{\mathbf{u}}' \cdot \left(\hat{\mathbf{b}} \times \hat{\mathbf{u}}'\right)\right] \hat{\mathbf{a}}' - \left(d\hat{\mathbf{b}} \cdot \hat{\mathbf{c}}'\right) \hat{\mathbf{b}}, \tag{2.7}$$

$$d\hat{\mathbf{a}}' = \left[d\Theta' - d\hat{\mathbf{u}}' \cdot \left(\hat{\mathbf{b}} \times \hat{\mathbf{u}}'\right)\right] \hat{\mathbf{c}}' - \left(d\hat{\mathbf{b}} \cdot \hat{\mathbf{a}}'\right) \hat{\mathbf{b}}. \tag{2.8}$$

These calculations gives the relation

$$d\hat{\mathbf{a}}' \cdot \hat{\mathbf{c}}' = -d\hat{\mathbf{c}}' \cdot \hat{\mathbf{a}}' = d\Theta' + \mathbf{R}_{\mathbf{X}} \cdot d\mathbf{X} + R_t dt, \tag{2.9}$$

where we introduce $\mathbf{R}_{\mathbf{X}} \equiv \nabla\hat{\mathbf{c}}' \cdot \hat{\mathbf{a}}' = \nabla\hat{\mathbf{u}}' \cdot \left(\hat{\mathbf{b}} \times \hat{\mathbf{u}}'\right)$ and $R_t \equiv (\partial\hat{\mathbf{c}}'/\partial t) \cdot \hat{\mathbf{a}}' = (\partial\hat{\mathbf{u}}'/\partial t) \cdot \left(\hat{\mathbf{b}} \times \hat{\mathbf{u}}'\right)$, which do not depend on the gyrophase. The infinitesimal change $d\hat{\mathbf{a}}' \cdot \hat{\mathbf{c}}'$ represents the variation of the angle which the vector $\hat{\mathbf{a}}'$ has during the infinitesimal period of time, dt, and consists of the contributions of the gyrophase, $d\Theta$, and spatial-temporal variation of

the base direction, $\mathbf{R}_\mathbf{X} \cdot d\mathbf{X} + R_t dt$. The latter contribution is caused by the arbitrariness in the definition of the base direction for the gyrophase, in other words a gyrophase symmetry existing in the dynamics. While Brizard and Qin proceed calculations using $\mathbf{R}_\mathbf{X}$ and R_t, Littlejohn removes the arbitrariness from the definition of the gyrophase through the gyrogauge transformation [17, 18] at the end of the formulation. According to the formulations by Brizard and Qin, this arbitrariness just causes an offset in the gyrophase and does not affect the resulting equations of motion physically. Although that fact imply that the gyrogauge transformation is not the essential step in the formulation, we utilize it before the Lie transformation because terms related to $\mathbf{R}_\mathbf{X}$ and R_t are canceled and the following calculations become simple.

We introduce a new gyrophase Θ as the angle pushed forward by a function $\varphi(t, \mathbf{X})$ from the original angle Θ';

$$\Theta \equiv \Theta' + \varphi. \tag{2.10}$$

In order to remove the arbitrariness from the gyrophase, the offset of the angle φ is determined so that the infinitesimal change of the angle which the new orthonormal vectors

$$\hat{\mathbf{c}} \equiv \hat{\mathbf{u}} \cos\Theta - \left(\hat{\mathbf{b}} \times \hat{\mathbf{u}}\right) \sin\Theta, \tag{2.11}$$

$$\hat{\mathbf{a}} \equiv \hat{\mathbf{u}} \sin\Theta + \left(\hat{\mathbf{b}} \times \hat{\mathbf{u}}\right) \cos\Theta, \tag{2.12}$$

have during the infinitesimal period reduces to only the contribution of the new gyrophase; $d\hat{\mathbf{a}} \cdot \hat{\mathbf{c}} = d\Theta$. The new base direction $\hat{\mathbf{u}}$ used in the definitions of the vector $\hat{\mathbf{c}}$ and $\hat{\mathbf{a}}$ is defined by $\hat{\mathbf{u}} \equiv \hat{\mathbf{u}}' \cos\varphi + \hat{\mathbf{b}} \times \hat{\mathbf{u}}' \sin\varphi$. From these equations, the exterior derivative of φ is determined; $d\varphi = d\Theta - d\Theta' = d\hat{\mathbf{a}} \cdot \hat{\mathbf{c}} - (d\hat{\mathbf{a}}' \cdot \hat{\mathbf{c}}' - \mathbf{R}_\mathbf{X} \cdot d\mathbf{X} - R_t dt) = \mathbf{R}_\mathbf{X} \cdot d\mathbf{X} + R_t dt$. Integrating $d\varphi$, we obtain the function φ as

$$\varphi = \int_0^t \left(\mathbf{R}_\mathbf{X} \cdot \frac{d\mathbf{X}}{dt} + R_t\right) dt. \tag{2.13}$$

Although Littlejohn uses slightly different expression, which has an additional term $\int \nabla \times \hat{\mathbf{b}}/2 \cdot d\mathbf{X}$, the difference is not essential because the additional term can be recovered through the Lie transformation later and does not make the calculation complicated at all. As long as one uses the new orthonormal vectors $\hat{\mathbf{a}}$, $\hat{\mathbf{b}}$, $\hat{\mathbf{c}}$, the vector $\mathbf{R}_\mathbf{X}$ and R_t related to the arbitrariness do not appear in calculations.

The infinitesimal change of the new base direction vector $\hat{\mathbf{u}}$ introduced through the gauge transformation can be written as $d\hat{\mathbf{u}} = -\left(d\hat{\mathbf{b}} \cdot \hat{\mathbf{u}}\right)\hat{\mathbf{b}}$, or explicitly

$$\frac{d\hat{\mathbf{u}}}{dt} = -\left(\frac{d\mathbf{X}}{dt} \cdot \nabla\hat{\mathbf{b}} \cdot \hat{\mathbf{u}} + \frac{d\hat{\mathbf{b}}}{dt}\right)\hat{\mathbf{b}}. \tag{2.14}$$

This differential equation coincides with the 'rotationless' transport equation introduced by Littlejohn [42]. We use the new gyrophase Θ, the orthonormal vectors $\hat{\mathbf{c}}$ and $\hat{\mathbf{a}}$ and the

direction vector $\hat{\mathbf{u}}$ in the remainder of this work instead of the corresponding vectors with the superscript ‘ ’. We note that the vector $\hat{\mathbf{u}}$ differs for each particle.

2.2.3 Potential perturbation and orderings

We introduce the potential perturbations as follows;

$$\phi = \phi_0 + \phi_1 \tag{2.15}$$

$$\mathbf{A} = \mathbf{A}_0 + \mathbf{A}_1 \tag{2.16}$$

The subscripts 0 and 1 represent the equilibrium and perturbation components, respectively. The drift-kinetic orderings,

$$\frac{\omega_0}{\Omega} \sim 0, \quad k_{\perp 0}\rho \sim \epsilon_\mathrm{d}, \quad k_{\parallel 0}\rho \sim \epsilon_\mathrm{d}, \quad \frac{\left|\hat{\mathbf{b}} \times \nabla \phi_0\right|}{B_0} \sim \epsilon_\mathrm{d} v_\mathrm{t}, \tag{2.17}$$

are applied to the equilibrium potentials. The gyrofrequency and gyroradius are denoted by $\Omega \equiv qB_0/m$ and $\rho \equiv v_\perp/\Omega$, respectively. Although we neglect the time dependence of the equilibrium potentials here, slow variations, i.e. $\omega_0/\Omega \sim \epsilon_\mathrm{d}$, can be treated in the same way. The gyrokinetic orderings

$$\frac{\omega_1}{\Omega} \sim \epsilon_\mathrm{g}, \quad k_{\perp 1}\rho \sim 1, \quad k_{\parallel 1}\rho \sim \epsilon_\mathrm{g}, \quad \frac{\left|\hat{\mathbf{b}} \times \nabla \phi_1\right|}{B_0} \sim \epsilon_\mathrm{g} v_\mathrm{t}, \tag{2.18}$$

are similarly applied to the perturbation components. Although we assume that the time scale of the perturbation is much longer than that of the gyration, fast variations, i.e. $\omega_0/\Omega \sim 1$, can be treated in the same way [19, 23].

2.2.4 Guiding-center 1-form

The fundamental 1-form of a single charged particle defined in the coordinate system $z = (z^0, z^1, \ldots, z^6) = (t, \mathbf{x}, \mathbf{v})$ is given by

$$\gamma \equiv \left[m\mathbf{v} + q\mathbf{A}(\mathbf{x})\right] \cdot d\mathbf{x} - \left[\frac{m}{2}v^2 + q\phi(\mathbf{x})\right] dt. \tag{2.19}$$

It can be rewritten in the guiding-center coordinate system introduced in Sec. 2.2.1 as

$$\gamma = \left[q\mathbf{A}(\mathbf{X} + \rho\hat{\mathbf{a}}) + mv_\perp \hat{\mathbf{c}} + mv_\parallel \hat{\mathbf{b}}\right] \cdot d(\mathbf{X} + \rho\hat{\mathbf{a}}) - \left[\frac{m}{2}\left(v_\parallel^2 + v_\perp^2\right) + q\phi_0(\mathbf{X} + \rho\hat{\mathbf{a}})\right] dt. \tag{2.20}$$

From a guiding-center representation of the 1-form $d\mathbf{x} = d(\mathbf{X} + \rho\hat{\mathbf{a}})$,

$$d\mathbf{x} = \left(\overleftrightarrow{I} - \rho\nabla \ln B_0 \hat{\mathbf{a}} - \rho\nabla\hat{\mathbf{b}} \cdot \hat{\mathbf{a}}\hat{\mathbf{b}}\right) \cdot d\mathbf{X} + \rho\hat{\mathbf{c}}\, d\Theta + \frac{\hat{\mathbf{a}}}{\Omega}\, dv_\perp, \tag{2.21}$$

we calculate $\hat{\mathbf{c}} \cdot d\mathbf{x}$ and $\hat{\mathbf{b}} \cdot d\mathbf{x}$ as $\hat{\mathbf{c}} \cdot d\mathbf{x} = \hat{\mathbf{c}} \cdot d\mathbf{X} + \rho\, d\Theta$ and $\hat{\mathbf{b}} \cdot d\mathbf{x} = \left(\hat{\mathbf{b}} - \rho \nabla \hat{\mathbf{b}} \cdot \hat{\mathbf{a}}\right) \cdot d\mathbf{X}$, respectively.

The calculation of $\mathbf{A}_0 \cdot d\mathbf{x}$ is rather complicated because of the dependences of the vector potential $\mathbf{A}_0$ on the velocity space variables. First, using the gauge transformation we obtain $\mathbf{A}_0 \cdot d\mathbf{x} = \mathbf{A}_0 \cdot d\mathbf{X} - d\mathbf{A}_0 \cdot \rho\hat{\mathbf{a}} + d\left(\mathbf{A}_0 \cdot \rho\hat{\mathbf{a}}\right)$. Second, since the equilibrium potential satisfies the drift-kinetic orderings, the term $\mathbf{A}_0(\mathbf{X} + \rho\hat{\mathbf{a}})$ can be Taylor expanded with $\epsilon_{\rm d}$; $\mathbf{A}_0(\mathbf{X} + \rho\hat{\mathbf{a}}) = \mathbf{A}_0 + \rho\hat{\mathbf{a}} \cdot \nabla \mathbf{A}_0 + \rho^2 \hat{\mathbf{a}}\hat{\mathbf{a}} : \nabla\nabla \mathbf{A}_0/2 + O(\epsilon_{\rm d}^3)$. Each term is reduced through the gauge transformation as

$$
\begin{aligned}
d\left(\rho\hat{\mathbf{a}} \cdot \nabla \mathbf{A}_0\right) \cdot \rho\hat{\mathbf{a}} &= -\frac{1}{2}\left[\rho\hat{\mathbf{a}} \times d(\rho\hat{\mathbf{a}})\right] \cdot \nabla \times \mathbf{A}_0 + \frac{\rho^2}{2}\hat{\mathbf{a}} \cdot d\nabla \mathbf{A}_0 \cdot \hat{\mathbf{a}} + d\left(\rho^2 \hat{\mathbf{a}} \cdot \nabla \mathbf{A}_0 \cdot \hat{\mathbf{a}}\right), \\
d\left(\frac{\rho^2}{2}\hat{\mathbf{a}}\hat{\mathbf{a}} : \nabla \mathbf{A}_0\right) \cdot \rho\hat{\mathbf{a}}, &= -\frac{1}{3}\rho\hat{\mathbf{a}} \cdot \nabla(\nabla \times \mathbf{A}_0) \cdot \left[\rho\mathbf{a} \times d(\rho\hat{\mathbf{a}})\right] + \frac{\rho^2}{6}\hat{\mathbf{a}}\hat{\mathbf{a}} : d(\nabla\nabla \mathbf{A}_0) \cdot \rho\hat{\mathbf{a}} \\
&\quad + d\left(\frac{\rho^2}{3}\hat{\mathbf{a}}\hat{\mathbf{a}} : \nabla\nabla \mathbf{A}_0 \cdot \rho\mathbf{a}\right),
\end{aligned}
$$

where we used the following relations;

$$
\begin{aligned}
d\left(\rho^2 \hat{\mathbf{a}} \cdot \nabla \mathbf{A}_0 \cdot \hat{\mathbf{a}}\right) &= \rho\hat{\mathbf{a}} \cdot \nabla \mathbf{A}_0 \cdot d(\rho\hat{\mathbf{a}}) + d(\rho\hat{\mathbf{a}}) \cdot \nabla \mathbf{A}_0 \cdot \rho\hat{\mathbf{a}} + \rho^2 \hat{\mathbf{a}} \cdot d(\nabla \mathbf{A}_0) \cdot \hat{\mathbf{a}}, \\
\left[\rho\hat{\mathbf{a}} \times d(\rho\hat{\mathbf{a}})\right] \cdot \nabla \times \mathbf{A}_0 &= \rho\hat{\mathbf{a}} \cdot \nabla \mathbf{A}_0 \cdot d(\rho\hat{\mathbf{a}}) - d(\rho\hat{\mathbf{a}}) \cdot \nabla \mathbf{A}_0 \cdot \rho\hat{\mathbf{a}}, \\
d\left(\rho^3 \hat{\mathbf{a}}\hat{\mathbf{a}} : \nabla\nabla \mathbf{A}_0 \cdot \hat{\mathbf{a}}\right) &= \rho\hat{\mathbf{a}}\rho\hat{\mathbf{a}} : \nabla\nabla \mathbf{A}_0 \cdot d(\rho\hat{\mathbf{a}}) + 2\rho\hat{\mathbf{a}} d(\rho\hat{\mathbf{a}}) : \nabla\nabla \mathbf{A}_0 \cdot \rho\hat{\mathbf{a}} \\
&\quad + \rho^2 \hat{\mathbf{a}}\hat{\mathbf{a}} : d(\nabla\nabla \mathbf{A}_0) \cdot \hat{\mathbf{a}}, \\
\rho\hat{\mathbf{a}} \cdot \nabla(\nabla \times \mathbf{A}_0) \cdot \left[\rho\mathbf{a} \times d(\rho\hat{\mathbf{a}})\right] &= \rho\hat{\mathbf{a}}\rho\hat{\mathbf{a}} : \nabla\nabla \mathbf{A}_0 \cdot d(\rho\hat{\mathbf{a}}) - \rho\hat{\mathbf{a}} d(\rho\hat{\mathbf{a}}) : \nabla\nabla \mathbf{A}_0 \cdot \rho\hat{\mathbf{a}}.
\end{aligned}
$$

Third, using the relations $d\mathbf{A}_0 = d\mathbf{X} \cdot \nabla \mathbf{A}_0$ and $\hat{\mathbf{a}} \cdot \nabla \mathbf{A}_0 - \nabla \mathbf{A}_0 \cdot \hat{\mathbf{a}} = (\nabla \times \mathbf{A}_0) \times \hat{\mathbf{a}} = -B_0 \hat{\mathbf{c}}$, we obtain

$$
\begin{aligned}
q\mathbf{A}_0(\mathbf{x}) \cdot d\mathbf{x} &= \left(q\mathbf{A}_0 - mv_\perp \hat{\mathbf{c}} + \frac{q\rho^2}{2}\hat{\mathbf{a}} \cdot \nabla \mathbf{B}_0 \times \hat{\mathbf{a}}\right) \cdot d\mathbf{X} + \frac{mv_\perp}{2}\left[\hat{\mathbf{a}} \times d(\rho\hat{\mathbf{a}})\right] \cdot \hat{\mathbf{b}} \\
&\quad + \frac{mv_\perp \rho}{2B_0}\hat{\mathbf{a}} \cdot \nabla \mathbf{B}_0 \cdot \left[\hat{\mathbf{a}} \times d(\rho\hat{\mathbf{a}})\right] - \frac{q\rho^2}{6}\hat{\mathbf{a}}\hat{\mathbf{a}} : d(\nabla\nabla \mathbf{A}_0) \cdot \rho\hat{\mathbf{a}} + dS + O(\epsilon_{\rm d}^3),
\end{aligned}
$$

where the gauge function S is given by $S \equiv q\rho\mathbf{A}_0(\mathbf{x}) \cdot \hat{\mathbf{a}} - q\rho^2 \hat{\mathbf{a}} \nabla \mathbf{A}_0 \cdot \hat{\mathbf{a}} - q\rho^3 \hat{\mathbf{a}}\hat{\mathbf{a}} : \nabla\nabla \mathbf{A}_0 \cdot \mathbf{a}/3$. Form the identity $\hat{\mathbf{a}} \cdot \nabla \mathbf{B}_0 \times \hat{\mathbf{a}} = B_0 \hat{\mathbf{a}} \cdot \nabla \hat{\mathbf{b}} \cdot \hat{\mathbf{c}}\hat{\mathbf{b}} - \hat{\mathbf{a}} \cdot \nabla B_0 \hat{\mathbf{c}}$, we obtain the gauge transformed expression of the 1-form $q\mathbf{A}_0 \cdot d\mathbf{x}$ up to the first order;

$$
\begin{aligned}
q\mathbf{A}_0(\mathbf{x}) \cdot d\mathbf{x} &= \left[q\mathbf{A}_0 - mv_\perp \hat{\mathbf{c}} + \frac{m^2 v_\perp^2}{2qB_0}\left(\hat{\mathbf{a}} \cdot \nabla \hat{\mathbf{b}} \cdot \hat{\mathbf{c}}\hat{\mathbf{b}} - \hat{\mathbf{a}} \cdot \nabla \ln B_0 \hat{\mathbf{c}}\right)\right] \cdot d\mathbf{X} \\
&\quad - \frac{m^2 v_\perp^2}{2qB_0}\left(1 + \rho\hat{\mathbf{a}} \cdot \nabla \ln B_0\right) d\Theta + dS + O(\epsilon_{\rm d}^2). \qquad (2.22)
\end{aligned}
$$

In summary, the fundamental 1-form in the guiding-center coordinate system is given by

$$
\begin{aligned}
\Gamma &= \Gamma_{\mathbf{X}} \cdot d\mathbf{X} + \Gamma_\Theta\, d\Theta + \Gamma_\mu\, d\mu + \Gamma_{v_\parallel}\, dv_\parallel + \Gamma_t\, dt, \qquad (2.23)\\
\Gamma_{\mathbf{X}} &= q\mathbf{A}_0 + \frac{m\mu}{q}\left(\hat{\mathbf{a}}\cdot\nabla\hat{\mathbf{b}}\cdot\hat{\mathbf{c}}\hat{\mathbf{b}} - \hat{\mathbf{a}}\cdot\nabla\ln B_0\hat{\mathbf{c}}\right) + mv_\parallel\hat{\mathbf{b}} - m\rho v_\parallel\nabla\hat{\mathbf{b}}\cdot\hat{\mathbf{a}},\\
&\quad + q\mathbf{A}_1 - \frac{q}{2}\rho\mathbf{A}_1\cdot\nabla\ln B_0\hat{\mathbf{a}} - q\rho\mathbf{A}_1\cdot\nabla\hat{\mathbf{b}}\cdot\hat{\mathbf{a}}\hat{\mathbf{b}},\\
\Gamma_\Theta &= \frac{m\mu}{q}\left(1-\rho\hat{\mathbf{a}}\cdot\nabla\ln B_0\right) + q\rho\mathbf{A}_1\cdot\hat{\mathbf{c}},\\
\Gamma_\mu &= \frac{1}{v_\perp}\mathbf{A}_1\cdot\hat{\mathbf{a}},\\
\Gamma_{v_\parallel} &= 0,\\
\Gamma_t &= -\left[\frac{m}{2}v_\parallel^2 + B_0\mu + \frac{m}{2}D^2 + q\phi_0 + q\phi_1\right],
\end{aligned}
$$

where the magnetic moment

$$
\mu \equiv \frac{mv_\perp^2}{2B_0} \qquad (2.24)
$$

has been introduced. The potentials except the equilibrium vector potential in the right hand side, i.e. $\mathbf{A}_1$, ϕ_0 and ϕ_1, are evaluated at the particle position $\mathbf{X} + \rho\hat{\mathbf{a}}$.

2.2.5 Drift-kinetic equations

The drift-kinetic equations can be obtained from the guiding-center 1-form, Eq. (2.23), by neglecting the potential perturbation or setting $\epsilon_{\mathrm{g}} = 0$. The higher order calculation requires the Lie perturbation analysis as Brizard [18] did. We take only the zeroth order terms in the 1-form;

$$
\Gamma_{\mathrm{drift}} = \left(q\mathbf{A}_0 + mv_\parallel\hat{\mathbf{b}}\right)\cdot d\mathbf{X} + \frac{m}{q}\mu d\Theta - \left[B_0\mu + \frac{m}{2}v_\parallel^2 + \frac{m}{2}D^2 + q\left\langle\phi_0\right\rangle\right]dt. \qquad (2.25)
$$

The Lagrange and Poisson tensors are calculated as

$$
\overleftrightarrow{\omega} = \left(\begin{array}{c|ccc}
-q\mathbf{B}^*\times\overleftrightarrow{I} & \mathbf{0} & \mathbf{0} & -m\hat{\mathbf{b}}\\
\hline
\mathbf{0} & 0 & -m/q & 0\\
\mathbf{0} & m/q & 0 & 0\\
m\hat{\mathbf{b}} & 0 & 0 & 0
\end{array}\right), \qquad (2.26)
$$

$$
\overleftrightarrow{\sigma} = \left(\begin{array}{c|ccc}
\hat{\mathbf{b}}\times\overleftrightarrow{I}/qB_\parallel^* & \mathbf{0} & \mathbf{0} & \mathbf{B}^*/mB_\parallel^*\\
\hline
\mathbf{0} & 0 & q/m & 0\\
\mathbf{0} & -q/m & 0 & 0\\
-\mathbf{B}^*/mB_\parallel^* & 0 & 0 & 0
\end{array}\right). \qquad (2.27)
$$

The Euler-Lagrange equations yield the drift-kinetic equations of motion;

$$\frac{d\mathbf{X}}{dt} = \frac{1}{B_{\parallel}^{*}}\left[\mathbf{B}^{*}v_{\parallel} + \hat{\mathbf{b}} \times \left(\nabla\phi_0 + \frac{\mu}{q}\nabla B_0\right)\right], \tag{2.28}$$

$$\frac{d\Theta}{dt} = \Omega, \tag{2.29}$$

$$\frac{d\mu}{dt} = 0, \tag{2.30}$$

$$\frac{dv_{\parallel}}{dt} = -\frac{q\mathbf{B}^{*}}{mB_{\parallel}^{*}} \cdot \left(\nabla\phi_0 + \frac{\mu}{q}\nabla B_0\right), \tag{2.31}$$

where a modified magnetic field is denoted by $\mathbf{B}^{*}$;

$$\mathbf{B}^{*} \equiv \mathbf{B}_0 + \frac{mv_{\parallel}}{q}\nabla \times \hat{\mathbf{b}} = B_{\parallel}^{*}\hat{\mathbf{b}} + \frac{mv_{\parallel}}{q}\hat{\mathbf{b}} \times \left(\hat{\mathbf{b}} \cdot \nabla\hat{\mathbf{b}}\right), \tag{2.32}$$

$$B_{\parallel}^{*} \equiv \hat{\mathbf{b}} \cdot \mathbf{B}^{*} = B_0 + \frac{mv_{\parallel}}{q}\hat{\mathbf{b}} \cdot \nabla \times \hat{\mathbf{b}}. \tag{2.33}$$

From the these equations, the velocity of the guiding-center is rewritten as

$$\frac{d\mathbf{X}}{dt} = v_{\parallel}\hat{\mathbf{b}} + \frac{1}{1 + (v_{\parallel}/\Omega)\hat{\mathbf{b}} \cdot \nabla \times \hat{\mathbf{b}}}\left[\frac{1}{B_0}\hat{\mathbf{b}} \times \nabla\phi_0 + \frac{\mu}{q}\hat{\mathbf{b}} \times \nabla \ln B_0 + \frac{v_{\parallel}^2}{\Omega}\hat{\mathbf{b}} \times \left(\hat{\mathbf{b}} \cdot \nabla\hat{\mathbf{b}}\right)\right]. \tag{2.34}$$

This expression implies that the drift-kinetic equations derived here include $\mathbf{E} \times \mathbf{B}$, grad$B$ and curvature drift motions. These drift velocities, however, differ from the familiar expression by the factor $1/\left(1 + (v_{\parallel}/\Omega)\hat{\mathbf{b}} \cdot \nabla \times \hat{\mathbf{b}}\right)$. This correction comes from the coupling of parallel motion and the magnetic shear along the magnetic field. If the magnetic field rotates spatially along the magnetic field itself in the same direction as the particle gyration, the effective gyrofrequency is reduced and thus the drift velocity becomes slower. The Baños drift [24] does not appear in the zeroth order equations. The detailed reason of the absence of the polarization drift is discussed in Sec. 2.3.5. From the equations of motion, the drift-kinetic Vlasov equation is obtained;

$$\frac{dF}{dt} + \frac{d\mathbf{X}}{dt} \cdot \frac{\partial F}{\partial \mathbf{X}} + \frac{d\Theta}{dt}\frac{\partial F}{\partial \Theta} + \frac{dv_{\parallel}}{dt}\frac{\partial F}{\partial v_{\parallel}} = 0. \tag{2.35}$$

The drift-kinetic equations derived here satisfy the Liouville's theorem

$$\frac{\partial}{\partial Z^i}\left(B_{\parallel}^{*}\dot{Z}^i\right) = \frac{\partial}{\partial t}\left(B_{\parallel}^{*}\frac{\partial t}{\partial t}\right) + \nabla \cdot \left(B_{\parallel}^{*}\frac{d\mathbf{X}}{dt}\right) + \frac{\partial}{\partial \Theta}\left(B_{\parallel}^{*}\frac{d\Theta}{dt}\right) + \frac{\partial}{\partial V_{\parallel}}\left(B_{\parallel}^{*}\frac{dV_{\parallel}}{dt}\right) = 0. \tag{2.36}$$

It can be easily confirmed using the relations

$$B_{\parallel}^{*}\frac{d\mathbf{X}}{dt} = \frac{1}{q}\nabla \times \left(\Gamma_t'\hat{\mathbf{b}}\right) - \frac{1}{m}\frac{\partial \Gamma_t'\mathbf{B}^{*}}{\partial v_{\parallel}},$$

$$B_{\parallel}^{*}\frac{dv_{\parallel}}{dt} = \frac{1}{m}\nabla \cdot \left(\Gamma_t'\mathbf{B}^{*}\right).$$

This fact implies that the phase-space volume is given by $B_\parallel^*/m$. From the Liouville's theorem, We can obtain the conservation form of the Vlasov equation;

$$\frac{\partial}{\partial t}\left(B_\parallel^* F\right) + \nabla\cdot\left(B_\parallel^* F\frac{d\mathbf{X}}{dt}\right) + \frac{\partial}{\partial\Theta}\left(B_\parallel^* F\frac{d\Theta}{dt}\right) + \frac{\partial}{\partial V_\parallel}\left(B_\parallel^* F\frac{dV_\parallel}{dt}\right) = 0. \tag{2.37}$$

2.3 Gyrokinetic equations

2.3.1 Lie perturbation analysis

In this section, we introduce the Lie transformation to eliminate the gyrophase dependences in the 1-form in the guiding-center coordinate system. First, we rewrite the guiding-center 1-form in power series of ϵ_g;

$$\begin{aligned}
\Gamma &= \Gamma_0 + \epsilon_\mathrm{g}\Gamma_1 + \epsilon_\mathrm{g}^2\Gamma_2 + \cdots, \qquad (2.38)\\
\Gamma_0 &= \left(q\mathbf{A}_0 + mv_\parallel\hat{\mathbf{b}}\right)\cdot d\mathbf{X} + \frac{m}{q}\mu\, d\Theta - \left[\frac{m}{2}v_\parallel^2 + B_0\mu + q\phi_0\right]dt,\\
\Gamma_1 &= q\mathbf{A}_1\cdot d\mathbf{X} + q\rho\mathbf{A}_1\cdot\hat{\mathbf{c}}\, d\Theta + \frac{1}{v_\perp}\mathbf{A}_1\cdot\hat{\mathbf{a}}\, d\mu - q\phi_1(\mathbf{X}+\rho\hat{\mathbf{a}})dt,\\
\Gamma_2 &= \left[\frac{m\mu}{q}\left(\hat{\mathbf{a}}\cdot\nabla\hat{\mathbf{b}}\cdot\hat{\mathbf{c}}\hat{\mathbf{b}} - \hat{\mathbf{a}}\cdot\nabla\ln B_0\hat{\mathbf{c}}\right) - m\rho v_\parallel\nabla\hat{\mathbf{b}}\cdot\hat{\mathbf{a}}\right]\cdot d\mathbf{X}\\
&\quad - \frac{m\mu}{q}\rho\hat{\mathbf{a}}\cdot\nabla\ln B_0\, d\Theta - q\rho\hat{\mathbf{a}}\cdot\nabla\phi_0\, dt,
\end{aligned}$$

where we assume that the spatial scale of the equilibrium fields are much longer than the gyroradius, or $\epsilon_\mathrm{d}\sim\epsilon_\mathrm{g}^2$. This assumption is justified for large devices where the plasma size is extremely larger than the gyroradius.

The Lie transformation is constructed from the Lie generator expanded in the power series of ϵ_g;

$$g \equiv \epsilon_\mathrm{g} g_1 + \epsilon_\mathrm{g}^2 g_2 + \cdots. \tag{2.39}$$

The time component of the Lie generator is set to zero because it is convenient to keep the time variable unchanged, i.e. $g_i^0 = 0$. The guiding-center coordinate variables Z^i and 1-form Γ are transformed to the new coordinate $\bar{Z}$ and 1-form $\bar{\Gamma}$;

$$\bar{Z} = \cdots\exp\left(\epsilon_\mathrm{g}^2\mathcal{L}_{g_2}\right)\exp\left(\epsilon_\mathrm{g}\mathcal{L}_{g_1}\right)Z, \tag{2.40}$$

$$\sum_n\bar{\Gamma}_n = \cdots\exp\left(-\epsilon_\mathrm{g}^2\mathcal{L}_{g_2}\right)\exp\left(-\epsilon_\mathrm{g}\mathcal{L}_{g_1}\right)\sum_m\Gamma_m + dS_1 + dS_2 + \cdots, \tag{2.41}$$

where the gauge functions and Lie derivative operators are denoted by S_n and $\mathcal{L}_{g_n}$, respectively. Although a Lie derivative operator is given by $\mathcal{L}_g f = i_g df - d(i_g f)$ for a vector field g, The second term, $-d(i_g f)$, vanishes when it operates on a scalar function and also

does not affect the dynamics when it operates on the fundamental 1-form. We, therefore, adopt a reduced form, $\mathcal{L}_g\psi = i_g d\psi$. The gyrocenter 1-form is calculated from the Lie generator as

$$\bar{\Gamma}_0 = \Gamma_0, \tag{2.42}$$

$$\bar{\Gamma}_1 = \Gamma_1 - i_{g_1} d\Gamma_0 + dS_1, \tag{2.43}$$

$$\bar{\Gamma}_2 = \Gamma_2 - i_{g_1} d\Gamma_1 + \left(\frac{1}{2}(i_{g_1} d)^2 - i_{g_2} d\right)\Gamma_0 + dS_2. \tag{2.44}$$

The n-th order gyrokinetic 1-form can be written as

$$\bar{\Gamma}_n = \Gamma_n - i_{g_n} d\Gamma_0 + C_n + dS_n, \tag{2.45}$$

where the term C_n represents all the remaining components coming from the higher order 1-forms, $\Gamma_1, \Gamma_2, \ldots$. The n-th order 1-form can be separated into the time component and the others;

$$\bar{\Gamma}_{n0} = \Gamma_{n0} - g_n^j \left(\frac{\partial \Gamma_{0t}}{\partial \bar{Z}^j} - \frac{\partial \Gamma_{0j}}{\partial t}\right) + C_{n0} + \frac{\partial S_n}{\partial t}, \tag{2.46}$$

$$\bar{\Gamma}_{ni} = \Gamma_{ni} - g_n^j \omega_{ji} + C_{ni} + \frac{\partial S_n}{\partial \bar{Z}^i}. \tag{2.47}$$

Using the relations $i_{g_n} d\Gamma_0 = g_n^j \omega_{ji} dz^i$ and $\sigma^{ij}\omega_{jk} \equiv \delta^i_j$, we can solve Eq. (2.47) for the Lie generator;

$$g_n^0 = 0, \quad g_n^j = \sigma^{ij}\left(\Gamma_{ni} - \bar{\Gamma}_{ni} + C_{ni} + \partial_i S_n\right). \tag{2.48}$$

Substituting it to Eq. (2.46), we obtain

$$\Gamma_{n0} - \bar{\Gamma}_{n0} + C_{n0} + \frac{\partial S_n}{\partial t} = \left(\Gamma_{ni} - \bar{\Gamma}_{ni} + C_{ni} + \frac{\partial S_n}{\partial \bar{Z}^i}\right)\sigma^{ij}\left(\frac{\partial \Gamma_{00}}{\partial \bar{Z}^j} - \frac{\partial \Gamma_{0j}}{\partial t}\right). \tag{2.49}$$

Using a vector field $\mathcal{V}_0$ created by the zeroth order equations of motion,

$$\mathcal{V}_0^0 = 1, \quad \mathcal{V}_0^i = \sigma^{ij}\left(\frac{\partial \Gamma_{00}}{\partial \bar{Z}^j} - \frac{\partial \Gamma_{0j}}{\partial t}\right), \tag{2.50}$$

the determining equation of the gauge function is obtained as

$$i_{\mathcal{V}_0} dS_n = \frac{dS_n}{dt} = \mathcal{V}_0^i \frac{\partial S_n}{\partial \bar{Z}^i} = -\mathcal{V}_0^i\left(\Gamma_{ni} - \bar{\Gamma}_{ni} + C_{ni}\right). \tag{2.51}$$

The gauge function is solved by integrating the right hand side along the zeroth order motion.

Since we obtain all the relations between the new gyrocenter 1-form, Lie generator and gauge function, the gyrocenter 1-form can be determined to be a suitable form. We

require the 1-form to be zero except the time component. This form does not change the Poisson tensor from that of the zeroth. The n-th gyrokinetic 1-form is, therefore, determined by

$$\bar{\Gamma}_n \equiv \mathcal{V}_0^i \langle \Gamma_{ni} + C_{ni} \rangle \, dt. \tag{2.52}$$

The new 1-form has only the gyroaveraged components of the guiding-center 1-form to be independent of the gyrophase. The remaining Θ dependent components are put into the gauge function;

$$\mathcal{V}_0^i \frac{\partial S_n}{\partial \bar{Z}^i} = -\mathcal{V}_0^i \left(\tilde{\Gamma}_{ni} + \tilde{C}_{ni} \right). \tag{2.53}$$

From the gauge function, The Lie generator is determined as

$$g_n^0 = 0, \quad g_n^j = \sigma^{ij} \left(\Gamma_{ni} + C_{ni} + \partial_i S_n \right). \tag{2.54}$$

We use the following notation here to separate the gyroaveraged component and gyrophase-dependent component;

$$\langle \psi \rangle \equiv \frac{1}{2\pi} \oint \psi \, d\Theta, \quad \tilde{\psi} \equiv \psi - \langle \psi \rangle. \tag{2.55}$$

2.3.2 First order analysis

We carry out the procedure presented in Sec. 2.3.1 and obtain the first order gyrokinetic equations of motion in this section. Although the second order analysis is omitted here, we can carry out in the same way. First, the zeroth order 1-form and the its Hamiltonian flow are given by

$$\bar{\Gamma}_0 = \left(q\mathbf{A}_0 + m\bar{v}_\parallel \hat{\mathbf{b}} \right) \cdot d\bar{\mathbf{X}} + \frac{m}{q} \bar{\mu} \, d\bar{\Theta} - \left[\frac{m}{2} \bar{v}_\parallel^2 + B\bar{\mu} + q\phi_0 \right] dt, \tag{2.56}$$

$$\begin{aligned} \mathcal{V}_0 = {} & \frac{\partial}{\partial t} + \frac{1}{B_\parallel^*} \left[\mathbf{B}^* \bar{v}_\parallel + \hat{\mathbf{b}} \times \nabla \left(\phi_0 + \frac{B_0 \bar{\mu}}{q} \right) \right] \cdot \frac{\partial}{\partial \bar{\mathbf{X}}} \\ & + \Omega \frac{\partial}{\partial \bar{\Theta}} - \frac{q\mathbf{B}^*}{m B_\parallel^*} \cdot \nabla \left(\phi_0 + \frac{B_0 \bar{\mu}}{q} \right) \frac{\partial}{\partial \bar{v}_\parallel}. \end{aligned} \tag{2.57}$$

The first order 1-form is determined from Eq. (2.52) as

$$\bar{\Gamma}_1 = -q \left\langle \phi_1 - \left(\bar{v}_\parallel \hat{\mathbf{b}} + \bar{v}_\perp \hat{\mathbf{c}} \right) \cdot \mathbf{A}_1 \right\rangle dt. \tag{2.58}$$

From the zeroth order flow $\mathcal{V}_0$ and the perturbation component of the first order 1-form

$$\tilde{\Gamma}_1 = q\tilde{\mathbf{A}}_1 \cdot d\mathbf{X} + q\rho \widetilde{\mathbf{A}_1 \cdot \hat{\mathbf{c}}} \, d\Theta + \frac{1}{v_\perp} \widetilde{\mathbf{A}_1 \cdot \hat{\mathbf{a}}} \, d\mu - q\tilde{\phi}_1 \, dt, \tag{2.59}$$

the determining equation of the first order gauge function is obtained as

$$\frac{\partial S_1}{\partial t} + \mathcal{V}_0^{\bar{\mathbf{X}}} \cdot \frac{\partial S_1}{\partial \bar{\mathbf{X}}} + \mathcal{V}_0^{\bar{\Theta}} \frac{\partial S_1}{\partial \bar{\Theta}} + \mathcal{V}_0^{\bar{v}_\parallel} \frac{\partial S_1}{\partial \bar{v}_\parallel} = q\tilde{\phi}_1 - q\mathcal{V}_0^{\bar{\mathbf{X}}} \cdot \tilde{\mathbf{A}}_1 - q\rho \mathcal{V}_0^{\bar{\Theta}} \widetilde{\mathbf{A}_1 \cdot \hat{\mathbf{c}}}. \tag{2.60}$$

Since obtaining the exact solution of this differential equation takes much time in numerical calculation, some approximations are applied to it. The Hamiltonian flow $\mathcal{V}_0$ is approximated to the dominant components, i.e. gyration, parallel motion and time evolution;

$$\mathcal{V}_0 \simeq \frac{\partial}{\partial t} + \bar{v}_\parallel \hat{\mathbf{b}} \cdot \frac{\partial}{\partial \bar{\mathbf{X}}} + \Omega \frac{\partial}{\partial \bar{\Theta}}. \tag{2.61}$$

The derivative of the gauge function S_1 is approximated as

$$dS_1 \simeq \frac{\partial S_1}{\partial \bar{\Theta}} d\bar{\Theta}. \tag{2.62}$$

Using these approximations, we can obtain the solution of the gauge function as

$$S_1 = \frac{q}{\Omega} \int \left[\phi_1 - (v_\perp \hat{\mathbf{c}} + v_\parallel \hat{\mathbf{b}}) \cdot \mathbf{A}_1 - \left\langle \phi_1 - (v_\perp \hat{\mathbf{c}} + v_\parallel \hat{\mathbf{b}}) \cdot \mathbf{A}_1 \right\rangle \right] d\Theta + \Delta, \tag{2.63}$$

where the constant of integration is denoted by Δ. The constant is caused by the approximation employed here, i.e. we ignore the dependences of S_1 to the other coordinate variables such as t, $\mathbf{X}$, μ and $v_\parallel$. Originally, the gauge function is determined by the integral along the Hamiltonian flow, or the particle trajectory, but now the path of integration is replaced with a mere gyration. The difference form the open path to close one results in the constant of integral instead of the initial value. Although the constant could be arbitrary, we have to choose the most appropriate one to reduce the error due to the approximation. Taking the gyroaverage of the original equation (2.60), we obtain the time evolution of the gyroaveraged component of the gauge function as $d\langle S_1 \rangle / dt = 0$. This relation indicates that the gyroaveraged component should not change in time. We, therefore, choose the constant of integral to make the gyroaveraged gauge function vanish;

$$\begin{aligned} S_1 &= \frac{q}{\Omega} \int_0^\Theta \tilde{\psi}_1(\Theta')\, d\Theta' - \left\langle \frac{q}{\Omega} \int_0^\Theta \tilde{\psi}_1(\Theta')\, d\Theta' \right\rangle \\ &= \frac{q}{2\pi\Omega} \int_\Theta^{\Theta+2\pi} (\Theta' - \Theta - \pi) \psi_1(\Theta') d\Theta', \end{aligned} \tag{2.64}$$

where we use the notation

$$\psi_1 \equiv \phi_1(\mathbf{X} + \rho\hat{\mathbf{a}}) - (v_\perp \hat{\mathbf{c}} + v_\parallel \hat{\mathbf{b}}) \cdot \mathbf{A}_1(\mathbf{X} + \rho\hat{\mathbf{a}}). \tag{2.65}$$

In the second equality in Eq. (2.64), the integration by part is applied. From the gauge function, the Lie generator is determined as

$$g_1^t = 0, \quad g_1^j = \sigma^{ij} \left(\Gamma_{1i} + \partial_i S_1 \right). \tag{2.66}$$

The gauge function S_1 is solved here by assuming $|dS_1/dt| \simeq |\Omega \partial S_1/\partial\theta| \gg |\partial S_1/\partial t + v_\parallel \cdot \partial S_1/\partial \mathbf{X}|$. This condition for the approximation can be relaxed by solving the determining equation of S_1, Eq. (2.60), in the following perturbative manner. The zeroth gauge

function is defined as a solution of the equation, $\Omega\partial_\Theta S_1^{(0)} = q\tilde{\psi}_1$;

$$S_1^{(0)} = \frac{q}{2\pi\Omega}\int_\Theta^{\Theta+2\pi}(\Theta'-\Theta-\pi)\psi_1 d\Theta'. \tag{2.67}$$

This solution is same as Eq. (2.64). The first order is determined by the equation, $\Omega\partial_\Theta S_1^{(1)} = q\tilde{\psi}_1 - (\partial_t + v_\parallel\hat{\mathbf{b}}\cdot\nabla)S_0^{(0)}$;

$$\begin{aligned}
S_1^{(1)} &= -\frac{1}{2\pi\Omega}\int_\Theta^{\Theta+2\pi}(\Theta'-\Theta-\pi)\left(\frac{\partial S_1^{(0)}}{\partial t} + v_\parallel\hat{\mathbf{b}}\cdot\frac{\partial S_1^{(0)}}{\partial \mathbf{X}}\right)d\Theta', \\
&= -\frac{q}{4\pi^2\Omega^2}\int_\Theta^{\Theta+2\pi}(\Theta'-\Theta-\pi)\int_{\Theta'}^{\Theta'+2\pi}(\Theta''-\Theta'-\pi)\left(\frac{\partial\psi_1}{\partial t} + v_\parallel\hat{\mathbf{b}}\cdot\frac{\partial\psi_1}{\partial\mathbf{X}}\right)d\Theta''d\Theta', \\
&= \frac{q}{4\pi\Omega^2}\int_\Theta^{\Theta+2\pi}(\Theta'-\Theta-\pi)^2\left(\frac{\partial\tilde{\psi}_1}{\partial t} + v_\parallel\hat{\mathbf{b}}\cdot\frac{\partial\tilde{\psi}_1}{\partial\mathbf{X}}\right)d\Theta'.
\end{aligned} \tag{2.68}$$

The second order is obtained similaly as

$$S_1^{(2)} = \frac{q}{12\pi\Omega^3}\int_\Theta^{\Theta+2\pi}(\Theta'-\Theta-2\pi)(\Theta'-\Theta-\pi)(\Theta'-\Theta)\left(\frac{\partial}{\partial t} + v_\parallel\hat{\mathbf{b}}\cdot\frac{\partial}{\partial\mathbf{X}}\right)^2\tilde{\psi}_1 d\Theta'. \tag{2.69}$$

This expansion was introduced by Brizard [18] and applied to a calculation of the compressional Alfvén wave by Qin [19,20]. The resulting gauge function $S_1 = S_1^{(0)} + S_1^{(1)} + S_1^{(2)}$ is given by

$$\begin{aligned}
S_1 = \frac{q}{2\pi\Omega}\int_\Theta^{\Theta+2\pi}(\Theta'-\Theta-\pi)\Bigg[1 &+ \frac{\Theta'-\Theta-\pi}{2\Omega}\left(\frac{\partial}{\partial t} + v_\parallel\hat{\mathbf{b}}\cdot\frac{\partial}{\partial\mathbf{X}}\right) \\
&+ \frac{(\Theta'-\Theta-2\pi)(\Theta'-\Theta)}{6\Omega^2}\left(\frac{\partial}{\partial t} + v_\parallel\hat{\mathbf{b}}\cdot\frac{\partial}{\partial\mathbf{X}}\right)^2\Bigg]\tilde{\psi}_1\, d\Theta'.
\end{aligned} \tag{2.70}$$

In summary, the gyrocenter 1-form up to the first order is given by

$$\bar{\Gamma}_0 + \bar{\Gamma}_1 = \left(q\mathbf{A}_0 + m\bar{v}_\parallel\hat{\mathbf{b}}\right)\cdot d\bar{\mathbf{X}} + \frac{m}{q}\bar{\mu}\, d\bar{\Theta} - \left[\frac{m}{2}\bar{v}_\parallel^2 + B_0\bar{\mu} + q\phi_0 + q\langle\psi_1\rangle\right]dt. \tag{2.71}$$

The gauge function and the Lie generator are given by

$$S_1 = \frac{q}{2\pi\Omega}\int_\Theta^{\Theta+2\pi}(\Theta'-\Theta-\pi)\psi_1(\Theta')d\Theta', \tag{2.72}$$

$$g_1^{\bar{\mathbf{X}}} = -\frac{1}{qB_\parallel^*}\hat{\mathbf{b}}\times\left(q\mathbf{A}_1 + \frac{\partial S_1}{\partial\mathbf{X}}\right) - \frac{\mathbf{B}^*}{mB_\parallel^*}\frac{\partial S_1}{\partial v_\parallel}, \tag{2.73}$$

$$g_1^{\bar{\Theta}} = -\frac{q}{m}\left(\frac{1}{v_\perp}\hat{\mathbf{a}}\cdot\mathbf{A}_1 + \frac{\partial S_1}{\partial\mu}\right), \tag{2.74}$$

$$g_1^{\bar{\mu}} = \frac{q}{m}\left(q\rho\hat{\mathbf{c}}\cdot\mathbf{A}_1 + \frac{\partial S_1}{\partial\Theta}\right), \tag{2.75}$$

$$g_1^{\bar{v}_\parallel} = \frac{\mathbf{B}^*}{mB_\parallel^*}\cdot\left(q\mathbf{A}_1 + \frac{\partial S_1}{\partial\mathbf{X}}\right). \tag{2.76}$$

The Lie generator is sometimes further approximated as

$$g_1 \simeq -\frac{1}{B_0}\hat{\mathbf{b}}\times\mathbf{A}_1\cdot\frac{\partial}{\partial\mathbf{X}} - \frac{q}{mv_\perp}\hat{\mathbf{a}}\cdot\mathbf{A}_1\frac{\partial}{\partial\Theta} + \frac{q}{m}\hat{\mathbf{b}}\cdot\mathbf{A}_1\frac{\partial}{\partial v_\parallel} + \frac{q^2}{m\Omega}\left(\tilde{\phi}_1 - v_\parallel\hat{\mathbf{b}}\cdot\tilde{\mathbf{A}}_1 + v_\perp\langle\hat{\mathbf{c}}\cdot\mathbf{A}_1\rangle\right)\frac{\partial}{\partial\mu}. \tag{2.77}$$

2.3.3 Second order analysis

The second order 1-form is given by

$$\begin{aligned}\bar{\Gamma}_2 &= i_{\mathcal{V}_0}\left\langle\Gamma_2 - i_{g_1}d\Gamma_1 + \frac{1}{2}\left(i_{g_1}d\right)^2\Gamma_0\right\rangle dt \\ &= i_{\mathcal{V}_0}\left\langle\Gamma_2 - i_{g_1}d\bar{\Gamma}_1 - \frac{1}{2}\left(i_{g_1}d\right)^2\Gamma_0\right\rangle dt,\end{aligned} \tag{2.78}$$

where the relation, $\bar{\Gamma}_1 = \Gamma_1 - i_{g_1}d\Gamma_0 + dS_1$, is use. Here the first term is calculated as

$$i_{\mathcal{V}_0}\langle\Gamma_2\rangle \simeq \frac{m\bar{v}_\parallel\bar{\mu}}{q}\left\langle\hat{\mathbf{a}}\cdot\nabla\hat{\mathbf{b}}\cdot\hat{\mathbf{c}}\right\rangle = -\frac{m\bar{v}_\parallel\bar{\mu}}{2q}\hat{\mathbf{b}}\cdot\nabla\times\hat{\mathbf{b}}, \tag{2.79}$$

where we make the approximation, $\mathcal{V}_0^{\bar{\mathbf{X}}} \simeq \bar{v}_\parallel\hat{\mathbf{b}}$. The second term is calculated as

$$-i_{\mathcal{V}_0}\left\langle i_{g_1}d\bar{\Gamma}_1\right\rangle \simeq -\frac{q^2}{m}\left\langle\hat{\mathbf{b}}\cdot\mathbf{A}_1\right\rangle^2 - \frac{q^3\bar{v}_\perp}{m\Omega}\langle\hat{\mathbf{c}}\cdot\mathbf{A}_1\rangle\frac{\partial\langle\psi_1\rangle}{\partial\bar{\mu}} - \frac{q}{B_\parallel^*}\hat{\mathbf{b}}\times\langle\mathbf{A}_1\rangle\cdot\nabla\langle\psi_1\rangle. \tag{2.80}$$

The third term is expanded as

$$\begin{aligned}-\frac{1}{2}i_{\mathcal{V}_0}\left\langle\left(i_{g_1}d\right)^2\Gamma_0\right\rangle &\simeq -\frac{1}{2}\left(i_{\partial_t} + \Omega i_{\partial_{\bar{\Theta}}}\right) \\ &\quad\times\left\langle i_{g_1}d\left(\frac{m}{q}g_1^{\bar{\mu}}d\bar{\Theta} - \frac{m}{q}g_1^{\bar{\Theta}}d\bar{\mu} - B_0g_1^{\bar{\mu}}dt - m\bar{v}_\parallel g_1^{\bar{v}_\parallel}dt\right)\right\rangle.\end{aligned} \tag{2.81}$$

It is approximated further as

$$\begin{aligned}-\frac{1}{2}i_{\mathcal{V}_0}\left\langle\left(i_{g_1}d\right)^2\Gamma_0\right\rangle &\simeq \frac{B_0}{2}\left\langle g_1^{\bar{\Theta}}\frac{\partial g_1^{\bar{\mu}}}{\partial\Theta} - g_1^{\bar{\mu}}\frac{\partial g_1^{\bar{\Theta}}}{\partial\Theta}\right\rangle + \frac{m}{2}\left\langle g_1^{\bar{v}_\parallel 2}\right\rangle + \frac{m\bar{v}_\parallel}{2}\left\langle g_1^{\bar{\theta}}\frac{\partial g_1^{\bar{v}_\parallel}}{\partial\theta}\right\rangle \\ &\simeq -B_0\left\langle g_1^{\bar{\mu}}\frac{\partial g_1^{\bar{\Theta}}}{\partial\bar{\Theta}}\right\rangle + \frac{q^2}{2m}\left\langle A_{1\parallel}^2\right\rangle - \frac{q\bar{v}_\parallel}{2B_0}\langle\hat{\mathbf{a}}\cdot\mathbf{A}_1\hat{\mathbf{c}}\cdot\nabla A_{1\parallel}\rangle.\end{aligned} \tag{2.82}$$

Therefore, the second order 1-form is obtained as

$$\begin{aligned}\bar{\Gamma}_{20} = &-\frac{m\bar{v}_\parallel\bar{\mu}}{2q}\hat{\mathbf{b}}\cdot\nabla\times\hat{\mathbf{b}} - \frac{q^2}{2m}\left\langle A_{1\parallel}^2\right\rangle - \frac{q^3\bar{v}_\perp}{m\Omega}\langle\hat{\mathbf{c}}\cdot\mathbf{A}_1\rangle\frac{\partial\langle\psi_1\rangle}{\partial\bar{\mu}} - \frac{q}{B_\parallel^*}\left(\hat{\mathbf{b}}\times\langle\mathbf{A}_1\rangle\right)\cdot\nabla\langle\psi_1\rangle \\ &- B_0\left\langle g_1^{\bar{\mu}}\frac{\partial g_1^{\bar{\Theta}}}{\partial\bar{\Theta}}\right\rangle - \frac{q\bar{v}_\parallel}{2B_0}\langle\hat{\mathbf{a}}\cdot\mathbf{A}_1\hat{\mathbf{c}}\cdot\nabla A_{1\parallel}\rangle.\end{aligned} \tag{2.83}$$

If the compressional component of the magnetic perturbation is negligible, i.e. $\mathbf{A}_{1\perp} \simeq 0$, the 1-form is further reduced to

$$\bar{\Gamma}_{20} = -\frac{m\bar{v}_{\parallel}\bar{\mu}}{2q}\hat{\mathbf{b}}\cdot\nabla\times\hat{\mathbf{b}} - \frac{q^2}{2m}\langle A_{1\parallel}\rangle^2 + \frac{q^3}{2m\Omega}\frac{\partial}{\partial\bar{\mu}}\left\langle\left(\tilde{\phi} - \bar{v}_{\parallel}\tilde{A}_{1\parallel}\right)^2\right\rangle. \tag{2.84}$$

The first term in the right hand side implies the recovery of the Baños drift.

2.3.4 Gyrokinetic equations

In the preceding sections we have obtained the fundamental 1-form for the gyrocenter coordinate system. The gyrokinetic equations of motion are easily obtained from the Hamiltonian $H \equiv -\bar{\Gamma}_{00} - \bar{\Gamma}_{10} - \bar{\Gamma}_{20}$ and the Poisson tensors, Eq. (2.27), as

$$\frac{d\bar{\mathbf{X}}}{dt} = \frac{1}{qB_{\parallel}^*}\hat{\mathbf{b}}\times\frac{\partial H}{\partial\bar{\mathbf{X}}} + \frac{\mathbf{B}^*}{mB_{\parallel}^*}\frac{\partial H}{\partial\bar{v}_{\parallel}}, \tag{2.85}$$

$$\frac{d\bar{\Theta}}{dt} = \frac{q}{m}\frac{\partial H}{\partial\bar{\mu}}, \tag{2.86}$$

$$\frac{d\bar{\mu}}{dt} = -\frac{q}{m}\frac{\partial H}{\partial\bar{\theta}} = 0, \tag{2.87}$$

$$\frac{d\bar{v}_{\parallel}}{dt} = -\frac{\mathbf{B}^*}{mB_{\parallel}^*}\frac{\partial H}{\partial\bar{\mathbf{X}}}. \tag{2.88}$$

The linearized gyrokinetic equations of motion are given by

$$\frac{d\bar{\mathbf{X}}}{dt} = \frac{1}{B_{\parallel}^*}\left[\mathbf{B}^*\bar{v}_{\parallel} + \hat{\mathbf{b}}\times\nabla\left(\phi_0 + \langle\psi_1\rangle + \frac{\bar{\mu}}{q}B_0\right)\right], \tag{2.89}$$

$$\frac{d\bar{\Theta}}{dt} = \Omega + \frac{q^2}{m}\frac{\partial\langle\psi_1\rangle}{\partial\bar{\mu}}, \tag{2.90}$$

$$\frac{d\bar{\mu}}{dt} = 0, \tag{2.91}$$

$$\frac{d\bar{v}_{\parallel}}{dt} = -\frac{q\mathbf{B}^*}{mB_{\parallel}^*}\cdot\nabla\left(\phi_0 + \langle\psi_1\rangle + \frac{\bar{\mu}}{q}B_0\right). \tag{2.92}$$

Using the gyrocenter distribution function $\bar{F}(\bar{\mathbf{X}}, \bar{\Theta}, \bar{\mu}, \bar{v}_{\parallel})$, the general gyrokinetic Vlasov equation is written as

$$\frac{d\bar{F}}{dt} + \frac{d\bar{\mathbf{X}}}{dt}\cdot\frac{\partial\bar{F}}{\partial\bar{\mathbf{X}}} + \frac{d\bar{\Theta}}{dt}\frac{\partial\bar{F}}{\partial\bar{\Theta}} + \frac{d\bar{v}_{\parallel}}{dt}\frac{\partial\bar{F}}{\partial\bar{v}_{\parallel}} = 0. \tag{2.93}$$

The distribution function used here is a six dimensional function of the gyrocenter coordinate variables. In order to reduce the numerical calculation cost, the distribution function is separated into the gyroaveraged component and the remaining gyrophase dependent

component; $\bar{F} = \left\langle \bar{F} \right\rangle + \tilde{\bar{F}}$. Since the equations of motion are independent of the gyrophase, the Vlasov equation is decoupled in the following two equations;

$$\left(\frac{d}{dt} + \frac{d\bar{\mathbf{X}}}{dt} \cdot \frac{\partial}{\partial \bar{\mathbf{X}}} + \frac{d\bar{v}_\parallel}{dt} \frac{\partial}{\partial \bar{v}_\parallel} \right) \left\langle \bar{F} \right\rangle = 0,$$
$$\left(\frac{d}{dt} + \frac{d\bar{\mathbf{X}}}{dt} \cdot \frac{\partial}{\partial \bar{\mathbf{X}}} + \frac{d\bar{\Theta}}{dt} \frac{\partial}{\partial \bar{\Theta}} + \frac{d\bar{v}_\parallel}{dt} \frac{\partial}{\partial \bar{v}_\parallel} \right) \tilde{\bar{F}} = 0.$$

In the collisionless limit, one can ignore the latter equation by setting $\tilde{\bar{F}} \equiv 0$ at the beginning of calculations, i.e. $\bar{F} = \left\langle \bar{F} \right\rangle$, because of the conservation property $d\tilde{\bar{F}}/dt = 0$. Therefore, the reduced equation describing the evolution of the five dimensional distribution function $\bar{F}(t, \bar{\mathbf{X}}, \bar{\mu}, \bar{v}_\parallel)$,

$$\frac{d\bar{F}}{dt} + \frac{d\bar{\mathbf{X}}}{dt} \cdot \frac{\partial \bar{F}}{\partial \bar{\mathbf{X}}} + \frac{d\bar{v}_\parallel}{dt} \frac{\partial \bar{F}}{\partial \bar{v}_\parallel} = 0, \tag{2.94}$$

is usually called the gyrokinetic Vlasov equation.

2.3.5 Pullback

A closed set of equations describing a plasma consists of the equations of motion, or Vlasov equation, and the Maxwell's equations. Since the Vlasov equation has been obtained, the remaining task we have to do is to write the Maxwell's equations in terms of the gyrocenter distribution function $\bar{F}$. In other words, the charge and current densities have to be derived from the gyrocenter distribution function. This can be curried out with the aid of the pullback technique introduced by Brizard [18] and Qin [20].

If the particle, guiding-center and gyrocenter variables, z, Z, $\bar{Z}$ represent the same position in the phase space, a distribution function can be expressed by each coordinate variable without any loss of accuracy;

$$f(z) \equiv F(Z) \equiv \bar{F}(\bar{Z}), \tag{2.95}$$

because the distribution function is a scalar field in the phase space. Using the Lie transformation introduced in Sec. 2.3.1, the guiding-center distribution can be expressed in terms of the gyrocenter one;

$$\begin{aligned} F(Z) = \bar{F}(\bar{Z}) &= \bar{F}\left(\exp\left(\mathcal{L}_g\right) Z\right) = \left[\exp\left(\mathcal{L}_g\right) \bar{F}\right](Z) \\ &= \bar{F}(\mathbf{X}, \Theta, \mu, v_\parallel) + g_1^i \frac{\partial \bar{F}}{\partial \bar{Z}^i} + \cdots . \end{aligned} \tag{2.96}$$

An observable macroscopic quantity $\bar{\lambda}(\mathbf{x})$ are calculated from the microscopic quantity $\lambda(\mathbf{x}, \mathbf{v})$ through the integral over the phase space;

$$\bar{\lambda}(\mathbf{x}) = \int \lambda(\mathbf{x}', \mathbf{v}') f(\mathbf{x}', \mathbf{v}') \delta(\mathbf{x}' - \mathbf{x}) \, d^3x' d^3v'. \tag{2.97}$$

This integral can be rewritten as the integral in the guiding-center coordinate.

$$\bar{\lambda}(\mathbf{x}) = \int \Lambda\left(\mathbf{X}, \Theta, \mu, V_{\parallel}\right) F\left(\mathbf{X}, \Theta, \mu, V_{\parallel}\right) \delta\left(\mathbf{X} + \rho\hat{\mathbf{a}} - \mathbf{x}\right) \frac{B_{\parallel}^{*}}{m} d^{3}X d\Theta d\mu dv_{\parallel}. \tag{2.98}$$

Using the pullback expression of the distribution function, Eq. (2.96), the macroscopic quantity $\bar{\lambda}$ is expressed in terms of the gyrocenter distribution function We, therefore, obtain the charge and current densities up to the first order as

$$\varrho(\mathbf{x}, t) = \int q\left(\bar{F} + g_{1}^{i} \frac{\partial \bar{F}}{\partial \bar{Z}^{i}}\right) \delta\left(\mathbf{X} + \frac{v_{\perp}}{\Omega}\hat{\mathbf{a}} - \mathbf{x}\right) \frac{B_{\parallel}^{*}}{m} d^{3}X d\Theta d\mu dv_{\parallel}, \tag{2.99}$$

$$\mathbf{j}(\mathbf{x}, t) = \int q\left(v_{\parallel}\hat{\mathbf{b}} + v_{\perp}\hat{\mathbf{c}}\right)\left(\bar{F} + g_{1}^{i} \frac{\partial \bar{F}}{\partial \bar{Z}^{i}}\right) \delta\left(\mathbf{X} + \frac{v_{\perp}}{\Omega}\hat{\mathbf{a}} - \mathbf{x}\right) \frac{B_{\parallel}^{*}}{m} d^{3}X d\Theta d\mu dv_{\parallel}. \tag{2.100}$$

We present four useful expressions employed in the gyrokinetic analysis of the micro-instabilities. The general form of the charge density under the assumption of the electrostatic plasma is given by

$$\varrho(\mathbf{x}, t) = \int q\left(\bar{F} + \frac{q\tilde{\phi}_{1}}{B_{0}} \frac{\partial \bar{F}}{\partial \bar{\mu}}\right) \delta\left(\mathbf{X} + \frac{v_{\perp}}{\Omega}\hat{\mathbf{a}} - \mathbf{x}\right) \frac{B_{\parallel}^{*}}{m} d^{3}X d\Theta d\mu dv_{\parallel}. \tag{2.101}$$

This expression uses some approximations described above, but can be used for general purposes such as analytical modelings and numerical simulations of micro-instabilities. If additional assumptions can be applied to the plasma, more simple expressions are available.

The simplest expression is obtained by the long-wavelength approximation, $v_{\perp}/\Omega \ll |\nabla \ln \phi_{1}|^{-1}$;

$$\begin{aligned}
\varrho(\mathbf{x}) \simeq & \int q\left\langle \bar{F} + \rho\hat{\mathbf{a}} \cdot \nabla \bar{F} + \frac{\rho^{2}}{2}\hat{\mathbf{a}}\hat{\mathbf{a}} : \nabla\nabla \bar{F} \right. \\
& \left. + \frac{q}{B_{0}}\rho\hat{\mathbf{a}} \cdot \nabla\left(\phi_{1} - \rho\hat{\mathbf{a}} \cdot \nabla\phi_{1}\right)\left(\frac{\partial \bar{F}}{\partial \mu} - \rho\hat{\mathbf{a}} \cdot \nabla \frac{\partial \bar{F}}{\partial \mu}\right)\right\rangle \frac{B_{\parallel}^{*}}{m} 2\pi d\mu, dv_{\parallel} \\
= & \int q\left\langle \bar{F} + \frac{\rho^{2}}{2}\hat{\mathbf{a}}\hat{\mathbf{a}} : \nabla\nabla \bar{F} - \frac{q\rho^{2}}{B_{0}}\hat{\mathbf{a}} \cdot \nabla\left(\frac{\partial \bar{F}}{\partial \mu}\hat{\mathbf{a}} \cdot \nabla\phi_{1}\right)\right\rangle \frac{B_{\parallel}^{*}}{m} 2\pi d\mu, dv_{\parallel} \\
= & qN + \frac{q}{2m\Omega^{2}}\nabla_{\perp}^{2} P + \frac{q^{2}}{m\Omega^{2}}\nabla_{\perp}(N\nabla_{\perp}\phi_{1}),
\end{aligned} \tag{2.102}$$

where the gyrocenter density N and pressure P are introduced as follows;

$$N(\bar{\mathbf{X}}) \equiv \int \bar{F}(t, \mathbf{x}, \bar{\mu}, \bar{v}_{\parallel}) \frac{B_{\parallel}^{*}}{m} 2\pi d\bar{\mu}, d\bar{v}_{\parallel}, \tag{2.103}$$

$$P(\bar{\mathbf{X}}) \equiv \int B_{0}\bar{\mu}\bar{F}(t, \mathbf{x}, \bar{\mu}, \bar{v}_{\parallel}) \frac{B_{\parallel}^{*}}{m} 2\pi d\bar{\mu}, d\bar{v}_{\parallel}. \tag{2.104}$$

The physical meaning of each term in Eq. (2.102) is understood as follows. The first term N represents the density of the gyrocenter, the second term represents the finite

Larmor radius (FLR) effect and the third term represents the polarization density. It can be interpreted as the induced charge density, $-\nabla_\perp \cdot \left[qN\Delta_\mathrm{p}\right]$, which caused by the polarization shift, $\Delta_\mathrm{p} = qE_1/m\Omega^2$, due to the perpendicular perturbation electric field, $E_1 = -\nabla_\perp \phi_1$. In other words, the time variation of the polarization density, $d\varrho_\mathrm{p}/dt = -\nabla \cdot \mathbf{j}_\mathrm{p}$, is caused by the current due to the polarization drift, $\mathbf{j}_\mathrm{pol} = qN(q/m\Omega^2)dE_1/dt$. As is shown in these observations, the polarization drift does not appear in the equations of motion, but in the density as an induced charge by the electric field. This apparently contradicted result is caused by the definition of the guiding-center coordinate. We constructed the guiding-center from only the magnetic field and the velocity and did not use the electric field. Consequently, the position of the guiding-center does not shift or drift if only the electric field changes. Since the gyrocenter transformation is an optimization to the guiding-center coordinate to decouple the gyrophase dependences, the gyrocenter position also does not have the polarization drift. The polarization effect dropped from the equations of motion appears as the polarization density through the coordinate transformation,

$$\mathbf{x} = \mathbf{X} + \rho\hat{\mathbf{a}} = \bar{\mathbf{X}} + \rho\hat{\mathbf{a}} - \frac{q}{m\Omega^2}\nabla_\perp \phi_1. \tag{2.105}$$

Another useful expression is obtained for the uniform plasma. When the distribution function is given by the sum of an uniform equilibrium Maxwellian and a perturbation,

$$\bar{F} = \bar{F}_0 + \delta\bar{F}\left(t, \bar{\mathbf{X}}, \bar{\mu}, \bar{v}_\parallel\right), \quad \bar{F}_0 = n_0 \frac{m}{2\pi T}\exp\left(-\frac{mv_\perp^2}{2T}\right), \tag{2.106}$$

the perturbation charge density is calculated up to the first order of the perturbation as

$$\varrho(\mathbf{x}) = qn_0 + \int q\left\langle \delta\bar{F}(\mathbf{x} - \rho\hat{\mathbf{a}}) - \frac{q}{T}\bar{F}_0\left[\phi(\mathbf{x}) - \langle\phi\rangle(\mathbf{x} - \rho\hat{\mathbf{a}})\right]\right\rangle \frac{B_\parallel^*}{m} 2\pi d\bar{\mu}, d\bar{v}_\parallel. \tag{2.107}$$

It is usually represented in the Fourier space;

$$\varrho(\mathbf{k}) = qn_0 + \int q\mathrm{J}_0(k_\perp\rho)\delta\bar{F}(\mathbf{k}, \mu, v_\parallel)\frac{B_\parallel^*}{m} 2\pi\, d\mu dv_\parallel - \frac{q^2 n_0}{T}\left[1 - \Gamma_0(k_\perp^2\rho_\mathrm{t}^2)\right]\phi_1(\mathbf{k}), \tag{2.108}$$

where the thermal gyroradius ρ_t and the function Γ_0 are introduced as $\rho_\mathrm{t} \equiv \sqrt{T/m}/\Omega$ and $\Gamma_0(z) \equiv \mathrm{I}_0(z)\exp(-z)$, respectively. We denote the Bessel and modified Bessel functions by J_0 and I_0. The Padé approximation of the function Γ_0, $\Gamma_0(z) \simeq 1/(1+z)$ or $1 - \Gamma_0(z) \simeq z/(1+(3/4)z)$, is sometimes employed in numerical calculations. According to Dubin [14] and Hahm [15], a more general expression for a nonuniform plasma is given by

$$\begin{aligned}\varrho(\mathbf{k}) = qn_0 + \int q\mathrm{J}_0(k_\perp\rho)\delta\bar{F}(\mathbf{k}, \mu, v_\parallel)\frac{B_\parallel^*}{m} 2\pi\, d\mu dv_\parallel - \frac{q^2 n_0}{T}\left[1 - \Gamma_0(k_\perp^2\rho_\mathrm{t}^2)\right]\phi_1(\mathbf{k}) \\ - \frac{q^2 n_0}{T}\left[\Gamma_1(k_\perp^2\rho_\mathrm{t}^2) - \Gamma_0(k_\perp^2\rho_\mathrm{t}^2)\right] i\mathbf{k}_\perp \cdot \ln\nabla n_0\rho_\mathrm{t}^2\phi_1(\mathbf{k}).\end{aligned} \tag{2.109}$$

2.4 Conclusions

The general derivation of the modern gyrokinetic equations was presented. The modern gyrokinetic theory has started from the early works by Littlejohn, which presents the advantages of the Lie perturbation analysis in the rigorous and mathematically clear treatment of the particle dynamics in an externally applied magnetic field. Brizard and Qin applied the Lie transformation technique for the perturbation electromagnetic field and obtained the closed set of the gyrokinetic equations in the context of plasma physics. Although their goal was same, their calculation processes were slightly different in the introduction of the guiding-center coordinate. We chose the most straightforward way in this work.

First in Sec. 2.2.1, the guiding-center position was used to evaluate the equilibrium magnetic field in the definition of the guiding-center coordinate instead of the particle position. This treatment is same as Qin's formulation and makes the preliminary calculation for the Lie perturbation analysis much simple. Second in Sec. 2.2.2, the gyrogauge transformation was utilized to exclude the arbitrariness in the definition of the gyrophase in the same way as Littlejohn did. Although this process is not essential in the formulation, the suppression of the physically unnecessary terms related to the arbitrariness is desirable for the general derivation in the case of nonuniform magnetic fields. Third in Sec. 2.2.4, we carried out only the gauge transformation in the preliminary stage as Qin did. The simple guiding-center coordinate adopted in this work does not provide the true adiabatic constant, i.e. the magnetic moment. Although Brizard employed the Lie perturbation analysis twice to obtain the guiding-center and gyrocenter coordinates, the first one can be omitted because it is sufficient to carried out the Lie transformation once at the last of the derivation to obtain the true adiabatic quantity.

In Sec. 2.3, the general expressions of the gyrokinetic equations up to the second order were obtained. The perturbation potentials are assumed to satisfy the gyrokinetic ordering in Sec. 2.2.3. The gauge function used to determine the Lie generator and the gyrocenter coordinate is approximated under the gyrokinetic ordering in Sec. 2.3.2. In addition to a commonly used expression of the gauge function, we obtained a more rigorous one, which relaxes the restriction on the time scale, $\omega/\Omega \ll 1$, and enables one to treat more short time-scale dynamics such as the compressional Alfv́en wave [19, 20]. If much more high frequency one such as the ion cyclotron wave has to be taken into account, fundamental improvements should be made. An attempt for the implementation in a numerical simulation is found in Ref. [23].

The general expression of the charge and current densities were obtained in Sec. 2.3.5 through the pullback transformations of the distribution function. We confirmed that the

conventional expressions of the charge density were recovered under the corresponding assumptions. Although a closed set of the gyrokinetic equations was presented, the conservation of the plasma energy was not provided here. Additional discussion using the field theory [25] may required to obtain the conservation law. Recently, a modern representation of the field theory is studied by Brizard [26, 27] and Qin [28, 29]. The self-consistency of the gyrokinetic theory will be an important topic of further studies.

Chapter 3

Refinement of the gyrokinetic equations with large flow shears

3.1 Introduction

Understanding the role of flow shears in the turbulent transport is one of the major issues in tokamak plasmas. The stabilizing effect [30–34] of the $\mathbf{E}\times\mathbf{B}$ flow shears on the toroidal ion-temperature-gradient (ITG) mode and various drift waves is believed to be one of the essential elements in the core and edge transport barriers. The existence of large flow shears associated with the short scale-length is a characteristic feature of the edge plasmas. In addition to the relatively short time-scale dynamics such as the micro-instabilities, the pedestal plasmas involves the longer time-scale equilibrium dynamics such as the edge localized modes (ELMs) and the L-H transition. In order to treat the multi-scale physics like the micro-instabilities and the equilibrium dynamics, a global full-f simulation is required for the understanding of the pedestal physics. Recently the development of such simulation codes [35, 36] has started. They employ the gyrokinetic equations [18, 19, 37] as the fundamental equations to describe the low frequency behavior of plasmas. The most distinct advantage of the gyrokinetic theory is in the separation of the time scale between the fast gyrating motion of particles and the relatively slow drift motions. Discarding the gyrating motion and the gyrophase dependence of the velocity distribution functions, one can choose much larger time-step than the gyroperiod in a simulation. It is also a benefit that the gyroaveraged expressions of the potentials and other physical quantities can reduce the numerical noise caused by the discreteness of the particles and the spatial grids.

The modern derivation of gyrokinetic equations has been developed with the aid of mathematics and the analytic mechanics such as 1-form representations of the particle dynamics, the Lie perturbation analysis and pullback representations. The commonly used

procedures in the derivation are understood as two steps of coordinate transformations and the formulation of the Maxwell's equations on the new coordinate. The first transformation introduces the guiding-center position, the gyrophase and the magnetic moment. The second one decompose the gyrophase dependences in the 1-form through successive Lie transformations. The gyrophase dependences in the original equations of motion are removed and thus the gyration and the drift motion are decoupled. The Vlasov equation and the Maxwell's equations expressed by pullbacks in the new coordinate enable one to treat the low frequency phenomena without resolving the fast gyrations of particles.

The improvement of the gyrokinetics for the strong $\mathbf{E} \times \mathbf{B}$ drift flow was provided by Littlejohn [17] for the first time and extended for the plasma with potential perturbations by Brizard [38], Hahm [39] and Qin [40]. Applications to the global linear analysis of ITG modes have been also made [31, 32]. We note that the gyrokinetic equations based on the conventional recursive method [2, 3, 11–13] also has been formulated for large flow shears by Sugama and Horton [41]. Although the formulation by Littlejohn slightly differs from others because of the difference in the expression of mechanics, their basic concepts are same. They introduced a reference frame moving with the $\mathbf{E} \times \mathbf{B}$ drift velocity in the guiding-center coordinate and decomposed the drift motion and the gyration not in the first order equations of motion but in the zeroth order equations. The physical meaning of this treatment is easily understood in an ideal case as follows. If the reference frame is moving with a constant velocity $\mathbf{D}$ and the electromagnetic fields are uniform, the Galilei transformation with $\mathbf{D}$ yields an uniform induced electromotive force, $q\mathbf{v} \times \mathbf{B}$. If the velocity $\mathbf{D}$ is given by the $\mathbf{E} \times \mathbf{B}$ drift velocity, $\mathbf{E} \times \mathbf{B}/B^2$, the perpendicular components of the electric field is canceled, and the particle simply gyrates as if the electric field is not applied from the beginning. In this case, the drift motion is successfully decomposed from the particle motion and included in the zeroth order equations of motion.

In the case of a general electric field, however, the velocity $\mathbf{D} = \mathbf{E} \times \mathbf{B}/B^2$ acquires the gyrophase dependence through the coupling of the gyration and spatial variation of the potential through $\mathbf{E} = -\nabla\phi(\mathbf{x})$. This dependence makes the derivation of the gyrokinetic equations complicated [17]. On the other hand, if the velocity $\mathbf{D}$ is defined as the $\mathbf{E} \times \mathbf{B}$ drift velocity measured at the guiding-center position as is common in the previous works [38–40], it differs from the averaged drift velocity of the gyrating particle in case of the nonuniform electric fields. In order to obtain the most appropriate zeroth order equation of motion, refinement of the velocity of the reference frame is necessary.

In the present study, using the conservation property of the magnetic moment as the criterion of the accuracy of the zeroth order equation of motion, we examine several kinds of drift velocities including the previous expression and obtain the practically most accurate expression of the velocity $\mathbf{D}$. The advantages of our gyrokinetic equations of

motion are verified through comparisons between the numerical solutions of the previous gyrokinetic equations and ours.

In Sec. 3.2, the guiding-center coordinate variables are introduced in the 1-form for a single particle. An equilibrium drift velocity **D** is also introduced in the transformation of the velocity coordinates so that the particle motion becomes a nearly simple gyration in the reference frame. In Sec. 3.3, the criterion to choose the appropriate velocity **D** is discussed. After examining several possible choices for **D**, a most practical expression is determined. The rest of the standard procedures, Lie perturbation analysis and the formulation of field equations, are curried out and the gyrokinetic equations are obtained in Sec. 3.5. The accuracy of the resultant equations are compared with those of Qin's formulation [40] in Sec. 3.6. Finally, conclusions are presented in Sec. 3.7.

3.2 Preliminary transformation

The first step in the derivation of gyrokinetic equations is a guiding-center transformation introducing a guiding-center position **X**, a gyrophase Θ, a perpendicular velocity $V_\perp$ and a parallel velocity $V_\parallel$. In the conventional derivations [18, 19, 37], the velocity is simply separated into the perpendicular and parallel components, i.e. $v_\perp \equiv \left|\hat{\mathbf{b}} \times \left(\mathbf{v} \times \hat{\mathbf{b}}\right)\right|$ and $v_\parallel \equiv \mathbf{v} \cdot \hat{\mathbf{b}}$, where the unit vector $\hat{\mathbf{b}}$ represents the magnetic field direction. In the gyrokinetic theory for large $\mathbf{E} \times \mathbf{B}$ drift flow shears [17, 38–40], however, the velocity space is defined on a reference frame moving with a equilibrium flow velocity **D**. The vector field of the flow plays an essential role in the improvement of the theory and is discussed in Sec. 3.3. In order to distinguish the modified velocity space variables from those on the stationary frame, $v_\perp$ and $v_\parallel$, we denote the new velocity components in the moving frame as capital letters, $V_\perp$ and $V_\parallel$. We note that if the velocity **D** is zero everywhere, the modified gyrokinetic theory coincides that of usual ordering, i.e. the equilibrium flow is much slower than the thermal velocity. In this case the guiding-center velocity variables also coincide, or $V_\perp = v_\perp$ and $V_\parallel = v_\parallel$.

We assume that the equilibrium flow is a function of the guiding-center position **X** to avoid undesirable complexities due to the dependences on the velocity space such as $\partial \mathbf{D}/\partial V_\parallel$. The guiding-center transformation is defined as inverse coordinate transformations;

$$\mathbf{x} \equiv \mathbf{X} + \frac{mV_\perp}{qB(\mathbf{X})}\hat{\mathbf{a}}'(\mathbf{X}, \Theta'), \tag{3.1}$$

$$\mathbf{v} \equiv \mathbf{D}(\mathbf{X}) + V_\perp \hat{\mathbf{c}}'(\mathbf{X}, \Theta') + V_\parallel \hat{\mathbf{b}}(\mathbf{X}), \tag{3.2}$$

where the gyrophase Θ', the orthonormal vectors $\hat{\mathbf{b}} \equiv \mathbf{B}/B$, $\hat{\mathbf{c}}' \equiv \hat{\mathbf{e}}_1 \cos\Theta' - \hat{\mathbf{e}}_2 \sin\Theta'$ and $\hat{\mathbf{a}}' \equiv \hat{\mathbf{e}}_1 \sin\Theta' + \hat{\mathbf{e}}_2 \cos\Theta'$ are introduced. The perpendicular unit vectors $\hat{\mathbf{e}}_1$ and $\hat{\mathbf{e}}_2$ are func-

tions of the guiding-center position $\mathbf{X}$ and assumed to be given beforehand. Since their definitions are arbitrary unless they have any singularities, the gyrogauge transformation [17, 18], $\Theta \equiv \Theta' + \varphi$, is introduced to remove the arbitrariness in the definition of the gyrophase Θ'. The gyrogauge φ is given by $\varphi \equiv \int_0^t [(d\mathbf{X}/dt) \cdot \nabla \hat{\mathbf{e}}_1 \cdot \hat{\mathbf{e}}_2 + (\partial \hat{\mathbf{e}}_1/\partial t) \cdot \hat{\mathbf{e}}_2]\, dt$. We denote the new direction vectors $\hat{\mathbf{c}}(\mathbf{X}, \Theta) \equiv \hat{\mathbf{c}}'(\mathbf{X}, \Theta - \varphi)$ and $\hat{\mathbf{a}}(\mathbf{X}, \Theta) \equiv \hat{\mathbf{a}}'(\mathbf{X}, \Theta - \varphi)$ simply by $\hat{\mathbf{c}}$ and $\hat{\mathbf{a}}$ in the remainder of this chapter. The usage of the new gyrophase Θ ensures the the uniqueness of the base direction for the gyrophase Θ. The relation, $d\hat{\mathbf{a}} \cdot \hat{\mathbf{c}} = d\mathbf{X} \cdot \nabla \hat{\mathbf{a}} \cdot \hat{\mathbf{c}} + dt(\partial \hat{\mathbf{a}}/\partial t) \cdot \hat{\mathbf{c}} = d\Theta$ is utilized later in the gauge transformation of 1-form to simplify the calculations.

Although the definition of the guiding-center $\mathbf{X}$ does not have the explicit dependence on $\mathbf{D}$, a difference arise from the modification of the perpendicular velocity $V_\perp$. When the guiding-center position for $\mathbf{D} = 0$ is denoted by $\mathbf{X}'$, the difference from the present guiding-center position is written as $\Delta_\mathrm{p} \equiv \mathbf{X} - \mathbf{X}' \simeq (m/qB)\hat{\mathbf{b}} \times \mathbf{D}$, where we used the approximation $B(\mathbf{X}) \simeq B(\mathbf{X}')$. If the velocity $\mathbf{D}$ is given by the simple $\mathbf{E} \times \mathbf{B}$ drift velocity, the quantity Δ_p is reduced to $\Delta_\mathrm{p} = -m\nabla_\perp \phi / qB^2$. The fact that its derivative with respect to time coincides the polarization drift velocity, $\mathbf{v}_\mathrm{p} \equiv -(d/dt) m\nabla_\perp \phi / qB^2$, indicates that the modified guiding-center coordinate $\mathbf{X}$ recovers the polarization drift due to the equilibrium electric fields in the zeroth order equations of motion, i.e. $d\mathbf{X}/dt - d\mathbf{X}'/dt = \mathbf{v}_\mathrm{p}$.

In order to separate the fundamental 1-form for a single charged particle,

$$\gamma \equiv [q\mathbf{A}(\mathbf{x}) + m\mathbf{v}] \cdot d\mathbf{x} - \left[\frac{m}{2}v^2 + q\phi(\mathbf{x})\right] dt, \tag{3.3}$$

into zeroth, first and successive higher order components, we introduce the perturbation potentials, $\phi = \phi_0 + \phi_1$ and $\mathbf{A} = \mathbf{A}_0 + \mathbf{A}_1$, and the following orderings;

$$\phi_1 \sim \epsilon \frac{m v_\mathrm{t}^2}{q}, \quad \mathbf{A}_1 \sim \epsilon \frac{m v_\mathrm{t}}{q}, \tag{3.4}$$

where quantity m, q and v_t are mass, charge and thermal speed of the particle species, respectively. The frequency of the perturbation ω is assumed to be much lower than the gyrofrequency Ω; $\omega \sim \epsilon\Omega$. The equilibrium $\mathbf{E} \times \mathbf{B}$ drift speed is assumed to be comparable to the thermal speed at most, and the the spatial scale of equilibrium magnetic field is assumed to be a second order quantity;

$$\frac{E_0}{B_0} \sim v_\mathrm{t}, \quad \frac{|\nabla B_0|}{B_0} \sim \epsilon^2 \frac{v_\mathrm{t}}{\Omega}. \tag{3.5}$$

The time scale of the equilibrium potentials are assumed as

$$\frac{\partial \phi_0}{\partial t} \sim \epsilon^2 v_\mathrm{t}^2 B_0, \quad \frac{\partial \mathbf{A}_0}{\partial t} \sim \mathbf{0}. \tag{3.6}$$

From the fundamental 1-form, Eq. (3.3), and the above orderings, the 1-form in the guiding-center coordinate can be written order by order;

$$\gamma_0 = \left(q\mathbf{A}_0 + mV_\parallel\hat{\mathbf{b}} + m\mathbf{D}\right)\cdot d\mathbf{X} + \frac{m}{q}\mu\, d\Theta - \left[\frac{m}{2}V_\parallel^2 + B_0\mu + \frac{m}{2}D^2 + q\bar{\phi}_0\right]dt, \tag{3.7}$$

$$\gamma_1 = (q\mathbf{A}_1 - m\rho\nabla\mathbf{D}\cdot\hat{\mathbf{a}})\cdot d\mathbf{X} + q\rho\mathbf{A}_1\cdot\hat{\mathbf{c}}\, d\Theta + \frac{1}{V_\perp}\mathbf{A}_1\cdot\hat{\mathbf{a}}\, d\mu - \left[q\tilde{\phi}_0 + mV_\perp\mathbf{D}\cdot\hat{\mathbf{c}} + q\phi_1(\mathbf{X}+\rho\hat{\mathbf{a}})\right]dt, \tag{3.8}$$

$$\gamma_2 = \left[\frac{m\mu}{q}\left(\hat{\mathbf{a}}\cdot\nabla\hat{\mathbf{b}}\cdot\hat{\mathbf{c}}\hat{\mathbf{b}} - \hat{\mathbf{a}}\cdot\nabla\ln B_0\hat{\mathbf{c}}\right) - \frac{mV_\perp V_\parallel}{\Omega}\nabla\hat{\mathbf{b}}\cdot\hat{\mathbf{a}}\right]\cdot d\mathbf{X} - \frac{m\mu}{q}\rho\hat{\mathbf{a}}\cdot\nabla\ln B_0\, d\Theta - m\rho\frac{\partial\mathbf{D}}{\partial t}\cdot\hat{\mathbf{a}}\, dt, \tag{3.9}$$

The higher order components, γ_3, γ_4, …, are omitted. Gyroaveraged quantities and their corresponding perturbation components for the electromagnetic potentials, $\psi = \phi_0$, ϕ_1 or $\mathbf{A}_1$, are denoted by $\bar{\psi} \equiv \oint \psi(\mathbf{X}+\rho\hat{\mathbf{a}})\, d\Theta/2\pi$ and $\tilde{\psi} \equiv \psi(\mathbf{X}+\rho\hat{\mathbf{a}}) - \bar{\psi}$. Here the perturbation of the equilibrium potential is expressed as $\tilde{\phi}_0$ instead of the Taylor expanded one, $\tilde{\phi}_0 \simeq \rho\hat{\mathbf{a}}\cdot\nabla\phi_0$. Although the latter form is commonly used in the previous works [38–40], the former exact form without the Taylor expansion are desirable in the case of the present ordering, $E_0/B_0 \sim v_\mathrm{t}$. The gyroradius and the direction of the equilibrium magnetic field at $\mathbf{X}$ are denoted by $\rho \equiv mV_\perp/qB_0(\mathbf{X})$ and $\hat{\mathbf{b}} \equiv \mathbf{B}_0/B_0$, respectively. The magnetic moment $\mu \equiv mV_\perp^2/B_0$ has been introduced and the gauge transformation, $\gamma \mapsto \gamma + dS$, has been applied to simplify the expressions.

From the truncated zeroth order 1-form under the assumption of the drift-kinetic ordering $k_\perp\rho \sim \epsilon \ll 1$;

$$\gamma_\mathrm{drift} = \left(q\mathbf{A}_0 + mV_\parallel\hat{\mathbf{b}} + m\mathbf{D}\right)\cdot d\mathbf{X} + \frac{m}{q}\mu\, d\Theta - \left[\frac{m}{2}V_\parallel^2 + B_0\mu + \frac{m}{2}D^2 + q\phi_0\right]dt, \tag{3.10}$$

we can obtain the zeroth order drift-kinetic equations

$$\frac{d\mathbf{X}}{dt} = \frac{1}{B_\parallel^*}\left[\mathbf{B}^* V_\parallel + \hat{\mathbf{b}}\times\left(\nabla\phi_0 + \frac{\mu}{q}\nabla B_0 + \frac{m}{2q}\nabla D^2 + \frac{m}{q}\frac{\partial\mathbf{D}}{\partial t}\right)\right], \tag{3.11}$$

$$\frac{d\Theta}{dt} = \frac{qB_0}{m}, \tag{3.12}$$

$$\frac{d\mu}{dt} = 0, \tag{3.13}$$

$$\frac{dV_\parallel}{dt} = -\frac{q\mathbf{B}^*}{mB_\parallel^*}\cdot\left(\nabla\phi_0 + \frac{\mu}{q}\nabla B_0 + \frac{m}{2q}\nabla D^2 + \frac{m}{q}\frac{\partial\mathbf{D}}{\partial t}\right), \tag{3.14}$$

where a modified magnetic field is introduced as

$$\mathbf{B}^* \equiv \nabla \times \left(\mathbf{A}_0 + \frac{mV_\parallel}{q}\hat{\mathbf{b}} + \frac{m}{q}\mathbf{D} \right) \tag{3.15}$$

$$= B_\parallel^* \hat{\mathbf{b}} + (mV_\parallel/q)\hat{\mathbf{b}} \times \left(\hat{\mathbf{b}} \cdot \nabla \hat{\mathbf{b}} \right) + (m/q)\nabla \times \mathbf{D}|_\perp, \tag{3.16}$$

where the parallel component of $\mathbf{B}^*$ is denoted by $B_\parallel^* \equiv \hat{\mathbf{b}} \cdot \mathbf{B}^*$. If the velocity $\mathbf{D}$ is given by the simple $\mathbf{E} \times \mathbf{B}$ drift velocity, it is confirmed that the polarization drift is recovered as

$$\frac{m}{qB_\parallel^*}\hat{\mathbf{b}} \times \frac{\partial \mathbf{D}}{\partial t} + \frac{mV_\parallel}{qB_\parallel^*}\nabla \times \mathbf{D}|_\perp = -\frac{1}{B_\parallel^* \Omega}\left(\frac{\partial \nabla_\perp \phi_0}{\partial t} + V_\parallel \hat{\mathbf{b}} \cdot \nabla \nabla \phi_0|_\perp \right) \tag{3.17}$$

The velocity of the guiding-center, therefore, involves $\mathbf{E} \times \mathbf{B}$, grad B, curvature and polarization drifts due to the temporal variation of ϕ_0 and due to the parallel motion. Although we omitted the Baños drift [24] in the above equations, it can be recovered from the second order 1-form. The phase space volume is calculated as $B_\parallel^*/m$ and the Liouville's theorem is confirmed; $(\partial/\partial Z^i)\left(B_\parallel^* \dot{Z}^i/m \right) = 0$, where the coordinate variables, $(t, \mathbf{X}, \Theta, \mu, V_\parallel)$, are denoted by Z^i for $i = 0, 1, \ldots, 6$.

3.3 Equilibrium drift velocity

In this section, we discuss how the equilibrium drift velocity $\mathbf{D}$ should be chosen. The introduction of the vector field $\mathbf{D}$ in Sec. 3.2 is aimed at decomposing the circular gyration from the particle dynamics. Therefore, one might expect the drift velocity obtained from the drift-kinetic equation (3.11) to be the best choice of $\mathbf{D}$. The dependences to the velocity space, however, cause difficulties in the calculations, i.e. the fundamental 1-form acquires some additional terms such as $\partial \mathbf{D}/\partial \mu$ and $\partial \mathbf{D}/\partial V_\parallel$. In order to keep the complexities in the same level as the previous study by Qin [40], we assume that the vector field $\mathbf{D}$ is an only function of the guiding-center position $\mathbf{X}$. From the guiding-center velocity, Eq. (3.11), and this assumption, we can obtain the practically most precise drift velocity;

$$\mathbf{D} \equiv \frac{\hat{\mathbf{b}}}{1 + \hat{\mathbf{b}} \cdot \nabla \times \mathbf{D}/\Omega} \times \left(\frac{\nabla \phi_0(\mathbf{X})}{B_0} + \frac{\nabla D^2}{2\Omega} \right). \tag{3.18}$$

Using the identity equation $\mathbf{D} \times \nabla \times \mathbf{D} = \nabla \mathbf{D} \cdot \mathbf{D} - \mathbf{D} \cdot \nabla \mathbf{D}$, we can obtain the relation

$$\left(\frac{\nabla \phi_0}{B} + \mathbf{D} \cdot \frac{\nabla \mathbf{D}}{\Omega} \right) - \frac{1}{1 + \hat{\mathbf{b}} \cdot \nabla \times \mathbf{D}/\Omega}\left(\frac{\nabla \phi_0}{B} + \frac{\nabla D^2}{2\Omega} \right)$$

$$= \frac{\hat{\mathbf{b}}}{1 + \hat{\mathbf{b}} \cdot \nabla \times \mathbf{D}/\Omega}\left(\frac{\nabla \phi_0}{B} + \frac{\nabla D^2}{2\Omega} \right) \cdot \nabla \times \mathbf{D}. \tag{3.19}$$

The vector product with $\hat{\mathbf{b}}$ yields a mathematically equivalent form to Eq. (3.18),

$$\mathbf{D} \equiv \hat{\mathbf{b}} \times \left(\frac{\nabla \phi_0}{B_0} + \mathbf{D} \cdot \frac{\nabla \mathbf{D}}{\Omega} \right). \tag{3.20}$$

Since the definition in the previous study is given by $\mathbf{D}_{\rm Qin} \equiv \hat{\mathbf{b}} \times \nabla \phi_0 / B$, the modification introduced into our definition is the second term in the right hand side in Eq. (3.20).

The physical meaning of Eq. (3.20) is easily understood through the vector product with the magnetic field;

$$m\mathbf{D} \cdot \nabla \mathbf{D}|_\perp = q\mathbf{D} \times \mathbf{B}_0 - q\nabla_\perp \phi_0. \tag{3.21}$$

This equation represents the perpendicular force balance in the stationary flow. The convection term in the left hand side is missing in $\mathbf{D}_{\rm Qin}$. A similar equation, $\mathbf{u} \cdot \nabla \mathbf{u} = \Omega \mathbf{u} \times \hat{\mathbf{b}} - (\Omega / B_0) \nabla \phi_0 - \nabla P / mN$, is discussed by Brizard [38] in the formulation of the gyrokinetic Vlasov equation for the plasma with toroidal rotation. Since their main interest is in the toroidal flow, their equilibrium velocity includes the parallel flow and they adopt an approximated expression of the flow, $\mathbf{u}_0 = u_{0\parallel} \hat{\mathbf{b}} + \hat{\mathbf{b}} \times \nabla \phi_0 / B_0$, as the vector field $\mathbf{D}$. Although the equilibrium parallel flow can be included in the definition of $\mathbf{D}$, we omit it for the clearness in the examination of the equilibrium perpendicular drift velocity.

One of the straightforward ways to examine the properness of this choice is to verify the conservation property of the magnetic moment μ. Since the gyrophase dependence is truncated in the drift-kinetic 1-form, Eq. (3.10), the drift-kinetic equation (3.13) conserves the magnetic moment. The general equation of motion, however, does not conserves μ;

$$\frac{d\mu}{dt} = qV_\perp \left(\mathbf{D} \cdot \hat{\mathbf{a}} - \hat{\mathbf{c}} \cdot \frac{\nabla \phi_0}{B_0} - \dot{X} \cdot \frac{\nabla \mathbf{D}}{\Omega} \cdot \hat{\mathbf{c}} \right), \tag{3.22}$$

because of the gyrophase dependence in the general 1-form

$$\begin{aligned} \gamma = & \left(q\mathbf{A}_0 + mV_\parallel \hat{\mathbf{b}} + m\mathbf{D} - m\rho \nabla \mathbf{D} \cdot \hat{\mathbf{a}} \right) \cdot d\mathbf{X} + \frac{m\mu}{q} d\Theta \\ & - \left[\frac{m}{2} V_\parallel^2 + B\mu + \frac{m}{2} D^2 + mV_\perp \mathbf{D} \cdot \hat{\mathbf{c}} + q\phi_0(\mathbf{X} + \rho \hat{\mathbf{a}}) \right] dt, \end{aligned} \tag{3.23}$$

where we neglect ∇B_0, $\nabla \hat{\mathbf{b}}$ and the perturbation potentials. If the gyration and the drift motion are decoupled well, the value of $d\mu/dt$ should be small. We calculate $d\mu/dt$ for three choices of $\mathbf{D}$. The first is zero velocity case, which corresponds to the conventional formulation with the equilibrium potential ϕ_0 but without special treatments for the large flow. The time derivative of μ becomes

$$\frac{d\mu}{dt} = -\frac{qV_\perp}{B} \hat{\mathbf{c}} \cdot \nabla \phi_0. \tag{3.24}$$

If the electric field is large, $E_0/B_0 \sim v_\mathrm{t}$, the variation of the magnetic moment becomes the same order as μ itself. In other words, the electric field has to be as small as the perturbation potential ϕ_1 in this case. The second is the simple $\mathbf{E}\times\mathbf{B}$ drift velocity, which corresponds to Qin's formulation;

$$\frac{d\mu}{dt} = -\frac{qV_\perp}{B}\hat{\mathbf{c}}\cdot\nabla(\phi_0 - \phi_0(\mathbf{X})) - qV_\perp\dot{\mathbf{X}}\hat{\mathbf{a}} : \frac{\nabla\nabla\phi_0(\mathbf{X})}{B}, \tag{3.25}$$

Since the most part of the electric field is canceled, it is applicable for a strong electric field in this case. The second derivative of ϕ, however, appears in $d\mu/dt$ and can be significant if the potential contour has a large curvature. The last is our definition, Eq. (3.20);

$$\frac{d\mu}{dt} = -qV_\perp\left(\frac{\nabla(\phi_0 - \phi_0(\mathbf{X}))}{B} + (\dot{X} - \mathbf{D})\cdot\frac{\nabla\mathbf{D}}{\Omega}\right)\cdot\hat{\mathbf{c}}, \tag{3.26}$$

Since the velocity of the guiding-center $\dot{X}$ can be approximated as $\dot{X} \simeq V_\parallel\mathbf{B}^*/B^*_\parallel + \mathbf{D}$, the second term proportional to $\nabla\mathbf{D}$ is considerably reduced. From the above observations, we confirm that the refinement of the gyrokinetic equations is achieved through our new choice of the vector field, Eq. (3.20). Numerical verifications of the new equilibrium velocity are given in Sec. 3.6.

3.4 Solution of the equilibrium velocity

We discuss the solution of Eq. (3.20) here. Since there is no analytic expression of the general solution, we have to employ a numerical solver for the general potential profile. We can, however, obtain the solution for special cases. First we consider the potential profile with plain contours. The electric field is written as $\mathbf{E} \equiv E(\mathbf{X}\cdot\hat{\mathbf{n}})\hat{\mathbf{n}}$ with the normal vector $\hat{\mathbf{n}}$. In this case, the solution is given by the ordinary $\mathbf{E}\times\mathbf{B}$ drift velocity.

$$\mathbf{D} = \hat{\mathbf{b}}\times\frac{\nabla\phi_0}{B}. \tag{3.27}$$

The solution is confirmed by the relation $\mathbf{D}\cdot\nabla\mathbf{D} = (E/B)(\hat{\mathbf{n}}\times\hat{\mathbf{b}})\cdot\nabla(E/B)(\hat{\mathbf{n}}\times\hat{\mathbf{b}}) = \mathbf{0}$.

Second we consider a more practical potential profile with circular contours. We rewrite Eq. (3.20) in a new orthogonal coordinate system where the base vectors are given by

$$\mathbf{e}^i = \left(\hat{\mathbf{b}},\ \nabla_\perp\phi_0,\ \hat{\mathbf{b}}\times\nabla_\perp\phi_0\right), \tag{3.28}$$

$$\mathbf{e}_i = \left(\hat{\mathbf{b}},\ \frac{\nabla_\perp\phi_0}{|\nabla_\perp\phi_0|^2}\ \frac{\hat{\mathbf{b}}\times\nabla_\perp\phi_0}{|\nabla_\perp\phi_0|^2}\right). \tag{3.29}$$

Using these bases, Eq. (3.20) is decomposed into

$$D_0 = \mathbf{D}\cdot\mathbf{e}_0 = 0, \tag{3.30}$$

$$D_1 = \mathbf{D}\cdot\mathbf{e}_1 = -\mathbf{D}\cdot\frac{\nabla\mathbf{D}}{\Omega}\cdot\mathbf{e}_2, \tag{3.31}$$

$$D_2 = \mathbf{D}\cdot\mathbf{e}_2 = \frac{1}{B} + \mathbf{D}\cdot\frac{\nabla\mathbf{D}}{\Omega}\cdot\mathbf{e}_1. \tag{3.32}$$

If the vector $\mathbf{D}$ is also written as $\mathbf{D} = D_i\hat{\mathbf{e}}^i = D^i\hat{\mathbf{e}}_i$, Each component of the differential equation is written as

$$(D_1\partial^1 + D_2\partial^2)D_2 + E_{112}(D_1)^2 + (E_{212}+E_{122})D_1D_2 + E_{222}(D_2)^2 = -\Omega D_1, \tag{3.33}$$

$$(D_1\partial^1 + D_2\partial^2)D_1 + E_{111}(D_1)^2 + (E_{211}+E_{121})D_1D_2 + E_{221}(D_2)^2 = \Omega D_2 - \frac{\Omega}{B}, \tag{3.34}$$

where the notation $\partial^i \equiv \hat{\mathbf{e}}^i\cdot\nabla$ and $E_{ijk} \equiv \mathbf{e}^i\cdot\nabla\mathbf{e}^j\cdot\mathbf{e}_k$ are introduced. In the case of the potential with circular contours, the coefficient E_{222} vanishes because of the symmetry;

$$E_{222} = (\hat{\mathbf{b}}\times\nabla\phi_0)\cdot\nabla\ln|\nabla_\perp\phi_0|^2 = 0. \tag{3.35}$$

The first component of the vector $\mathbf{D}$, therefore, vanishes and the differential equation reduces to

$$D_0 = 0, \quad D_1 = 0, \quad \frac{1}{B} - D_2 + \frac{E_{221}}{\Omega}(D_2)^2 = 0. \tag{3.36}$$

This quadratic equation is solved as

$$D_2 = \frac{1}{B}\frac{2}{1+\sqrt{1-4E_{221}/B\Omega}}, \tag{3.37}$$

The coefficient E_{221} is calculated as

$$E_{221} = \mathbf{e}^2\cdot\nabla\mathbf{e}^2\cdot\mathbf{e}_1 = \frac{\nabla\phi_0}{|\nabla_\perp\phi_0|}\cdot\hat{\mathbf{b}}\times\nabla\nabla\phi_0\times\hat{\mathbf{b}}\cdot\frac{\nabla\phi_0}{|\nabla_\perp\phi_0|}. \tag{3.38}$$

Since the potential with circular contours can be expressed as $\phi_0(|\mathbf{r}|)$ with the radial vector $\mathbf{r}$, the coefficient E_{221} is reduced to

$$E_{221} = \frac{\mathbf{r}}{r}\cdot\hat{\mathbf{b}}\times\left[\left(\phi_0'' - \frac{\phi_0'}{r}\right)\frac{\mathbf{rr}}{r^2} + \frac{\phi_0'}{r}\overleftrightarrow{I}\right]\times\hat{\mathbf{b}}\cdot\frac{\mathbf{r}}{r} = -\frac{\phi_0'}{r}\left|\hat{\mathbf{b}}\times\frac{\mathbf{r}}{r}\right|^2, \tag{3.39}$$

and thus the solution is given by

$$\mathbf{D} = \frac{2}{1+\sqrt{1-4C}}\frac{\hat{\mathbf{b}}\times\nabla\phi}{B}, \quad C \equiv \frac{E_r}{rB\Omega}\left|\hat{\mathbf{b}}\times\frac{\mathbf{r}}{r}\right|^2, \tag{3.40}$$

where the radial electric field is denoted by $E_r = -\partial\phi_0/\partial r$. This velocity is larger (smaller) than the simple $\mathbf{E}\times\mathbf{B}$ drift velocity for positive (negative) qE by a factor of

$2/\left(1+\sqrt{1-4C}\right)$ and the polarization shift $\hat{\mathbf{b}}\times\mathbf{D}/\Omega$ is also larger (smaller). We note that if the coefficient C is larger than $1/4$, i.e. the electric field is too large, the velocity $\mathbf{D}$ can not be defined. Above the marginal value, the trajectory of the particle diverges exponentially.

Lastly, the numerical scheme for the general potential profile is presented. We used a simple recurrence equation to solve the equilibrium drift velocity;

$$\mathbf{D}_0 = \hat{\mathbf{b}}\times\frac{\nabla\phi_0}{B}, \tag{3.41}$$

$$\mathbf{D}_{n+1} = \hat{\mathbf{b}}\times\left(\frac{\nabla\phi_0}{B}+\mathbf{D}_{n+1}\cdot\frac{\nabla\mathbf{D}_n}{\Omega}\right), \tag{3.42}$$

where the gradient of the vector $\mathbf{D}_n(\mathbf{X})$ is calculated as

$$\nabla\mathbf{D}_n(\mathbf{X}) = \sum_i \hat{\mathbf{z}}^i\frac{\mathbf{D}_n\left(\mathbf{X}+\delta\hat{\mathbf{z}}^i\right)-\mathbf{D}_n\left(\mathbf{X}-\delta\hat{\mathbf{z}}^i\right)}{2\delta}. \tag{3.43}$$

The small quantity δ is chosen to be much smaller than the scale length of the potential ϕ_0. Sufficient accuracy for general purposes can be obtained by two or three times of the iteration.

3.5 Gyrokinetic equations

3.5.1 The general derivation of the gyrokinetic equations

The remaining procedures to obtain the gyrokinetic equations are the Lie perturbation analysis and the formulation of the gyrokinetic Maxwell's equations. Since these treatments are essentially same as the previous works [17–19, 37–40], we omit detailed discussions and describe the outline and the results.

Successive Lie transformations are introduced; $\mathcal{T}\equiv\cdots\exp(\epsilon^2\mathcal{L}_2)\exp(\epsilon\mathcal{L}_1)$. The i th order operator $\mathcal{L}_i$ is a Lie derivative operator defined by an i th order Lie generator g_i; $\mathcal{L}_i v\equiv i_{g_i}(dv)$. Although the correct Lie derivative has the form $i_g(dv)+d(i_g v)$, we adopt the truncated expression because the second term does not affect to scalars and resultant equations of motion. In other words, the second term $d(i_g v)$ is eliminated through the gauge transformation. The guiding-center coordinate variables $Z^i=(t,\mathbf{X},\Theta,\mu,V_\parallel)$ are transformed to the gyrocenter coordinate variables $\overline{Z}^i=(t,\overline{\mathbf{X}},\overline{\Theta},\overline{\mu},\overline{V}_\parallel)$; $\overline{Z}=\mathcal{T}Z=\cdots\exp(\epsilon^2 i_{g_2}d)\exp(\epsilon i_{g_1}d)Z$, where the time variable t is not changed through the Lie transformation. The 1-form in the guiding-center coordinate, $\gamma=\gamma_0+\epsilon\gamma_1+\epsilon^2\gamma_2+\cdots$, is also transformed to the gyrokinetic 1-form, $\Gamma=\Gamma_0+\epsilon\Gamma_1+\epsilon^2\Gamma_2+\cdots$, in the gyrocenter coordinate. The new 1-form Γ is determined by the Lie generator g_i and the gauge function

S_i;

$$\Gamma_0 = \gamma_0, \tag{3.44}$$

$$\Gamma_1 = \gamma_1 - i_{g_1} d\gamma_0 + dS_1, \tag{3.45}$$

$$\Gamma_2 = \gamma_2 - i_{g_1} d\gamma_1 + \frac{1}{2}\left((i_{g_1} d)^2 - i_{g_2} d\right)\gamma_0 + dS_2. \tag{3.46}$$

The first order gauge function S_1 and the first order Lie generator g_1 are determined as follows;

$$\mathcal{V}_0^i \frac{\partial S_1}{\partial \bar{Z}^i} = -\mathcal{V}_0^i \left(\gamma_{1i} - \langle \gamma_{1i} \rangle\right), \tag{3.47}$$

$$g_1^j = \sigma^{ij}\left(\gamma_{1i} + \frac{\partial S_1}{\partial \bar{Z}^i}\right) \quad \text{for } j \neq 0, \tag{3.48}$$

where the vector field $\mathcal{V}_0^i$ is defined as the flow created by the zeroth order equation of motion;

$$\mathcal{V}_0^i = \sigma^{ij}\left(\frac{\partial \gamma_{0j}}{\partial \bar{Z}^0} - \frac{\partial \gamma_{00}}{\partial \bar{Z}^j}\right). \tag{3.49}$$

The time-component of the Lie generator, g_1^0, is defined as zero, which corresponds to the identical transformation for the variable t. The tensor $\overleftrightarrow{\sigma}$ represents the Poisson tensor calculated from the zeroth order 1-form, Eq. (3.7);

$$\overleftrightarrow{\sigma} = \left(\begin{array}{c|ccc} \hat{\mathbf{b}} \times \overleftrightarrow{I}/qB_\parallel^* & \mathbf{0} & \mathbf{0} & \mathbf{B}^*/mB_\parallel^* \\ \hline \mathbf{0} & 0 & q/m & 0 \\ \mathbf{0} & -q/m & 0 & 0 \\ -\mathbf{B}^*/mB_\parallel^* & 0 & 0 & 0 \end{array}\right). \tag{3.50}$$

The gyrokinetic 1-form is obtained up to the first order;

$$\Gamma = \Gamma_0 + \Gamma_1 = \gamma_0 - \mathcal{V}_0^i \langle \gamma_{1i} \rangle \, dt. \tag{3.51}$$

This 1-form yields the gyrokinetic equations of motion

$$\frac{dZ^i}{dt} = \sigma^{ij}\left(\frac{\partial \Gamma_j}{\partial t} - \frac{\partial \Gamma_0}{\partial Z^j}\right). \tag{3.52}$$

The Vlasov equation and its conservation form are also obtained as $\dot{Z}^i\left(\partial \bar{F}/\partial Z^i\right) = 0$ and $(\partial/\partial Z^i)\left(\dot{Z}^i B_\parallel^* \bar{F}\right) = 0$, respectively.

The gyrokinetic expressions of Maxwell's equations can be obtained by writing the charge density and current density with the distribution function in gyrocenter coordinate. The formulation is achieved by pullback technique introduced by Brizard [18] and Qin [19,20]. When a physical quantity is given by $\lambda(\mathbf{x}, \mathbf{v})$, e.g. $\lambda = q$ for the charge density and

$\lambda = q\mathbf{v}$ for the current density, its moment is expressed as $\bar{\lambda}(\mathbf{x}) = \int \lambda(\mathbf{x}', \mathbf{v}') f(\mathbf{x}', \mathbf{v}') \delta(\mathbf{x}' - \mathbf{x})\, d^3x' d^3v'$. Thus, the pullback expression of λ, $\Lambda(Z) = \lambda(\mathbf{X} + \rho\hat{\mathbf{a}}, \mathbf{v}(\Theta, \mu, V_\parallel))$, yields the averaged quantity in the guiding-center coordinate; $\bar{\lambda}(\mathbf{x}) = \int \Lambda(Z') F(Z') \delta(\mathbf{X}' + \rho\hat{\mathbf{a}} - \mathbf{x}) B_\parallel^* / m\, d^6Z'$. The distribution function $F(Z)$ is that of guiding-center and also can be written in the gyrocenter coordinate as $f(z) = F(Z) = \bar{F}(\bar{Z})$. The gyrocenter distribution function $\bar{F}$ is usually assumed to be independent of the gyrophase $\bar{\Theta}$. From the pullback expressions, we can write the moment integral of arbitrary physical quantities with the gyrocenter distribution function $\bar{F}$;

$$\bar{\lambda}(\mathbf{x}) = \int \Lambda(Z') \mathcal{T}^* \bar{F}(Z') \delta(\mathbf{X}' + \rho\hat{\mathbf{a}} - \mathbf{x}) \frac{B_\parallel^*}{m}\, d^6Z'. \tag{3.53}$$

3.5.2 Limiting case with electrostatic perturbation

We show the gyrokinetic equations with the electrostatic perturbation as an example of limiting case. The equations of motion in this section are used in Sec. 3.6 for numerical verifications. We use some approximations commonly assumed in the analysis of the micro-instabilities [39, 43, 44]. First, the vector field of the zeroth order, $\mathcal{V}_0$, used in the determining equations of the gauge function S_1, Eq. (3.47), and the 1-form, Eq. (3.51), is reduced to $\mathcal{V}_0 \simeq (\bar{V}_\parallel \hat{\mathbf{b}} + \mathbf{D})\partial_{\bar{\mathbf{X}}} + \Omega \partial_{\bar{\Theta}} + \partial_t$. Second, we assume that the dependences of the gauge function S_1 on the coordinate variables $(\bar{\mathbf{X}}, \bar{\mu}, \bar{V}_\parallel, t)$ are much smaller than on the gyrophase $\bar{\Theta}$, i.e. $dS_1 \simeq \partial_{\bar{\Theta}} S_1 d\bar{\Theta}$.

Under these approximations, the gyrokinetic 1-form is obtained up to the first order as

$$\begin{aligned}\Gamma = &\left(q\mathbf{A}_0 + m\bar{V}_\parallel \hat{\mathbf{b}} + m\mathbf{D}\right) \cdot d\bar{\mathbf{X}} + \frac{m}{q}\bar{\mu}\, d\bar{\Theta} \\ &- \left[\frac{m}{2}\bar{V}_\parallel^2 + B\bar{\mu} + \frac{m}{2}D^2 + q\bar{\phi}_0 + q\bar{\phi}_1\right] dt.\end{aligned} \tag{3.54}$$

Although this equation is almost same as the corresponding equations in the previous works of Hahm [39] and Qin [40], there are two differences. One is the definition of $\mathbf{D}$ from the simple $\mathbf{E} \times \mathbf{B}$ drift velocity to the generalized one. The other difference is the expression of the gyroaveraged equilibrium potential ϕ_0. Hahm and Qin employ $\phi_0 + (m\mu/2q^2)\hat{\mathbf{b}} \cdot \nabla \times \mathbf{D}$ and $\phi_0 + (\mu/2q\Omega)\nabla_\perp^2 \phi_0$ as the gyroaveraged potential, respectively. The term $(m\mu/2q^2)\hat{\mathbf{b}} \cdot \nabla \times \mathbf{D}$ is also found in Brizard's paper [38] and can be written as $(\mu/2q\Omega)\nabla_\perp^2 \phi_0$ approximately. Since our expression of the gyroaveraged potential is also approximated as $\bar{\phi}_0 \simeq \phi_0 + (\mu/2q\Omega)\nabla_\perp^2 \phi_0$, these three expressions are essentially same. Our equation, however, has an advantage in the rigorousness because of the absence of the truncation due to the Taylor expansion.

The first order gauge function is obtained as

$$S_1 = \frac{q}{\Omega}\tilde{\Phi}_0 + \frac{q}{\Omega}\tilde{\Phi}_1 - \frac{m\rho}{\Omega}\left(\bar{V}_\parallel \hat{\mathbf{b}} + \mathbf{D}\right)\cdot\nabla\mathbf{D}\cdot\hat{\mathbf{c}} + m\rho\hat{\mathbf{a}}\cdot\mathbf{D}, \tag{3.55}$$

where the notation $\tilde{\Phi} \equiv \oint \tilde{\phi}\, d\bar{\Theta} - \left\langle \oint \tilde{\phi}\, d\bar{\Theta} \right\rangle_{\bar{\Theta}}$ is introduced for $\tilde{\Phi}_0$ and $\tilde{\Phi}_1$. It is calculated by the partial integral;

$$\tilde{\Phi} = \frac{1}{2\pi}\int_{\Theta}^{\Theta+2\pi} (\Theta' - \Theta - \pi)\phi\left(\mathbf{X} + \rho\hat{\mathbf{a}}(\Theta')\right) d\Theta'. \tag{3.56}$$

Using the definition of the velocity field $\mathbf{D}$, Eq. (3.20), we can rewrite Eq. (3.55) in a simpler form,

$$S_1 = \frac{q}{\Omega}\tilde{\Phi}_0 + \frac{q\rho}{\Omega}\hat{\mathbf{c}}\cdot\nabla\phi_0 - \frac{m\bar{V}_\parallel\rho}{\Omega}\hat{\mathbf{b}}\cdot\nabla\mathbf{D}\cdot\hat{\mathbf{c}} + \frac{q}{\Omega}\tilde{\Phi}_1. \tag{3.57}$$

The first two terms in Eq. (3.57) can be written also as

$$\frac{q}{\Omega}\tilde{\Phi}_0 + \frac{q\rho}{\Omega}\hat{\mathbf{c}}\cdot\nabla\phi_0 = \frac{1}{2\pi}\int_{\Theta}^{\Theta+2\pi} (\Theta' - \Theta - \pi)\left[\phi_0\left(\mathbf{X} + \rho\hat{\mathbf{a}}(\Theta')\right) - \phi_0(\mathbf{X}) - \hat{\mathbf{a}}(\Theta')\cdot\nabla\phi_0(\mathbf{X})\right] d\Theta'. \tag{3.58}$$

The previous expression given by Qin for the simple equilibrium velocity $\mathbf{D}_{\mathrm{Qin}} \equiv \hat{\mathbf{b}} \times \nabla\phi_0/B$ is

$$S_{1\,\mathrm{Qin}} = \frac{q}{\Omega}\tilde{\Phi}_0 + \frac{q\rho}{\Omega}\hat{\mathbf{c}}\cdot\nabla\phi_0 - \frac{V_\perp}{B^2}\mathbf{D}_{\mathrm{Qin}}\cdot\nabla\mathbf{D}_{\mathrm{Qin}}\cdot\hat{\mathbf{c}} - \frac{V_\perp V_\parallel}{B^2}\hat{\mathbf{b}}\cdot\nabla\mathbf{D}_{\mathrm{Qin}}\cdot\mathbf{c} + \frac{q}{\Omega}\tilde{\Phi}_1. \tag{3.59}$$

The third term in $S_{1\,\mathrm{Qin}}$ has been canceled in our gauge function S_1. This fact shows that the zeroth order equations of motion adopted here is more accurate than that of Qin's study. The first order Lie generator g_1 is calculated from this approximated S_1 as

$$g_1^{\bar{\mathbf{X}}} = -\frac{1}{qB_\parallel^*}\hat{\mathbf{b}}\times\left[-m\rho\nabla\mathbf{D}\cdot\hat{\mathbf{a}} + \nabla\left(\frac{q}{\Omega}\tilde{\Phi}_0 + \frac{q}{\Omega}\tilde{\Phi}_1 + \frac{q\rho}{\Omega}\hat{\mathbf{c}}\cdot\nabla\phi_0 - \frac{mV_\parallel\rho}{\Omega}\hat{\mathbf{b}}\cdot\nabla\mathbf{D}\cdot\hat{\mathbf{c}}\right)\right] - \frac{\mathbf{B}^*}{mB_\parallel^*}\left(-\frac{m\rho}{\Omega}\hat{\mathbf{b}}\cdot\nabla\mathbf{D}\cdot\hat{\mathbf{c}}\right), \tag{3.60}$$

$$g_1^{\bar{\Theta}} = -\frac{q^2}{m\Omega}\left(\frac{\partial\tilde{\Phi}_0}{\partial\bar{\mu}} + \frac{\partial\tilde{\Phi}_1}{\partial\bar{\mu}} + \frac{1}{qV_\perp}\hat{\mathbf{c}}\cdot\nabla\phi_0 - \frac{mV_\parallel}{q^2V_\perp}\hat{\mathbf{b}}\cdot\nabla\mathbf{D}\cdot\hat{\mathbf{c}}\right), \tag{3.61}$$

$$g_1^{\bar{\mu}} = \frac{q^2}{m\Omega}\left(\tilde{\phi}_0 + \tilde{\phi}_1 - \rho\hat{\mathbf{a}}\cdot\nabla\phi_0 + \frac{m\rho V_\parallel}{q}\hat{\mathbf{b}}\cdot\nabla\mathbf{D}\cdot\hat{\mathbf{a}}\right), \tag{3.62}$$

$$g_1^{\bar{V}_\parallel} = \frac{\mathbf{B}^*}{mB_\parallel^*}\cdot\left[-m\rho\nabla\mathbf{D}\cdot\hat{\mathbf{a}} + \nabla\left(\frac{q}{\Omega}\tilde{\Phi}_0 + \frac{q}{\Omega}\tilde{\Phi}_1 + \frac{q\rho}{\Omega}\hat{\mathbf{c}}\cdot\nabla\phi_0 - \frac{mV_\parallel\rho}{\Omega}\hat{\mathbf{b}}\cdot\nabla\mathbf{D}\cdot\hat{\mathbf{c}}\right)\right]. \tag{3.63}$$

Terms proportional to $\mathbf{D}\cdot\nabla\mathbf{D}$ have been canceled also in the Lie generator.

From the gyrokinetic 1-form, the gyrokinetic equations of motion are obtained as

$$\frac{d\mathbf{X}}{dt} = \frac{1}{B_\parallel^*}\left[\mathbf{B}^* V_\parallel + \hat{\mathbf{b}}\times\left(\nabla\bar{\phi}_0 + \nabla\bar{\phi}_1 + \frac{\mu}{q}\nabla B_0 + \frac{m}{2q}\nabla D^2 + \frac{m}{q}\frac{\partial\mathbf{D}}{\partial t}\right)\right], \tag{3.64}$$

$$\frac{d\Theta}{dt} = \frac{qB_0}{m} + \frac{q^2}{m}\frac{\partial\bar{\phi}_0}{\partial\bar{\mu}} + \frac{q^2}{m}\frac{\partial\bar{\phi}_1}{\partial\bar{\mu}}, \tag{3.65}$$

$$\frac{d\mu}{dt} = 0, \tag{3.66}$$

$$\frac{dV_\parallel}{dt} = -\frac{q\mathbf{B}^*}{mB_\parallel^*}\cdot\left(\nabla\bar{\phi}_0 + \nabla\bar{\phi}_1 + \frac{\mu}{q}\nabla B_0 + \frac{m}{2q}\nabla D^2 + \frac{m}{q}\frac{\partial\mathbf{D}}{\partial t}\right). \tag{3.67}$$

The term proportional to $\partial\mathbf{D}/\partial t$ in Eq. (3.64) represents the polarization drift due to the temporal variation of the equilibrium electric field. This term lacks in Hahm's paper [39] because of the assumption that the equilibrium potential is constant in time. The $\bar{\mu}$ derivative of the gyroaveraged potential is also expressed as

$$\frac{\partial\bar{\phi}}{\partial\bar{\mu}} = \frac{1}{q\bar{V}_\perp}\left\langle\hat{\mathbf{a}}\cdot\nabla\phi(\mathbf{X}+\rho\hat{\mathbf{a}})\right\rangle = \frac{1}{B}\left\langle\hat{\mathbf{c}}\hat{\mathbf{c}}:\nabla\nabla\phi(\mathbf{X}+\rho\hat{\mathbf{a}})\right\rangle. \tag{3.68}$$

If the spatial scale of the equilibrium potential is much larger than the gyroradius, we can use approximated expressions, $\bar{\phi}_0 \simeq \phi_0 + (\rho^2/4)\nabla_\perp^2\phi_0$ and $\partial\bar{\phi}_0/\partial\bar{\mu} \simeq \nabla_\perp^2\phi_0/2B$.

The particle density is calculated up to the first order as a pullback expression;

$$n(\mathbf{x}) = \int\left(\bar{F} + g_1^{\bar{\mathbf{X}}}\cdot\frac{\partial\bar{F}}{\partial\mathbf{X}} + g_1^{\bar{\mu}}\frac{\partial\bar{F}}{\partial\mu} + g_1^{\bar{V}_\parallel}\frac{\partial\bar{F}}{\partial V_\parallel}\right)\frac{B_\parallel^*}{m}\delta(\mathbf{X}+\rho\hat{\mathbf{a}}-\mathbf{x})\,d^3Xd\Theta d\mu dV_\parallel. \tag{3.69}$$

If we used the approximated expression of the Lie generator, $g_1 \simeq g_1^{\bar{\mu}}$, as is often the case with the most of the gyrokinetic analyses, the density equation is reduced to

$$n = \int\left(\bar{F} + g_1^{\bar{\mu}}\partial_{\bar{\mu}}\bar{F}\right)\frac{B_\parallel^*}{m}\delta(\mathbf{X}+\rho\hat{\mathbf{a}}-\mathbf{x})\,d^3Xd\Theta d\mu dV_\parallel. \tag{3.70}$$

Using the partial integral for $\bar{\mu}$ and assuming that the spatial scale of the equilibrium potential is much larger than the gyroradius, we can obtain the reduced expression

$$n \simeq N + \frac{1}{\Omega^2}\nabla_\perp\cdot(U_\parallel\nabla_\parallel\mathbf{D}) + N_\mathrm{p}, \tag{3.71}$$

where we define the gyrocenter density N, the parallel velocity $U_\parallel$ and the polarization density N_p due to the potential perturbation as

$$N \equiv \int\bar{F}\frac{B_\parallel^*}{m}\delta\left(\mathbf{X}+\rho\hat{\mathbf{a}}-\mathbf{x}\right)d^3Xd\Theta d\mu dV_\parallel, \tag{3.72}$$

$$U_\parallel \equiv \int V_\parallel\bar{F}\frac{B_\parallel^*}{m}\delta\left(\mathbf{X}+\rho\hat{\mathbf{a}}-\mathbf{x}\right)d^3Xd\Theta d\mu dV_\parallel, \tag{3.73}$$

$$N_\mathrm{p} \equiv \int\frac{q^2}{m\Omega}\tilde{\phi}_1\frac{\partial\bar{F}}{\partial\bar{\mu}}\frac{B_\parallel^*}{m}\delta(\mathbf{X}+\rho\hat{\mathbf{a}}-\mathbf{x})\,d^3Xd\Theta d\mu dV_\parallel. \tag{3.74}$$

The density equation for Qin's equilibrium velocity is given by

$$n_\mathrm{Qin} = N + \frac{1}{\Omega^2}\nabla_\perp\cdot\left[\left(N\mathbf{D}_\mathrm{Qin} + U_\parallel\hat{\mathbf{b}}\right)\cdot\nabla\mathbf{D}_\mathrm{Qin}\right] + N_\mathrm{p}. \tag{3.75}$$

The term proportional to $\mathbf{D} \cdot \nabla \mathbf{D}$ has been canceled also in the equation of the density. This relation gives the Poisson equation and thus we have obtained the whole set of the gyrokinetic equations.

3.6 Numerical comparisons

In this section, numerical verifications are given to confirm the advantages of the present equilibrium drift velocity. We solve the gyrokinetic equations of motion (3.64) – (3.67) and compare the solutions with that of the full-kinetic equations and the previous gyrokinetic equations for three kinds of potential profiles.

First, we examine the particle trajectories for the potential $\phi_0 = -Ey$ and $\phi_1 = 0$. The solution of the new equilibrium drift velocity, Eq. (3.20), for the uniform electric field is given by a simple $\mathbf{E} \times \mathbf{B}$ drift velocity $\mathbf{D} = E/B\hat{\mathbf{x}}$ for $\mathbf{B} = B\hat{\mathbf{z}}$. Therefore, the equations of motion for the previous definition of $\mathbf{D} = \mathbf{D}_{\mathrm{Qin}}$ and our definition coincide with each other for the uniform electric field. We solved the full-kinetic equations and the gyrokinetic equations and plotted the particle position and the gyrocenter position in Fig. 3.1. The initial position and velocity used in solving the gyrokinetic equations are determined from those of the full-kinetic calculation through the coordinate transformation, $\bar{\mathbf{X}} = \mathbf{x} - \rho\hat{\mathbf{a}} + g_1^{\mathbf{X}}$. The last term $g_1^{\mathbf{X}}$ comes from the Lie transformation between the guiding-center and the gyrocenter coordinates. It represents a correction of the gyrocenter position related to the perturbation generated from the nonuniformity of the equilibrium potential and the particle gyration. The solution of the gyrokinetic equations are transformed inversely to the particle positions, $\mathbf{x} = \bar{\mathbf{X}} + \rho\hat{\mathbf{a}} - g_1^{\bar{\mathbf{X}}}$, and plotted. The gyrating curve labeled "full" in Fig. 3.1 represents the particle trajectory calculated from the full-kinetic equations. The plus cross marks represent the particle positions calculated from the gyrokinetic equations with and without $\mathbf{D}$, respectively. From the fact that the particle positions with $\mathbf{D}$ are just on the curve of the full-kinetic solution, while those of $\mathbf{D} = 0$ are not, the effectiveness of the employment of the equilibrium drift velocity $\mathbf{D}$ for the strong electric field is confirmed.

The upper and lower horizontal lines represent the trajectories of the gyrocenter with and without $\mathbf{D}$, respectively. The difference in the gyrocenter positions are caused by the modification of the velocity space. Since the velocity in the gyrokinetics with $\mathbf{D}$ is defined in the frame moving with the velocity $\mathbf{D}$, the gyrocenter position shifts along the electric field. The amount of the shift is given by $\hat{\mathbf{b}} \times \mathbf{D}/\Omega = E/B\Omega\hat{\mathbf{y}}$ and corresponds to the polarization due to the equilibrium electric field.

Secondly, we use a potential profile with circular contours, $\phi_0(r) = -Er$. A particle drifts along the contour to the clockwise direction for a positive E. The solution of

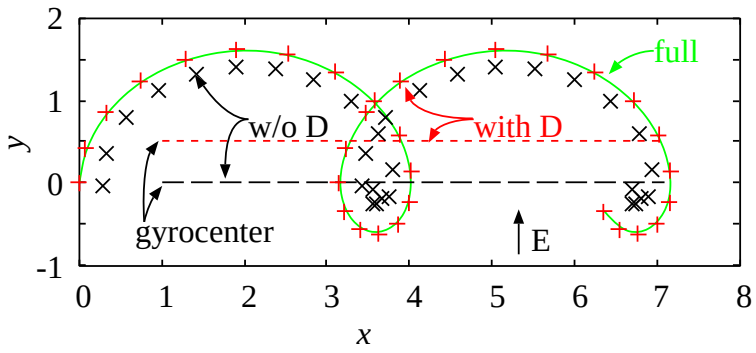

Figure 3.1: Comparisons of particle trajectories calculated from the full-kinetic, gyrokinetic equations with and without **D**. The curve labeled "full" represents the particle orbit calculated from the full-kinetic equations of motion. The plus and cross marks correspond to the solutions of the gyrokinetic equations with and without **D**, respectively. The gyrocenter orbits with and without **D** are shown as dashed and dotted lines, respectively.

Eq. (3.20) for this potential is given by

$$\mathbf{D} = \frac{2}{1+\sqrt{1-4E/rB\Omega}}\hat{\mathbf{b}} \times \frac{\nabla\phi_0}{B}, \tag{3.76}$$

where we denote the radius by $r = \sqrt{x^2+y^2}$. In order to confirm the accuracy of the equation in the nonuniform electric field, the conservation of the energy is examined. There are two expressions for the energy according to the coordinate systems;

$$H_{\mathrm{f}}(\mathbf{x},\mathbf{v}) = \frac{m}{2}v^2 + q\phi_0, \tag{3.77}$$

$$H_{\mathrm{g}}(\bar{\mathbf{X}},\bar{\mu},\bar{V}_{\parallel}) = \frac{m}{2}\bar{V}_{\parallel}^2 + B\bar{\mu} + \frac{m}{2}D^2 + q\left\langle\phi_0\right\rangle. \tag{3.78}$$

The former is the Hamiltonian on the particle coordinate system and represents the energy of the particle at the phase space position $(\mathbf{x},\mathbf{v})$. The latter expression, H_{g} is the gyrokinetic Hamiltonian on the gyrocenter coordinate system $(\bar{\mathbf{X}},\bar{\Theta},\bar{\mu},\bar{V}_{\parallel})$. Since the description of dynamics consists of the definition of the coordinate system and the equations of motion, or time derivative of the coordinate variables, the Hamiltonian becomes an invariant if and only if the corresponding equations of motion are employed. Thus, the full-kinetic equation conserves the particle energy H_{f} but not the gyrokinetic energy H_{g}, and *vice versa* for the gyrokinetic equations. The reason for the nonconservation is that the gyrokinetic 1-form and the coordinate transformation between the particle and the gyrocenter involves truncation errors through the Taylor expansions with respect to ϵ. Therefore, the degree of energy conservation is a suitable criterion to evaluate the accuracy of the equations.

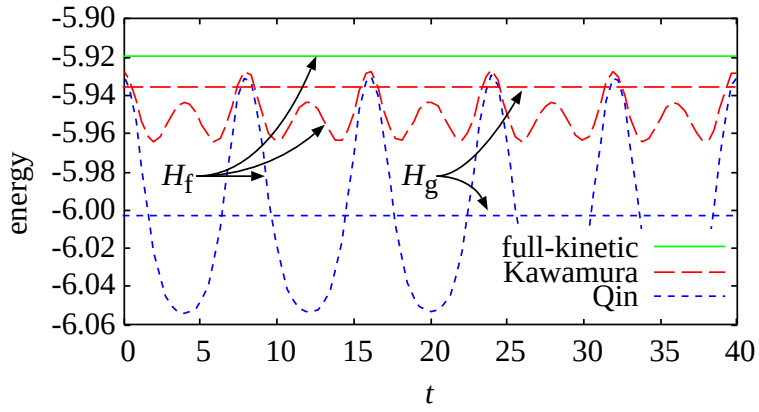

Figure 3.2: Time evolution of the particle energy H_f, Eq. (3.77), and the gyrokinetic energy H_g, Eq. (3.78). They are calculated from the full-kinetic equations (solid) and the gyrokinetic equations with the equilibrium velocity field $\mathbf{D}$ (dashed) and $\mathbf{D}_{\rm Qin}$ (dotted).

We employ two combinations of the energy expressions and equations of motion. One is the 'proper' pair of the particle energy, H_f, and the full-kinetic equations of motion, and also H_g and the gyrokinetic equations. In this case, the energy is conserved rigorously. From the numerical comparison with the full-kinetic one, the consistency of the gyrokinetic equations are examined. The other combination, i.e. H_f and the gyrokinetic equations, is useful to examine the accuracy of the equations of motion and the coordinate transformations used in the calculation of H_f from the gyrokinetic coordinate variables. Although the time evolution of the energy is not stationary, it does not have a secular variation but oscillates with the gyrofrequency and its harmonics. The amplitude of the oscillation is employed as the criterion of the accuracy.

We solve the full-kinetic and the gyrokinetic equations numerically and plot three kinds of energy values in Fig. 3.2. First is the particle energy H_f calculated from the full-kinetic solution. It is shown as a solid horizontal line labeled 'H_f' in the figure. Second is the gyrokinetic energy H_g calculated from the gyrokinetic solution. The dashed and dotted horizontal lines labeled 'H_g' represent the gyrokinetic energy for our equilibrium drift velocity field $\mathbf{D}$ and that of Qin, respectively. Their conservation indicates the consistency of the gyrokinetic equations derived here. The reduction of the derivation from the value of the full-kinetic energy is also observed. The third energy value is the particle energy H_f calculated from the gyrokinetic solution. Since H_f is a function on the particle coordinate system, it is evaluated with the particle coordinate variables transformed from the gyrocenter coordinate variables. The dashed and dotted oscillatory curves correspond to the solutions obtained from the equations for $\mathbf{D}$ and $\mathbf{D}_{\rm Qin}$, respectively. Since the amplitude of the energy oscillation for the present $\mathbf{D}$ is reduced by a factor of three compared with

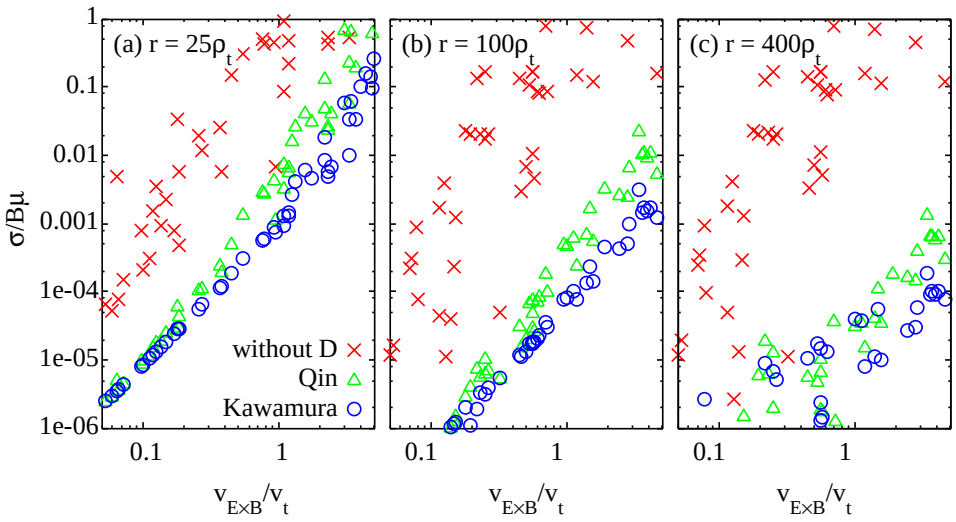

Figure 3.3: Standard deviations of energy oscillations for the $\mathbf{E}\times\mathbf{B}$ drift velocity. Figures (a), (b) and (c) correspond to three kinds of the initial positions of the particles, r/ρ_t = 25, 100 and 400, respectively. The cross, triangle and circle marks correspond to the gyrokinetic equations for $\mathbf{D} = 0$, the improved equations of Qin and the equations derived here, respectively.

that for the previous $\mathbf{D}_{\rm Qin}$, we confirm that the refinement of the gyrokinetic equations has been achieved by the new equilibrium velocity.

In order to study the dependence of the error on the various plasma parameters, we plot the standard deviations of the energy oscillation for various E, B, v_t and the initial velocity in Fig. 3.3. The standard deviation σ is normalized by the perpendicular energy $B\mu$ and can be interpreted as a relative error. The horizontal axis represents the $\mathbf{E}\times\mathbf{B}$ drift velocity normalized by the thermal velocity. Fig. 3.3(a), (b) and (c) correspond to three kinds of initial positions of the particle, r/ρ_t = 25, 100 and 400, respectively. The cross, triangle and circle marks correspond to the gyrokinetic equations for $\mathbf{D} = 0$, the improved equations of Qin and the equations derived here, respectively. The broad distributions in $\sigma/B\mu$, especially for the equations for $\mathbf{D} = 0$, are caused by the thermal spread in the perpendicular velocity space, which has a Maxwellian distribution. The relative error of the equations for $\mathbf{D} = 0$ does not depend on the initial position, which corresponds to the curvature of the potential contour in this case, while the error of the improved equations with $\mathbf{D}$ decreases for smaller curvature. This fact indicates that the error in the equations for $\mathbf{D} = 0$ depends on the electric field strength, while that of the equations with $\mathbf{D}$ depends on the second derivative of ϕ_0 rather than the first derivative or the strength of the electric field. This tendency agrees with the observation on the conservation of the magnetic moment in Sec. 3.3. The relative error with the present $\mathbf{D}$ is roughly estimated from

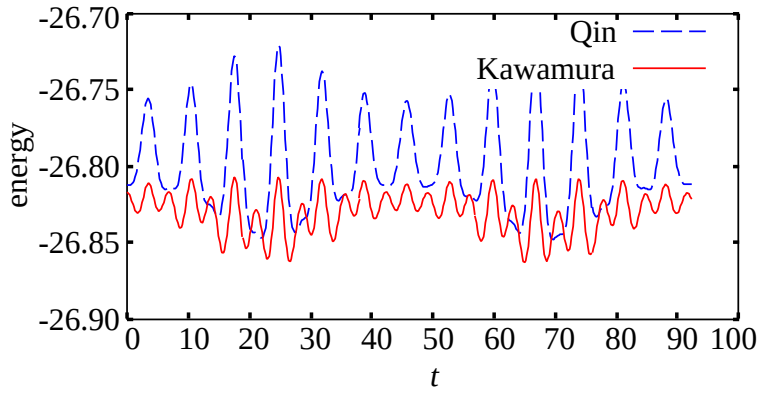

Figure 3.4: Time evolution of the particle energy. The solid and dashed lines correspond to the solution of our gyrokinetic equations and those of Qin, respectively.

Fig.3.3 as $\Delta \simeq (v_{\mathbf{E}\times\mathbf{B}}/v_t)^2/2(r/\rho_t)^2 = (E/rB\Omega)^2/2 \simeq (\nabla^2\phi/B\Omega)^2/2$. From the comparisons between the Qin's previous solutions (triangle marks in Fig. 3.3) and ours (circle marks), the reduction of the error is achieved when the $\mathbf{E}\times\mathbf{B}$ drift velocity exceeds approximately $1/10$ of the thermal velocity. The maximum reduction around $1/10$ is achieved when $v_{\mathbf{E}\times\mathbf{B}} > v_t$.

Finally, we examine the energy oscillation for a more general potential profile. We used an equilibrium potential with elliptic contours as an example; $\phi_0 = -E\sqrt{4x^2+y^2}$. The solution of Eq. (3.20) is numerically calculated. The time evolution of the particle energy calculated from the gyrokinetic equations for $\mathbf{D}$ and $\mathbf{D}_{\mathrm{Qin}}$ are shown in Fig. 3.4. The period, $T = 92$, equals to a one cycle of the rotation along the contour. At the beginning of the calculation, the particle is located on the x axis, $(x, y) = (l, 0)$, and drifts clockwise to $(0, -2l)$ at $t = T/4 = 23$. The slow variation of the envelope is caused by the spatial difference of the curvature of the potential contour. The amplitude of the energy oscillation is reduced by a factor of three also in the potential with elliptic contours.

The time evolution of the gyrocenter positions are also compared for the potential with elliptic contours. We solve the full-kinetic equations, the gyrokinetic equations formulated by Qin and ours from the same initial position and velocity. The deviation of the gyrocenter position from that of the full-kinetic results is presented in Fig. 3.5. The dashed and solid curves correspond to the solution of Qin's equations and ours. Our equations gives less deviation by a factor of three. The smallness of the deviation of the position represents the accuracy of the velocity given by the equations of motion.

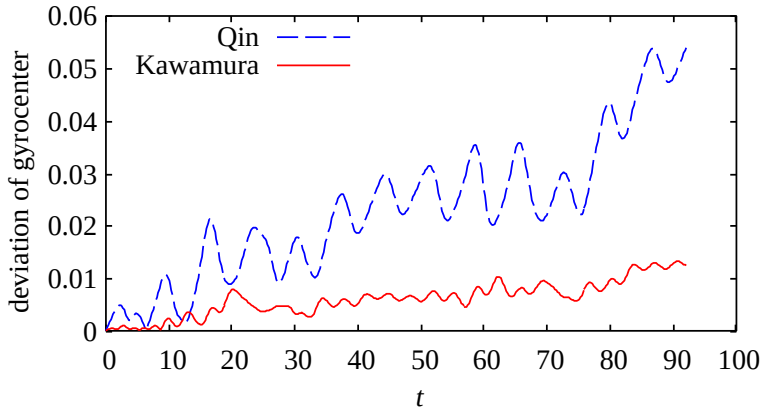

Figure 3.5: Time evolution of the deviation of gyrocenter position calculated by the gyrokinetic equations from that by the full-kinetic equations. The solid and dashed lines correspond to the results of Qin's gyrokinetic equations and those of ours, respectively.

3.7 Conclusions

Refinement of the equilibrium drift velocity in the gyrokinetic theory has been proposed for edge plasmas with large $\mathbf{E}\times\mathbf{B}$ flow shears. An equilibrium velocity field $\mathbf{D}$ is introduced in the coordinate transformations, Eqs. (3.1) and (3.2), to decouple the drift motion and gyration of a charged particle in the zeroth order dynamics in Eq. (3.7). We investigated the effects of the velocity $\mathbf{D}$ on the zeroth order equation of motion, especially on the magnetic moment μ, and obtained the practically most accurate expression of $\mathbf{D}$, Eq. (3.20).

Using the standard procedures of Lie perturbation analysis, we obtained the general expressions of Lie generator. Eq. (3.48), and the gyrokinetic 1-form, Eq. (3.51), up to the first order. As a limiting case, the electrostatic gyrokinetic equations of motion, (3.64) – (3.67), and the particle density, Eq. (3.71), were derived. It was confirmed that a term proportional to $\mathbf{D}\cdot\nabla\mathbf{D}$ in the gauge function, Eq. (3.59), used by Qin was canceled through the refinement of $\mathbf{D}$ in our gauge function, Eq. (3.57). This fact indicates that our modification in $\mathbf{D}$ reduces the error involved in the zeroth order dynamics.

The advantages of our formulation were also confirmed in the numerical verifications in Sec. 3.6. The accuracy of the equations of motion was estimated through the conservation of the particle energy calculated from the gyrocenter coordinate variables $\bar{Z} = (\bar{\mathbf{X}}, \bar{\Theta}, \bar{\mu}, \bar{V}_{\parallel})$. When the $\mathbf{E}\times\mathbf{B}$ drift velocity is comparable to the thermal velocity, the oscillatory behavior of the energy due to the truncations at the second order was reduced up to 1/10 in its standard deviation compared with the previous formulation by Qin.

From the analytic investigation and the numerical verifications, it has been confirmed

that the refinement of the equilibrium velocity **D** succeeds in obtaining more accurate equations of motion and gyrocenter coordinate. The general expressions of the charge and current densities were formulated and the approximated density equation (3.71) for the electrostatic potential was also obtained. Our formulation is, however, based on the single particle 1-form and thus the self-consistency for collective dynamics, or a plasma, is not fully ensured by itself. The self-consistency, e.g. conservation of the plasma energy, for the gyrokinetics without large equilibrium flow has been confirmed by the field theory [25]. The self-consistency is essential not only for the theoretical completeness but for the numerical simulation as a guarantee of the conservation of energy and momentum. The application of the field theory to the gyrokinetic theory with the strong $\mathbf{E} \times \mathbf{B}$ flow will be an important topic of further studies.

Chapter 4

Kinetic modeling of a sheath layer in a magnetized collisionless plasma

4.1 Introduction

Plasmas in the laboratory are usually contacting with walls. If the walls are electrically floating, negative charges accumulate on the walls and repel electrons until the electron flux balances with the ion flux. The repulsion of electrons causes a decrease of electron density and generates a nonneutral layer, namely sheath, in front of the wall. The strong electric field in the sheath layer with a width of a few Debye lengths causes acceleration of ions toward the wall. In fusion plasmas, the plasma is continuously produced in the core region and transported across the magnetic field over the separatrix. Since the magnetic field is open outside the separatrix, the plasma is transported mainly along the magnetic field toward the divertor plate. The core plasma, the peripheral plasma and the sheath layer are strongly linked with each other. A proper modeling of the sheath layer in a magnetic field is one of the important issues in transport analysis of the fusion plasmas.

In addition to the global transport study, local physical quantities near the wall surface are also important to understand the physics in the plasma-wall interaction. For examples, the electric field profile is essential information for the prediction of the behavior of dust particles [45]. The incident angle distribution of ions to the surface is also essential for obtaining the production rate of secondary electrons and the sputtering at the surface [46–48]. An analytic model of the sheath layer can provide physical insights about the dependences of these quantities on various plasma parameters and physical processes such as the polarization drift and the finite Larmor radius effect. The condition for a stable sheath formation is also a quite important issue in the analytic modeling of the sheath layer. The analytic treatment is superior to the particle-in-cell (PIC) simulation in order to extract these fundamental informations.

Recent theoretical investigations of unmagnetized plasmas [49–52] have been made to reveal the property of the self-consistent potential profile for the plasmas generated by ionization. The geometry used in these studies is one dimensional with length $2L$ and bounded by two facing walls at $x = \pm L$, which is called a fully bounded model. Plasma equations are solved in the half region $0 \leq x \leq L$ by virtue of the symmetry. This model is usually used for studies of a presheath, in which the ions are accelerated till the sheath edge defined by the equality of the generalized Bohm criterion, [53] i.e. $\left\langle v_{\mathrm{i}}^{-2} \right\rangle = m_{\mathrm{i}}/T_{\mathrm{e}}$. Since the electron Debye length λ_{De} is much shorter than the system length, the ratio λ_{De}/L is usually assumed to be zero.

A geometry such that a sheath layer connected with an infinite plasma is called a half-bounded model. The half-bounded model is usually used to study a sheath layer rather than a presheath layer and the the ratio of the Debye length to the system length is finite. [54–56] This model has an arbitrariness in the choice of the plasma at the source boundary and velocity distribution of the plasma source has to be specified. We adopt this geometry and use a shifted Maxwellian for the velocity distribution function of the plasma source. The velocity distribution of small velocity ions are truncated for the fulfillment of the generalized Bohm criterion.

The sheath formation in a magnetized plasma has drawn a lot of attention since Chodura and Daybelge revealed the properties of the magnetic presheath in the fluid and particle-in-cell (PIC) simulation study [56] and the kinetic study [57]. The most distinctive property is the existence of a characteristic length related to the magnetic field. The length of the magnetic presheath is roughly proportional to the ion Larmor radius, which was predicted by Chodura and confirmed by simulation studies [55, 58]. When the plasma is moderately magnetized, i.e. the ion Larmor radius is comparable or larger than the characteristic length, the full-kinetic equations including the cyclotron motion are usually solved in simulations [55, 58–60]. The dynamics of the magnetized plasma is sometimes described by the gyrokinetic theory on the assumption that the characteristic time is much longer than the gyration period. The extension of the theory to the plasmas with strong electric field has been developed by Littlejohn [17], Hahm [39] and Qin [28]. Recently Qin *et al.* published a review on the derivation of gyrokinetic equation which can be applied to the edge plasma with a strong electric field [40]. We adopt this theory to describe the potential profile in a magnetized plasma.

This chapter is organized as follows. First, we derive a equation which describes a potential profile in the sheath layer for an unmagnetized plasma from the stationary collisionless Vlasov equation in Sec. 4.2.1. In Sec. 4.3, a potential equation for a magnetized plasma is derived from the gyrokinetic Vlasov equation on the assumption that the ion gyroradius is smaller than the characteristic length of the potential profile. The gener-

alized Bohm criterion for a magnetized plasma is formulated. In Sec. 4.4, the numerical solutions of the potential equations for the magnetized sheath layer are obtained. Comparisons of the potential profiles between the analytical solutions and the full-kinetic particle simulation results for the same parameters are made and the validity of our modeling is discussed. Finally, conclusions are presented in Sec. 4.5.

4.2 Basic equations for a unmagnetized plasma

4.2.1 Model equations based on the Vlasov equation

We consider a plasma without magnetic field in this section prior to a magnetized plasma. Plasma profiles near a wall are essentially one-dimensional if the wall is large enough to be treated as an infinite flat plane. We assume a one-dimensional plasma and a plasma source which compensates the loss of particles at the wall. Fig. 4.1 shows the geometry of the plasma. The system length along the x axis is denoted by L and a perfectly absorbing wall is placed at $x = L$. The source plasma consists of electrons and ions of one species filling the region $x < 0$ and flows into the region in consideration, $0 < x < L$. The electrostatic potential ϕ is measured from the value at the source end, $x = 0$.

In the present analysis, we neglect the effect of collisions and particle generations in the sheath layer. The one dimensional system we consider here is similar to that in the simulation study [58, 61] except that there is no particle source in the sheath layer. For simplicity, we assume that the source region is sufficiently large and is not affected by the wall. The source plasma in the region $x < 0$ plays a role of source and also sink. All particles passing through the boundary $x = 0$ from positive x are just removed. The rate and the velocity distribution of newly injected particles from $x = 0$ have no correlation with the removed particles.

The equilibrium of the plasma can be determined from the energy conservation, $mv^2/2 + q\phi(x) = \text{const.}$, and the collisionless stationary Vlasov equation for a particle distribution function $f(x, v)$, $df/dt = 0$ or $f = \text{const.}$ along the particle trajectory. Here, the constants m and q represent the mass and the charge, respectively. The velocity distribution f at arbitrary x and v can be expressed as $f(x, v) = f_0\left(\sqrt{v^2 + 2q\phi/m}\right)$, where $f_0(v)$ is an initial distribution function at $x = 0$. By solving the Poisson equation $\partial^2\phi/\partial x^2 = -(1/\epsilon_0)\int_{-\infty}^{\infty}(q_i f_i + q_e f_e)\, dv$, we can obtain the potential profile as a function of x.

The plasma source and the sheath layer are strongly linked with each other and the distribution function at the source boundary $x = 0$ can not be determined by itself. We, however, have some clues on the distribution function in the presheath region. The velocity distribution of the plasma source can be assumed to be close to a Maxwellian be-

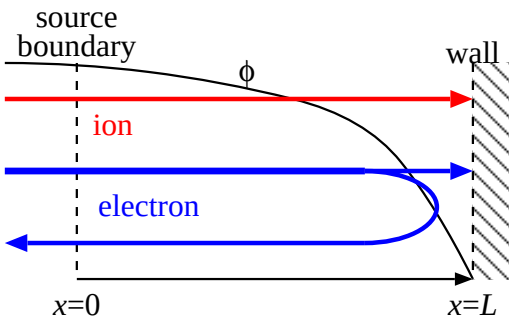

Figure 4.1: The schematic diagram of the sheath layer.

cause of the collisionality. The velocity distributions in the presheath region have been investigated in many studies [51, 58, 60–62]. These studies suggest the existence of a weak electric field in the presheath region which accelerates the ions until the generalized Bohm criterion, $\left\langle v_{\mathrm{i}}^{-2}\right\rangle \leq m_{\mathrm{i}}/T_{\mathrm{e}}$, is satisfied. The notation $\langle\ \rangle$ represents the average over the velocity space with a weight f;

$$\langle A(x,v)\rangle \equiv \frac{\int_{-\infty}^{\infty} A(x,v)f(x,v)\,dx}{\int_{-\infty}^{\infty} f(x,v)\,dx} \tag{4.1}$$

In this work, the distribution functions of electrons and ions at the source boundary, $x = 0$, are assumed to be shifted Maxwellians,

$$f_{0\mathrm{e}}(v) \equiv \frac{\nu_{\mathrm{e}} n_0}{\sqrt{2\pi}v_{\mathrm{te}}} \exp\left(-\frac{(v-\overline{v}_{\mathrm{e}})^2}{2v_{\mathrm{te}}^2}\right) \quad \text{for } v_{\mathrm{ce}} < v < \infty, \tag{4.2}$$

$$f_{0\mathrm{i}}(v) \equiv \frac{\nu_{\mathrm{i}} n_0}{Z\sqrt{2\pi}v_{\mathrm{ti}}} \exp\left(-\frac{(v-\overline{v}_{\mathrm{i}})^2}{2v_{\mathrm{ti}}^2}\right) \quad \text{for } v_{\mathrm{ci}} < v < \infty, \tag{4.3}$$

where the electron and ion drifting velocities $\overline{v}_{\mathrm{e}}$ and $\overline{v}_{\mathrm{i}}$ represent the amount of the velocity shift of the electron and ion velocity distributions, respectively. We note that the temperatures T_{e} and T_{i} and the corresponding thermal velocities $v_{\mathrm{te}} = \sqrt{T_{\mathrm{e}}/m_{\mathrm{e}}}$ and $v_{\mathrm{ti}} = \sqrt{T_{\mathrm{i}}/m_{\mathrm{i}}}$ in Eqs. (4.2) and (4.3) can deviate from the actual second-order velocity moment because of the existence of the cut-off in the velocity distributions by the minimum velocities $v_{\mathrm{ce}} < 0$ and $v_{\mathrm{ci}} > 0$. We write the effective temperature with a superscript '*', $T_{\mathrm{i}}^{*} \equiv \left\langle m_{\mathrm{i}} v_{\mathrm{i}}^2\right\rangle$. The electron cut-off velocity v_{ce} is determined by the wall potential $\Phi = \phi(L)$ as $v_{\mathrm{ce}} = -\sqrt{2e\Phi/m_{\mathrm{e}}}$. This cut-off velocity yields the electron normalization coefficient $\nu_{\mathrm{e}} = 2/\left[1 + \mathrm{erf}\left(\overline{v}_{\mathrm{e}}/\sqrt{2}v_{\mathrm{te}} + \sqrt{e\Phi/T_{\mathrm{e}}}\right)\right]$, where n_0 represents the density at $x = 0$. The ion normalization coefficient ν_{i} are also calculated as $\nu_{\mathrm{i}} = 2/\left[1 + \mathrm{erf}\left((\overline{v}_{\mathrm{i}} - v_{\mathrm{ci}})/\sqrt{2}v_{\mathrm{ti}}\right)\right]$. These normalization coefficients satisfy the charge neutrality, $n_{\mathrm{e}}(0) = Zn_{\mathrm{i}}(0) = n_0$.

Since zero-velocity ions violate the generalized Bohm criterion, the ions distribution function used here is truncated at a positive velocity v_{ci}. We solve the equality of the

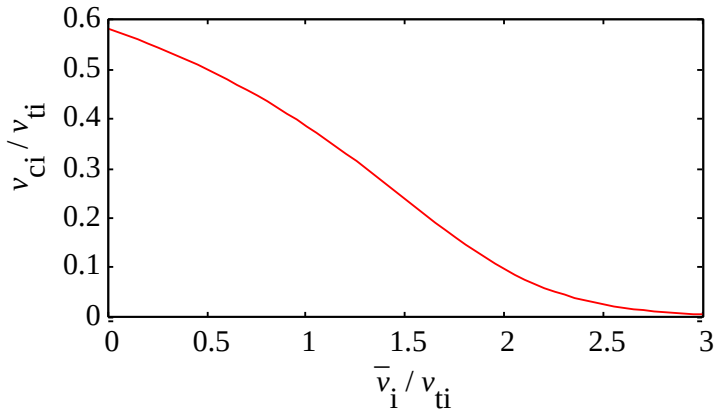

Figure 4.2: Minimum cut-off velocity v_{ci} as a function of $\overline{v}_i$. The generalized Bohm criterion is satisfied in the region above the curve.

generalized Bohm criterion, $B(\overline{v}_i, v_{ci}) \equiv Z(m_i/m_e)\left(\left\langle v_e^2\right\rangle - \langle v_e\rangle^2\right)\left\langle v_i^{-2}\right\rangle = 1$, and plot the numerical solution of v_{ci} as a function of $\overline{v}_i$ in Fig. 4.2. Here, we assume a hot hydrogen plasma; $T_i = T_e$, $m_i/m_e = 1836$, $q_i/q_e = -1$ and $\overline{v}_e = 0$. We note that the effective temperature ratio can varies according to the cut-off velocity v_{ci}. We should choose a set of parameters $\overline{v}_i$ and v_{ci} in the region above the curve to assure the generalized Bohm criterion $B \leq 1$. The minimum cut-off velocity has a value $v_{ci} \simeq 0.58 v_{ti}$ for $\overline{v}_i = 0$, and monotonically decreases as $\overline{v}_i$ increases. In the following discussions, we use $\overline{v}_e = 0$, $\overline{v}_i = 2v_{ti}$ and $v_{ci} = 0.1 v_{ti}$. The Bohm parameter has a slightly smaller value than unity, $B \simeq 0.96$, the wall potential is $\Phi \simeq -2.13 T_e/e$ and the actual temperature ratio is $T_i^*/T_e^* \simeq 0.97$ in this case.

The electric potential ϕ is assumed to be a monotonically decreasing function of the position x. The density and the particle flux can be calculated by the integral over the velocity space v;

$$n_s(x) = \int_{v_{min\,s}}^{\infty} f_{0s}\left(\sqrt{v^2 + \frac{2q_s}{m_s}\phi(x)}\right) dv, \tag{4.4}$$

$$\Gamma_s(x) = \int_{v_{min\,s}}^{\infty} v\, f_{0s}\left(\sqrt{v^2 + \frac{2q_s}{m_s}\phi(x)}\right) dv = \int_{v_{cs}}^{\infty} v\, f_{0s}(v)\, dv. \tag{4.5}$$

The lower limit of the integral, $v_{min\,s}$, represents the minimum velocity of the particles at the position x, and has a different form for each particle species according to the charge of the particles, $q_e = -e$ and $q_i = Ze$;

$$v_{min\,e} = -\sqrt{-\frac{2e}{m_e}(\Phi - \phi(x))}, \tag{4.6}$$

$$v_{min\,i} = \sqrt{v_{ci}^2 - \frac{2Ze}{m_i}\phi(x)}, \tag{4.7}$$

where Φ is a wall potential and $\Phi \le \phi \le 0$. The electron which has the velocity $v_{\min\,\mathrm{e}} < 0$ at the position x corresponds to the particle which was reflected just at the wall. The ion which has the velocity $v_{\min\,\mathrm{i}}$ at the position x corresponds to the particle which was injected at the velocity v_{ci} from $x = 0$. The wall potential Φ is determined from the particle flux balance between electrons and ions;

$$\Gamma_{\mathrm{e}} = Z\Gamma_{\mathrm{i}}. \tag{4.8}$$

This condition means the wall is perfectly absorbing and electrically floating.

For simplicity, we introduce the electron Debye length $\lambda_{\mathrm{De}} \equiv \sqrt{n_0 e^2/\epsilon_0 T_{\mathrm{e}}}$ and dimensionless parameters $\mu \equiv m_{\mathrm{i}}/m_{\mathrm{e}}$, $\tau \equiv T_{\mathrm{i}}/T_{\mathrm{e}}$, $\psi \equiv -e\phi/T_{\mathrm{e}}$, $M_{\mathrm{e}} \equiv \bar{v}_{\mathrm{e}}\sqrt{m_{\mathrm{i}}/T_{\mathrm{e}}} = \sqrt{\mu}\bar{v}_{\mathrm{e}}/v_{\mathrm{te}}$, $M_{\mathrm{i}} \equiv \bar{v}_{\mathrm{i}}\sqrt{m_{\mathrm{i}}/T_{\mathrm{e}}} = \sqrt{\tau}\bar{v}_{\mathrm{i}}/v_{\mathrm{ti}}$ and $C \equiv v_{\mathrm{ci}}\sqrt{m_{\mathrm{i}}/T_{\mathrm{e}}} = \sqrt{\tau}v_{\mathrm{ci}}/v_{\mathrm{ti}}$, where M_{e} and M_{i} represent the ratios of the drifting velocities $\bar{v}_{\mathrm{s}}$ to the cold-ion sound velocity $\sqrt{T_{\mathrm{e}}/m_{\mathrm{i}}}$ and C represents the ion cut-off velocity. We note that the normalized potential ψ has opposite sign to ϕ, thus $0 \le \psi \le \Psi \equiv -e\Phi/T_{\mathrm{e}}$. By using these parameters and the source velocity distribution function (4.2) and (4.3), the densities and the fluxes are calculated as

$$\frac{n_{\mathrm{e}}}{n_0} = \int_{-\sqrt{2(\Psi-\psi)}}^{\infty} \frac{\nu_{\mathrm{e}}}{\sqrt{2\pi}} \exp\left[-\frac{1}{2}\left(\sqrt{\hat{v}^2 + 2\psi} - \frac{M_{\mathrm{e}}}{\sqrt{\mu}}\right)^2\right] d\hat{v}, \tag{4.9}$$

$$\frac{n_{\mathrm{i}}}{n_0} = \int_{\sqrt{C^2+2Z\psi}}^{\infty} \frac{\nu_{\mathrm{i}}}{\sqrt{2\pi\tau}Z} \exp\left[-\frac{1}{2\tau}\left(\sqrt{\hat{v}^2 - 2Z\psi} - M_{\mathrm{i}}\right)^2\right] d\hat{v}, \tag{4.10}$$

$$\frac{\Gamma_{\mathrm{e}}}{n_0 v_{\mathrm{te}}} = \frac{\nu_{\mathrm{e}}}{\sqrt{2\pi}} \exp\left[-\left(\sqrt{\psi} - \frac{M_{\mathrm{e}}}{\sqrt{2\mu}}\right)^2\right] + \frac{\nu_{\mathrm{e}} M_{\mathrm{e}}}{2\sqrt{\mu}}\left[1 - \mathrm{erf}\left(\sqrt{\psi} - \frac{M_{\mathrm{e}}}{\sqrt{2\mu}}\right)\right], \tag{4.11}$$

$$\frac{\Gamma_{\mathrm{i}}}{n_0 v_{\mathrm{ti}}} = \frac{\nu_{\mathrm{i}}}{\sqrt{2\pi}Z} \exp\left(-\frac{(M_{\mathrm{i}} - C)^2}{2\tau}\right) + \frac{\nu_{\mathrm{i}} M_{\mathrm{i}}}{2\sqrt{\tau}Z}\left[1 + \mathrm{erf}\left(\frac{M_{\mathrm{i}} - C}{\sqrt{2\tau}}\right)\right]. \tag{4.12}$$

The wall potential Ψ is determined by the flux balance equation (4.8);

$$\begin{aligned}&\sqrt{\frac{2\mu}{\pi}} \exp\left[-\left(\sqrt{\Psi} - \frac{M_{\mathrm{e}}}{\sqrt{2\mu}}\right)^2\right] + M_{\mathrm{e}}\left[1 - \mathrm{erf}\left(\sqrt{\Psi} - \frac{M_{\mathrm{e}}}{\sqrt{2\mu}}\right)\right] \\ &= \frac{\nu_{\mathrm{i}}}{\nu_{\mathrm{e}}}\sqrt{\frac{2\tau}{\pi}} \exp\left(-\frac{(M_{\mathrm{i}} - C)^2}{2\tau}\right) + \frac{\nu_{\mathrm{i}}}{\nu_{\mathrm{e}}} M_{\mathrm{i}}\left[1 + \mathrm{erf}\left(\frac{M_{\mathrm{i}} - C}{\sqrt{2\tau}}\right)\right].\end{aligned} \tag{4.13}$$

The density profile is obtained from these equations as a function of potential ψ. By solving the Poisson equation

$$\lambda_{\mathrm{De}}^2 \frac{d^2\psi}{dx^2} = Z\frac{n_{\mathrm{i}}}{n_0} - \frac{n_{\mathrm{e}}}{n_0} \tag{4.14}$$

with the boundary conditions $\psi(0) = 0$ and $\psi(L) = \Psi$, a unique self-consistent potential is obtained as a function of the position x.

4.2.2 Generalized Bohm criterion for an unmagnetized plasma

The generalized Bohm criterion has been formulated by Harrison and Thompson [53] as a generalization of the original Bohm criterion for a plasma with a finite ion temperature. The physical meaning of the criterion is that the charge density increases as the potential decreases toward the wall, i.e. $d(Zen_\mathrm{i} - en_\mathrm{e})/d\phi \leq 0$. A stable sheath layer is automatically formed only if this condition is satisfied. In this section we recover the generalized Bohm criterion from the equations obtained in Sec. 4.2.1.

Before discussing the physical interpretation of the Bohm criterion, we calculate the derivative of the electron and ion density with respect of the potential. The electron and ion densities are given by

$$n_\mathrm{e}(x) = \int_{v_{\mathrm{min\,e}}}^{\infty} f_{\mathrm{e}0}\left(\sqrt{v^2 - \frac{2e}{m_\mathrm{e}}\phi}\right) dv, \tag{4.15}$$

$$n_\mathrm{i}(x) = \int_{v_{\mathrm{min\,i}}}^{\infty} f_{\mathrm{i}0}\left(\sqrt{v^2 + \frac{2Ze}{m_\mathrm{i}}\phi}\right) dv, \tag{4.16}$$

where the lower limits of the integrals are given in Eqs. (4.6) and (4.7). We assume the electron velocity distribution to be a Maxwellian at $x = 0$;

$$f_{\mathrm{e}0}(v) = \frac{n_0}{\sqrt{2\pi}v_\mathrm{te}} \exp\left(-\frac{v^2}{2v_\mathrm{te}^2}\right)\left[\frac{1}{2} + \frac{1}{2}\mathrm{erf}\left(\sqrt{-\frac{e\Phi}{T_\mathrm{e}}}\right)\right]^{-1}. \tag{4.17}$$

The value of the distribution function for the velocity below $v_{\mathrm{min\,e}}$ is defined as zero. Here we calculate the derivative of the electron density with respect to the potential ϕ as follows;

$$\begin{aligned}\frac{dn_\mathrm{e}}{d\phi} &= -\frac{dv_{\mathrm{min\,e}}}{d\phi} f_{\mathrm{e}0}\left(\sqrt{v_{\mathrm{min\,e}}^2 - \frac{2e}{m_\mathrm{e}}\phi}\right) - \int_{v_{\mathrm{min\,e}}}^{\infty} \frac{e}{m_\mathrm{e}\sqrt{v^2 - \frac{2e}{m_\mathrm{e}}\phi}} \frac{df_{\mathrm{e}0}}{dv}\left(\sqrt{v^2 - \frac{2e}{m_\mathrm{e}}\phi}\right) dv \\ &= \sqrt{-\frac{e}{2m_\mathrm{e}(\Phi - \phi)}} f_{\mathrm{e}0}\left(-\sqrt{-\frac{2e}{m_\mathrm{e}}\Phi}\right) + \int_{v_{\mathrm{min\,e}}}^{\infty} \frac{e}{m_\mathrm{e}v_\mathrm{te}^2} f_{\mathrm{e}0}\left(\sqrt{v^2 - \frac{2e}{m_\mathrm{e}}\phi}\right) dv, \end{aligned} \tag{4.18}$$

where the relation $df_{\mathrm{e}0}/dv = -vf_{\mathrm{e}0}/v_\mathrm{te}^2$ is used. In the limit of $x \to 0$, we obtain

$$\frac{dn_\mathrm{e}}{d\phi} = \sqrt{-\frac{e}{2m_\mathrm{e}\Phi}} f_{\mathrm{e}0}\left(-\sqrt{-\frac{2e}{m_\mathrm{e}}\Phi}\right) + \frac{n_0 e}{m_\mathrm{e}v_\mathrm{te}^2} \simeq \frac{n_0 e}{T_\mathrm{e}}. \tag{4.19}$$

We employ the approximation $\exp(e\Phi/m_\mathrm{e}v_\mathrm{te}^2) \ll 1$ in the second equality. The derivative of the ion density is obtained similarly as

$$\frac{dn_\mathrm{i}}{d\phi} = -\frac{dv_{\mathrm{min\,i}}}{d\phi}\left[f_{\mathrm{i}0}\left(\sqrt{v_{\mathrm{min\,i}}^2 + \frac{2Ze}{m_\mathrm{i}}\phi}\right) + f_{\mathrm{i}0}\left(-\sqrt{v_{\mathrm{min\,i}}^2 + \frac{2Ze}{m_\mathrm{i}}\phi}\right)\right]$$

$$
\begin{aligned}
&+\int_{v_{\mathrm{min\,i}}}^{\infty}\frac{Ze}{m_{\mathrm{i}}\sqrt{v^2+\frac{2Ze}{m_{\mathrm{i}}}\phi}}\frac{df_{\mathrm{i0}}}{dv}\left(\sqrt{v^2+\frac{2Ze}{m_{\mathrm{i}}}\phi}\right)dv\\
&+\int_{-\infty}^{-v_{\mathrm{min\,i}}}\frac{Ze}{m_{\mathrm{i}}\sqrt{v^2+\frac{2Ze}{m_{\mathrm{i}}}\phi}}\frac{df_{\mathrm{i0}}}{dv}\left(-\sqrt{v^2+\frac{2Ze}{m_{\mathrm{i}}}\phi}\right)dv\\
=&\sqrt{-\frac{Ze}{2m_{\mathrm{i}}\phi}}f_{\mathrm{i0}}(0)+\int_{v_{\mathrm{min\,i}}}^{\infty}\frac{Ze}{m_{\mathrm{i}}\sqrt{v^2+\frac{2Ze}{m_{\mathrm{i}}}\phi}}\frac{df_{\mathrm{i0}}}{dv}\left(\sqrt{v^2+\frac{2Ze}{m_{\mathrm{i}}}\phi}\right)dv\\
&+\int_{-\infty}^{-v_{\mathrm{min\,i}}}\frac{Ze}{m_{\mathrm{i}}\sqrt{v^2+\frac{2Ze}{m_{\mathrm{i}}}\phi}}\frac{df_{\mathrm{i0}}}{dv}\left(-\sqrt{v^2+\frac{2Ze}{m_{\mathrm{i}}}\phi}\right)dv. \qquad (4.20)
\end{aligned}
$$

We require the condition $f_{\mathrm{i0}}(0)=0$ to take the limit of $x\to 0$ and then we obtain

$$
\begin{aligned}
\left.\frac{dn_{\mathrm{i}}}{d\phi}\right|_{x=0}&=\int_{+0}^{\infty}\frac{Ze}{m_{\mathrm{i}}v}\frac{df_{\mathrm{i0}}}{dv}(v)dv+\int_{-\infty}^{-0}\frac{Ze}{m_{\mathrm{i}}v}\frac{df_{\mathrm{i0}}}{dv}(-v)dv\\
&=\mathrm{P}\!\int_{-\infty}^{\infty}\frac{Ze}{m_{\mathrm{i}}v}\frac{df_{\mathrm{i0}}}{dv}(v)dv, \qquad (4.21)
\end{aligned}
$$

where the notation $\mathrm{P}\!\int$ represents the principal integration. We require also the condition $(df_{\mathrm{i0}}/dv)(0)=0$ for the integral to be finite. The integration by parts yields

$$
\left.\frac{dn_{\mathrm{i}}}{d\phi}\right|_{x=0}=\mathrm{P}\!\int_{-\infty}^{\infty}\frac{Ze}{m_{\mathrm{i}}v^2}f_{\mathrm{i0}}(v)dv \qquad (4.22)
$$

From the above calculations we obtain the derivative of the charge density as

$$
\frac{d\rho}{d\phi}=\frac{Z^2e^2}{m_{\mathrm{i}}}\mathrm{P}\!\int_{-\infty}^{\infty}\frac{f_{\mathrm{i0}}(v)}{v^2}dv-\frac{n_0e^2}{T_{\mathrm{e}}}. \qquad (4.23)
$$

The spatial potential profile is determined by the Poisson equation, $\nabla^2\phi=-\rho/\epsilon_0$, for a given charge density ρ. Using the relation, $d/dx=(d\phi/dx)d/d\phi$, we can rewrite the Poisson equation as

$$
\frac{\epsilon_0}{2}\frac{d}{d\phi}\left(\frac{d\phi}{dx}\right)^2=-\rho. \qquad (4.24)
$$

Since the squire of the electric field, $(d\phi/dx)^2$, should be positive and the charge density is practically zero at the sheath edge, the monotonically decreasing potential requires $d\rho/d\phi\le 0$, i.e. $d\phi/dx\le 0$ and $d\rho/dx\ge 0$. This requirement is the generalized Bohm criterion;

$$
\frac{Z^2e^2}{m_{\mathrm{i}}}\mathrm{P}\!\int_{-\infty}^{\infty}\frac{f_{\mathrm{i0}}(v)}{v^2}dv\le\frac{n_{\mathrm{e0}}e^2}{T_{\mathrm{e}}}\quad\text{or}\quad Z\left\langle v_{\mathrm{i}}^{-2}\right\rangle\le\frac{m_{\mathrm{i}}}{T_{\mathrm{e}}}, \qquad (4.25)
$$

where the charge neutrality, $Zn_{\mathrm{i0}}=n_{\mathrm{e0}}$, is use. We note that the expression derived here relies on the following assumptions; $f_{\mathrm{i0}}|_{v=0}=0$, $df_{\mathrm{i0}}/dv|_{v=0}=0$ and $\exp(e\Phi/m_{\mathrm{e}}v_{\mathrm{te}}^2)\ll 1$.

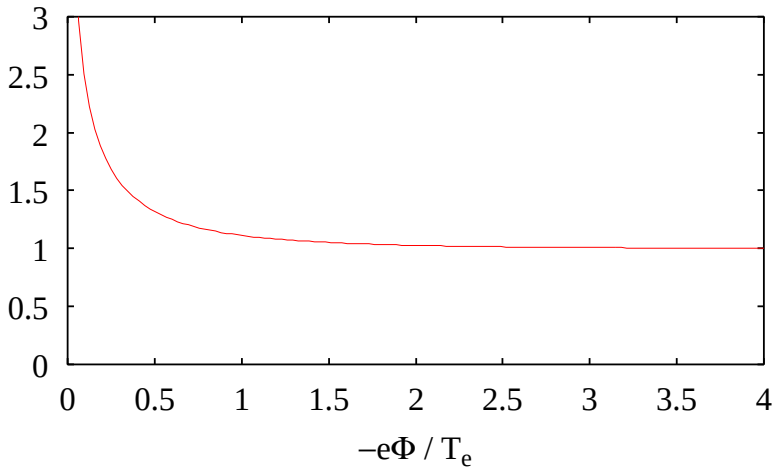

Figure 4.3: The influence of the correction term in Eq. (4.26). The right hand side of the equation is plotted as a function of the normalized potential $e\Phi/T_e$.

The last one can be excluded by using the more general expression;

$$\frac{ZT_e}{m_i}\left\langle v_i^{-2}\right\rangle \leq 1+\frac{1}{2\sqrt{\pi}}\sqrt{-\frac{T_e}{e\Phi}}\exp\left(\frac{e\Phi}{T_e}\right)\left[\frac{1}{2}+\frac{1}{2}\mathrm{erf}\left(\sqrt{-\frac{e\Phi}{T_e}}\right)\right]^{-1} \tag{4.26}$$
$$\simeq \left[1-\frac{1}{2\sqrt{\pi}}\sqrt{-\frac{T_e}{e\Phi}}\exp\left(\frac{e\Phi}{T_e}\right)\right]^{-1}.$$

The approximation in the second equality is valid for $-e\Phi/T_e \gtrsim 0.5$. The second term in the right hand side is a correction due to the electron cut-off velocity caused by the absorption at the wall. The right hand side is plotted as a function of the normalized potential $e\Phi/T_e$ in Fig. 4.3. The influence of the correction term is restrictive. If the normalized wall potential is larger than unity as is often the case, the deviation of Eq. (4.26) from unity is relatively small.

4.3 Basic equations for a magnetized plasma

4.3.1 Model equations based on the gyrokinetic theory

In this section, we derive a set of equations describing a potential profile in a magnetized sheath layer. The motion of a magnetized particle is essentially four dimensional at least; one dimension for a space coordinate normal to the wall and three dimensions for the parallel velocity along the magnetic field and the perpendicular velocities. It means that the system has additional degrees of freedom compared with the unmagnetic case in the last section, therefore obtaining a rigorous solution is a rather difficult task. In some cases

where the Larmor radius is sufficiently smaller than the characteristic length of the sheath potential profile, however, we can separate the dynamics of the parallel and perpendicular motions, eliminate the perpendicular velocities and treat the plasma as one dimensional system.

Magnetized plasmas have three kinds of characteristic lengths, Debye length λ_{De}, thermal Larmor radius ρ and mean free path l_{mfp}. Ions and electrons have their Larmor radii and mean free paths, respectively. We discuss a one component plasma first. The mean free path is usually much longer than the Debye length, but the ratios of ρ to λ_{De} and l_{mfp} differ according to the plasma parameters. Thus, we classify the relative magnitudes of the Larmor radius to the other lengths into three cases; (i) $0 < \rho < \lambda_{\mathrm{De}}$, (ii) $\lambda_{\mathrm{De}} < \rho < l_{\mathrm{mfp}}$ and (iii) $l_{\mathrm{mfp}} < \rho$. The first case corresponds to a strong magnetic field case or a low pressure plasma. The particle motion is dominated by the cyclotron motion and thus, the velocity spaces can be separated to the parallel and perpendicular velocities. The velocity coordinates $v_{\parallel}$ and $v_{\perp}$ can be described by two different equation of motion. Since the perpendicular velocity coordinate can be ignored because of the conservation law of the magnetic momentum in a uniform magnetic field, the dynamics of the plasma can be reduced to one dimensional. The third case, $\rho > l_{\mathrm{mfp}}$, corresponds to weak magnetic field. Since a particle suffers collisions during a gyration period, the velocity spaces tend to be isotropic except the average flow toward the wall. Therefore, the plasma in this case can be also treated as one dimensional system on the assumption of the high collisionality. In the second case, however, the dynamics of a particle is quite complicated because of the shorter characteristic length of the potential profile and the existence of collisions. The dynamics in velocity spaces must be treated as three dimensional and described directly by the full-kinetic equations of motion. Therefore, PIC or Vlasov simulations are required to obtain the potential profile in the sheath layer.

When the plasma consists of ions and electrons, the ratio $\rho/\lambda_{\mathrm{De}}$ is classified into five regions as shown in Fig. 4.4. We assume that the ion mean free path $l_{\mathrm{mfp\,i}}$ is much shorter than $\sqrt{m_{\mathrm{i}}/m_{\mathrm{e}}}\lambda_{\mathrm{De}}$. The horizontal axis represents the squared ratio $\rho_{\mathrm{i}}^2/\lambda_{\mathrm{De}}^2$. The actual range near the divertor plates of fusion devices [55] is around $1 \lesssim \rho_{\mathrm{i}}^2/\lambda_{\mathrm{De}}^2 \lesssim 1000$. The regions where the plasma can be treated as one dimension is the first from the left end, $\rho_{\mathrm{i}} < \lambda_{\mathrm{De}}$, the third, $l_{\mathrm{mfp\,i}} < \rho_{\mathrm{i}} < \sqrt{m_{\mathrm{i}}/m_{\mathrm{e}}}\lambda_{\mathrm{De}}$ and the fifth, $\rho_{\mathrm{i}} > \sqrt{m_{\mathrm{i}}/m_{\mathrm{e}}}f_{\mathrm{mfp\,e}}$ or $\rho_{\mathrm{e}} > f_{\mathrm{mfp\,e}}$. The other regions, $\lambda_{\mathrm{De}} < \rho_{\mathrm{i}} < f_{\mathrm{mfp\,i}}$ and $\lambda_{\mathrm{De}} < \rho_{\mathrm{e}} < f_{\mathrm{mfp\,e}}$ require three dimensional full-kinetic description for ions or electrons, respectively.

In this work, we concentrate on the first case, $\rho_{\mathrm{i}} < \lambda_{\mathrm{De}}$. The magnetic field is assumed to be sufficiently strong so that a gyrating orbit of ion can be regarded as a small but finite circle around a guiding center. The motion of guiding center is described by the gyrokinetics on the assumption that the gyroradius is much smaller than the charac-

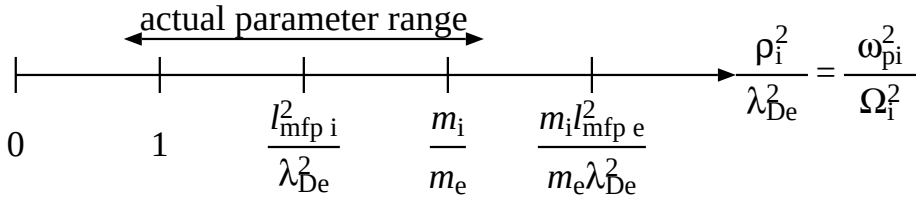

Figure 4.4: Schematic diagram of various characteristic lengths, Debye length λ_{De}, Larmor radius ρ_i and mean free path l_{mfp}. The actual parameter range of $\rho_\mathrm{i}/\lambda_{\mathrm{De}}$ is around $1 \lesssim \rho_\mathrm{i}^2/\lambda_{\mathrm{De}}^2 \lesssim 1000$ near divertor plates of fusion devices.

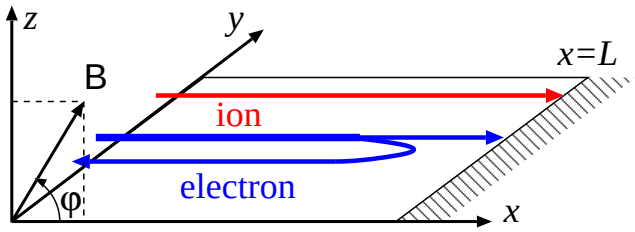

Figure 4.5: Geometry of the magnetic sheath model.

teristic scale length of the spatial inhomogeneity. The gyrokinetic theories generalized for a strong electric field [17, 28, 39, 40] have been developed to describe a edge plasma accompanied with a large equilibrium radial electric field. The difference from the ordinal gyrokinetic theory is that the particle velocity is measured on a frame moving with the $\mathbf{E}\times\mathbf{B}$ drift velocity. This gyrokinetic theory enables one to obtain the potential equations in a magnetized sheath layer.

We assume a one dimensional system shown in Fig. 4.5. The potential and density profiles along y and z directions are uniform and the uniform magnetic field B is on the y-z plain. The formulation is similar to that of the unmagnetized case except that the equations are expressed in the gyrocenter coordinates $(\mathbf{X}, \theta, \bar{\mu}, v_\parallel)$. The magnetic momentum $\bar{\mu}$ is measured on the moving frame with the $\mathbf{E}\times\mathbf{B}$ drift velocity $\mathbf{D} = \hat{\mathbf{b}}\times\nabla\phi(\mathbf{X})/B$;

$$\bar{\mu} = \frac{m\left|\mathbf{v} - v_\parallel\hat{\mathbf{b}} - \mathbf{D}\right|^2}{2B} = \frac{mv_\perp^2}{2B} + \frac{qv_\perp}{B\Omega}\hat{\mathbf{r}}\cdot\nabla\phi + \frac{q^2}{2mB\Omega^2}|\nabla_\perp\phi|^2, \tag{4.27}$$

where the vector $\hat{\mathbf{b}} = \mathbf{B}/B$ is an unit vector parallel to the magnetic field. The gyrocenter position $\mathbf{X}$ is defined also in the moving frame;

$$\mathbf{X} = \mathbf{x} - \frac{|\mathbf{v} - v_\parallel\hat{\mathbf{b}} - \mathbf{D}|}{\Omega}\hat{\mathbf{r}} = \mathbf{x} - \frac{\sqrt{2B\bar{\mu}/m}}{\Omega}\hat{\mathbf{r}}. \tag{4.28}$$

The unit vector $\hat{\mathbf{r}}$ represents the gyro-radius vector and is a function of the gyrophase θ; $\hat{\mathbf{r}}(\theta) = \hat{\mathbf{y}}\times\hat{\mathbf{b}}\cos\theta - \hat{\mathbf{y}}\sin\theta$. The particle velocity on the stationary frame is expressed as

$\mathbf{v} = v_\parallel \hat{\mathbf{b}} + \sqrt{2B\bar{\mu}/m}\hat{\mathbf{r}} \times \hat{\mathbf{b}} + \mathbf{D}$. The gyrocenter $\mathbf{X}$ and the ordinary guiding-center $\mathbf{X}'$ are related by the equation

$$\begin{aligned}\mathbf{X} - \mathbf{X}' &= \left[\mathbf{x} - \frac{\sqrt{2B\bar{\mu}/m}}{\Omega}\hat{\mathbf{r}}(\theta)\right] - \left[\mathbf{x} - \frac{v_\perp}{\Omega}\hat{\mathbf{r}}(\theta')\right] \\ &= -\frac{1}{B\Omega}\nabla_\perp \phi(\mathbf{X}),\end{aligned} \tag{4.29}$$

where the relation of the perpendicular velocity $v_\perp \hat{\mathbf{r}}(\theta') \times \hat{\mathbf{b}} = \sqrt{2B\bar{\mu}/m}\hat{\mathbf{r}}(\theta) \times \hat{\mathbf{b}} + \mathbf{D}$ is used. The gyrophase θ' is measured in the stationary frame. From Eq. (4.29), we can confirm that the gyrocenter $\mathbf{X}$ includes the polarization shift $\mathbf{E}_\perp / B\Omega$. The two kinds of gyrophases θ and θ' are also related by the equation

$$v_\perp \cos\theta' - \sqrt{2B\bar{\mu}/m}\cos\theta = -\hat{\mathbf{y}} \cdot \mathbf{D} = -\frac{1}{B}\hat{\mathbf{y}} \times \hat{\mathbf{b}} \cdot \nabla\phi. \tag{4.30}$$

The energy conservation equation is rewritten in the gyrocenter coordinates $(\mathbf{X}, \theta, \bar{\mu}, v_\parallel)$ as

$$H = \frac{m}{2}v_\parallel^2 + B\bar{\mu} + q\phi + \frac{\bar{\mu}}{2\Omega}\nabla_\perp^2\phi + \frac{q^2}{2m\Omega^2}|\nabla_\perp \phi|^2 = \text{const.} \tag{4.31}$$

The particle density is expressed by an integral of a gyrocenter distribution function F with respect to the stationary velocity space $(\theta, v_\perp, v_\parallel)$;

$$n(\mathbf{x}) = \int F(\mathbf{X}, \theta, \bar{\mu}, v_\parallel) v_\perp d\theta dv_\perp dv_\parallel. \tag{4.32}$$

The arguments of the function $F(\mathbf{X}, \theta, \bar{\mu}, v_\parallel)$ are treated as functions of the stationary velocity space. This transformation is called pullback [20] and provides expressions of physical quantities on both the stationary and the gyrocenter coordinate systems.

The formulation itself is quite similar to that in Sec. 4.2.1. The magnetic momentum $\bar{\mu}$ in Eq. (4.31) can be ignored because of the conservation property, $\bar{\mu} = \text{const}$, and the energy conservation equation becomes one dimensional;

$$\frac{m}{2}v_\parallel^2 + q\phi_{\text{gyro}} = \text{const.} \tag{4.33}$$

This equation is almost the same as the unmagnetized expression except that the potential is modified to the effective potential

$$\phi_{\text{gyro}} = \phi + \frac{\bar{\mu}}{2q\Omega}\nabla_\perp^2\phi + \frac{q}{2m\Omega^2}|\nabla_\perp \phi|^2. \tag{4.34}$$

When the perpendicular velocity distributions are simple Maxwellian and the parallel velocity distributions are given by the shifted Maxwellian (4.2) and (4.3), the densities

and the fluxes are expressed as

$$\frac{n_\mathrm{e}}{n_0} = \int_{-\sqrt{2(\Psi-\psi)}}^{\infty} \frac{\nu_\mathrm{e}}{\sqrt{2\pi}} \exp\left[-\frac{1}{2}\left(\sqrt{v_\parallel^2 + 2\psi} - \frac{M_\mathrm{e}}{\sqrt{\mu}}\right)^2\right] dv_\parallel, \tag{4.35}$$

$$\frac{n_\mathrm{i}}{n_0} = \int_0^{2\pi}\int_0^{\infty}\int_{\sqrt{2\psi_\mathrm{gyro}}}^{\infty} \frac{\nu_\mathrm{i}}{\sqrt{2\pi\tau}Z} \exp\left[-\frac{1}{2\tau}\left(\sqrt{v_\parallel^2 - 2\psi_\mathrm{gyro}} - M_\mathrm{i}\right)^2\right] \times \exp\left(-\frac{\hat{V}_\perp^2}{2}\right)(1 - f_\mathrm{loss}) v_\perp \, dv_\parallel dv_\perp d\theta, \tag{4.36}$$

$$\frac{\Gamma_\mathrm{e}}{n_0 v_\mathrm{te}} = \mathbf{N}\cdot\hat{\mathbf{b}}\nu_\mathrm{e}\left\{\frac{1}{\sqrt{2\pi}}\exp\left[-\left(\sqrt{\Psi} - \frac{M_\mathrm{e}}{\sqrt{2\mu}}\right)^2\right] + \frac{M_\mathrm{e}}{2\sqrt{\mu}}\left[1 - \mathrm{erf}\left(\sqrt{\Psi} - \frac{M_\mathrm{e}}{\sqrt{2\mu}}\right)\right]\right\} \tag{4.37}$$

$$\frac{\Gamma_\mathrm{i}}{n_0 v_\mathrm{ti}} = \mathbf{N}\cdot\hat{\mathbf{b}}\nu_\mathrm{i}\left\{\frac{1}{\sqrt{2\pi}Z}\exp\left(-\frac{M_\mathrm{i}^2}{2\tau}\right) + \frac{M_\mathrm{i}}{2\sqrt{\tau}}\left[1 + \mathrm{erf}\left(\frac{M_\mathrm{i}}{\sqrt{2\tau}}\right)\right]\right\}. \tag{4.38}$$

The newly introduced function f_loss represents the particle loss due to the absorption of particles in gyration at the wall. The detail of f_loss is discussed in the next section. We defined, here, a normalized gyration velocity $\hat{V}_\perp = \sqrt{2B\bar{\mu}/m_\mathrm{i}}/v_\mathrm{ti}$, a unit vector $\mathbf{N}$ normal to the wall and a normalized effective potential for ions

$$\psi_\mathrm{gyro} = \psi + \frac{\tau\omega_\mathrm{pe}^2}{2\mu\Omega_\mathrm{i}^2}\left(\frac{\hat{V}_\perp^2}{2}\nabla_\perp^2\psi - \frac{Z}{\tau}|\nabla_\perp\psi|^2\right). \tag{4.39}$$

The Poisson equation is the same as Eq. (4.14). These equations are similar to those of the unmagnetized plasma (4.9) – (4.14) except three points, the effective potential for ion, the ion density equation and the parallel flux coefficient $\mathbf{N}\cdot\hat{\mathbf{b}}$.

4.3.2 Particle loss at a wall

In the gyrokinetic theory, a particle is usually treated as a charged 'ring' driven by a force due to the effective potential ψ_gyro representing the averaged potential over the ring. This concept makes the rigorous treatment of finite size plasmas, especially bounded by walls, difficult, because a wall may cut the ring and cause some inconsistency. If the ring is assumed to keep its shape when it overlaps with the wall, the density will be overestimated and the temperature will be also overestimated because faster particles tend to be lost more rapidly even if the gyrocenters are at the same distance from the wall. If the ring is assumed to be lost when some part of it touches the wall, the density and the temperature will be underestimated.

The concept of 'ring' is based on the assumption that the gyrocenter distribution has no gyrophase dependence, i.e. $\partial F/\partial\theta = 0$. That is true in many cases without wall or some other spatial discrete effect. In the sheath analyses, however, we need to consider

an inhomogeneous gyrophase distribution near the wall. Therefore, we have introduced the particle loss factor $f_{\rm loss}$ into the ion distribution function.

$$F(\mathbf{X}, \theta, \bar{\mu}, v_{\parallel}) = [1 - f_{\rm loss}(\mathbf{X}, \theta, \bar{\mu}, v_{\parallel})]\bar{F}(\mathbf{X}, \bar{\mu}, v_{\parallel}) \tag{4.40}$$

The factor $f_{\rm loss}$ represents simply whether a particle is lost or not. If the point $(\mathbf{X}, \theta, \bar{\mu}, v_{\parallel})$ is on the trajectory which has cross points with the wall in the past, $f_{\rm loss}$ takes the value one. If the particle on the point experiences no collision with the wall in the past, $f_{\rm loss}$ is zero.

In order to evaluate $f_{\rm loss}$, we examined three kinds of coordinate system, the stationary frame, the guiding-center frame and the gyrocenter frame. We calculated a particle trajectory numerically for the fields $\mathbf{B} = 1/4\,\hat{\mathbf{x}} + \sqrt{15/16}\,\hat{\mathbf{z}}$ and $\mathbf{E}(x) = x/8$ from the initial point $\mathbf{x}_0 = \mathbf{0}$ and $\mathbf{v}_0 = \hat{\mathbf{x}}$. The results are shown in Fig. 4.6. The three curves correspond to the stationary frame (dashed curve), the guiding-center frame (dotted curve) and the gyrocenter frame (solid curve). The original trajectory on the stationary frame is too complex to determine whether the particle hits the wall. The second one is rather simple because the $\mathbf{E} \times \mathbf{B}$ motion and the parallel motion is canceled. However, it still includes the polarization drift which is caused by the change of the electric field due to the parallel motion. The third one is almost completely circular motion because the gyrocenter used in this work includes the polarization shift.

The calculation of the loss factor $f_{\rm loss}$ is carried out on the frame of the gyrocenter. Since the gyrocenter motion includes the parallel, $\mathbf{E} \times \mathbf{B}$ drift and polarization drift velocities, the particle motion on this frame is just a simple gyration with a perpendicular velocity $v_{\perp} = \sqrt{2B\bar{\mu}/m}$. The wall approaches from the right hand side with a velocity $v_{\parallel} \cos\phi$, where φ represents a angle between the magnetic field and the normal direction to the wall. These motions are illustrated in Fig. 4.7. The two figures show the projections of the particle orbits to the z-x and y-x planes. The wall is assumed to locate at the distance l from the gyrocenter. Since we assume that a particle is absorbed once it touches the wall, the loss factor can be obtained to see whether the distance $\Delta(t)$ between the particle and the wall has been negative in the past $t < 0$;

$$\Delta(t) = l - v_{\parallel} t \cos\varphi + \frac{v_{\perp}}{\Omega} \sin\varphi \cos(\theta + \Omega t). \tag{4.41}$$

We neglect the acceleration due to the electric field because the change of the parallel velocity during the one cyclotron period $2\pi/\Omega$ is small. Since the parallel velocity is always positive, it is sufficient to examine only a gyro-period. The algorithm used in our code is as follows. (i) if the distance $\Delta(0)$ is negative, $f_{\rm loss} = 1$. (ii) if $\Delta(t)$ is monotonically decreasing function, i.e. the time derivative of $\Delta(t)$ is non-positive, $v_{\parallel} \cos\varphi \geq v_{\perp} \sin\varphi$, the function $\Delta(t)$ is always positive for $t < 0$, therefore $f_{\rm loss} = 0$. The time derivative of $\Delta(t)$

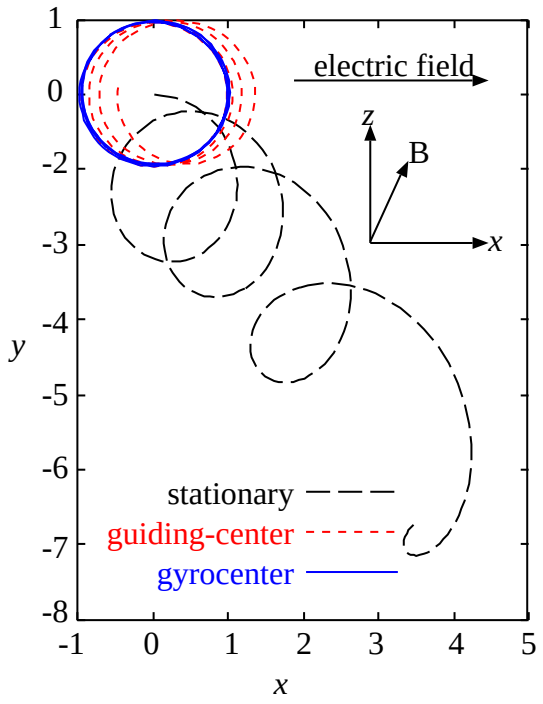

Figure 4.6: Particle trajectories on the stationary frame (dashed curve), the guiding-center frame (dotted curve) and the gyrocenter frame (solid curve).

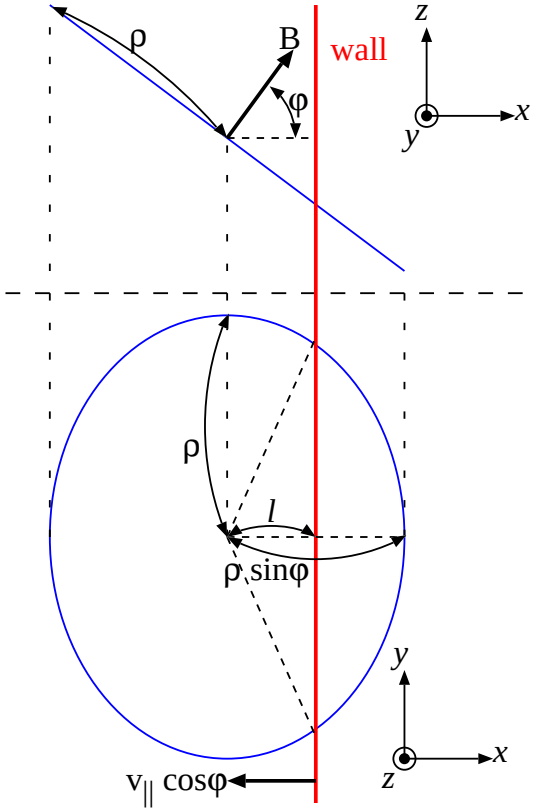

Figure 4.7: Schematic diagrams of a particle trajectory on the gyrocenter frame. The particle motion is simple gyration and the wall is approaching from the right hand side with the velocity $v_{\parallel}\cos\varphi$.

is given by $d\Delta/dt = -v_{\parallel}\cos\varphi - v_{\perp}\sin\varphi\sin(\theta+\Omega t)$. (iii) if a negative extremal value exists in $-2\pi \le \Omega t < 0$, $f_{\rm loss} = 1$. The extremal values are given by solving the equation $d\Delta/dt = 0$. Two solutions always exist;

$$\begin{cases} \Omega t_1 &= -\theta - \sin^{-1}\left(-\dfrac{v_{\parallel}\cos\varphi}{v_{\perp}\sin\varphi}\right) & (\mathrm{mod}\ -2\pi), \\ \Omega t_2 &= -\theta + \sin^{-1}\left(-\dfrac{v_{\parallel}\cos\varphi}{v_{\perp}\sin\varphi}\right) + \pi & (\mathrm{mod}\ -2\pi), \end{cases} \tag{4.42}$$

where the notation (mod -2π) represents the selection of the solutions in $-2\pi \le \Omega t < 0$. (iv) if the condition (iii) does not hold true, $f_{\rm loss} = 0$.

4.3.3 Generalized Bohm criterion for a magnetized plasma

As the analytic model equation of a magnetized plasma has been obtained, now we can formulate the corresponding criterion for the magnetized plasma. In the formulation of the magnetized Bohm criterion here, we assume that the ion Larmor radius is much smaller than the system length and also much smaller than the scale length of the density and the potential in the presheath, i.e. $v_\perp/\Omega \ll L$ and $v_\perp/\Omega \ll L_\phi$. We note that the scale length of the density and the potential is comparable in the presheath, $Zn_\mathrm{i} = n_\mathrm{e} \simeq n_0(1 + e\phi/T_\mathrm{e})$. Since the sheath edge, which is defined by the equality of the Bohm criterion, is far from the wall, the ion loss factor is ignored, i.e $f_\mathrm{loss} = 0$. For simplicity, we use the so called long wave length approximation, $\epsilon \sim (v_\mathrm{t}/\Omega)/L_\phi \ll 1$, and expand terms up to the second order, e.g. $\phi(\mathbf{x}) \simeq \phi(\mathbf{X}) + (v_\perp/\Omega)\hat{\mathbf{a}} \cdot \nabla\phi + (v_\perp/\Omega)^2 \hat{\mathbf{a}}\hat{\mathbf{a}} : \nabla\nabla\phi/2$ and $\langle\phi\rangle \simeq \phi(\mathbf{X}) + (v_\perp/\Omega)^2\nabla_\perp^2\phi/4$. After straightforward calculations, the ion density equation (4.36) yields the familiar equation used in many gyrokinetic theories;

$$\begin{aligned} n_\mathrm{i} &= \overline{n}_\mathrm{i} + \frac{T_\mathrm{i}}{2m_\mathrm{i}\Omega_\mathrm{i}^2}\nabla_\perp^2\overline{n}_\mathrm{i} + \frac{Ze}{m_\mathrm{i}\Omega_\mathrm{i}^2}\nabla_\perp\cdot(\overline{n}_\mathrm{i}\nabla_\perp\phi) \\ &= \overline{n}_\mathrm{i} + \frac{b_z^2 T_\mathrm{i}}{2m_\mathrm{i}\Omega_\mathrm{i}^2}\frac{d^2\overline{n}_\mathrm{i}}{dx^2} + \frac{b_z^2 Ze}{m_\mathrm{i}\Omega_\mathrm{i}^2}\frac{d}{dx}\left(\overline{n}_\mathrm{i}\frac{d\phi}{dx}\right) \\ &= \overline{n}_\mathrm{i} + \frac{b_z^2 ZT_\mathrm{i}}{2m_\mathrm{i}\Omega_\mathrm{i}^2}\left[\frac{d^2\overline{n}_\mathrm{i}}{d\phi^2}\left(\frac{d\phi}{dx}\right)^2 - \frac{\rho}{\epsilon_0}\frac{\partial\overline{n}_\mathrm{i}}{\partial\phi}\right] + \frac{b_z^2 Ze}{m_\mathrm{i}\Omega_\mathrm{i}^2}\left[\frac{d\overline{n}_\mathrm{i}}{d\phi}\left(\frac{d\phi}{dx}\right)^2 - \frac{\rho}{\epsilon_0}\overline{n}_\mathrm{i}\right], \end{aligned} \tag{4.43}$$

where the charge density is denoted by ρ and a gyro-particle density is introduced as $\overline{n}_\mathrm{i}(\mathbf{X}) \equiv \int \overline{f}_{\mathrm{i}\parallel}(\mathbf{X}, v_\parallel)\, dv_\parallel$ and $\overline{f}_{\mathrm{i}\parallel}$ is a gyro-particle distribution function. The second and third terms in Eq. (4.43) represent the finite Larmor radius and polarization effects, respectively. The potential derivative of the ion density (4.43) can be calculated by using the following relations.

$$\frac{d}{d\phi}\frac{d^2\overline{n}_\mathrm{i}}{dx^2} = \left(\frac{d\phi}{dx}\right)^2\frac{d^3\overline{n}_\mathrm{i}}{d\phi^3} - 3\frac{\rho}{\epsilon_0}\frac{d^2\overline{n}_\mathrm{i}}{d\phi^2} - \frac{1}{\epsilon_0}\frac{d\rho}{d\phi}\frac{d\overline{n}_\mathrm{i}}{d\phi}, \tag{4.44}$$

$$\frac{d}{d\phi}\frac{d}{dx}\left(\overline{n}_\mathrm{i}\frac{d\phi}{dx}\right) = \left(\frac{d\phi}{dx}\right)^2\frac{d^2\overline{n}_\mathrm{i}}{d\phi^2} - 3\frac{\rho}{\epsilon_0}\frac{d\overline{n}_\mathrm{i}}{d\phi} - \frac{\overline{n}_\mathrm{i}}{\epsilon_0}\frac{d\rho}{d\phi}. \tag{4.45}$$

Since we can assume that $\rho \simeq 0$ at the sheath edge, the ion density is estimated by taking leading order terms as

$$\frac{dn_\mathrm{i}}{d\phi} \simeq \frac{d\overline{n}_\mathrm{e}}{d\phi} - \frac{b_z^2 Ze\overline{n}_\mathrm{i}}{\epsilon_0 m_\mathrm{i}\Omega_\mathrm{i}^2}\frac{d\rho}{d\phi} = \frac{d\overline{n}_\mathrm{i}}{d\phi} - \frac{b_z^2 Z\overline{n}_\mathrm{i}T_\mathrm{e}}{\lambda_\mathrm{De}^2 en_0 m_\mathrm{i}\Omega_\mathrm{i}^2}\frac{d\rho}{d\phi}, \tag{4.46}$$

where the definition of the Debye length $\lambda_\mathrm{De}^2 = \epsilon_0 T_\mathrm{e}/n_\mathrm{e}e^2$ is used. The derivative of the gyrocenter ion density is calculated as

$$\frac{d\overline{n}_\mathrm{i}}{d\phi} = \frac{d}{d\phi}\int_0^\infty\int_{v_{\min\mathrm{i}}}^\infty f_{0\mathrm{i}}\left(\sqrt{v_\parallel^2 + \frac{2Ze}{m_\mathrm{i}}\phi + \frac{\overline{\mu}}{m_\mathrm{i}\Omega_\mathrm{i}}\nabla_\perp^2\phi + \frac{Z^2e^2}{m_\mathrm{i}^2\Omega_\mathrm{i}^2}|\nabla_\perp\phi|^2}\right)\exp\left(-\frac{B\overline{\mu}}{T_\mathrm{i}}\right)dv_\parallel dv_\perp$$

$$\simeq \frac{Ze\overline{n}_\mathrm{i}}{m_\mathrm{i}} \left\langle v_{\|\mathrm{i}}^{-2} \right\rangle \left(1 - \frac{b_z^2 T_\mathrm{e} T_\mathrm{i}}{4\lambda_\mathrm{De}^2 e^2 m_\mathrm{i} \Omega_\mathrm{i}^2 n_0} \frac{d\rho}{d\phi} \right), \tag{4.47}$$

where the condition, $\rho = 0$ at $x = 0$, is used. The derivative of the electron density,

$$\frac{dn_\mathrm{e}}{d\phi} = \frac{n_0 e}{T_\mathrm{e}}, \tag{4.48}$$

is also obtained similarly. From Eqs. (4.46), (4.47), (4.48) and the definition of the charge density, $\rho = Zen_\mathrm{i} - en_\mathrm{e}$, the potential derivative of the charge density is obtained as

$$\frac{d\rho}{d\phi} \simeq \left(\frac{Z^2 \overline{n}_\mathrm{i} T_\mathrm{e}}{n_0 m_\mathrm{i}} \left\langle v_{\|\mathrm{i}}^{-2} \right\rangle - 1 \right) \frac{n_0 e^2}{T_\mathrm{e}} - \left(\frac{ZT_\mathrm{i}}{4m_\mathrm{i}} \left\langle v_{\|\mathrm{i}}^{-2} \right\rangle + 1 \right) \frac{b_z^2 Z T_\mathrm{e}}{\lambda_\mathrm{De}^2 m_\mathrm{i} \Omega_\mathrm{i}^2} \frac{d\rho}{d\phi}. \tag{4.49}$$

The relation between the ion particle density n_i and the ion gyrocenter density $\overline{n}_\mathrm{i}$ is calculated from the charge neutrality condition at $x = 0$, $Zen_\mathrm{i} = en_\mathrm{e} = en_0$;

$$\begin{aligned} Z\overline{n}_\mathrm{i} &\simeq n_0 - \frac{b_z^2 Z^2 e}{m_\mathrm{i} \Omega_\mathrm{i}^2} \frac{d\overline{n}_\mathrm{i}}{d\phi} \left(\frac{d\phi}{dx} \right)^2 \\ &\simeq n_0 \left[1 + \frac{b_z^2 Z^2 e^2}{m_\mathrm{i} \Omega_\mathrm{i}^2} \left(\frac{d\phi}{dx} \right)^2 \left\langle v_{\|\mathrm{i}}^{-2} \right\rangle \left(1 - \frac{b_z^2 T_\mathrm{e} T_\mathrm{i}}{4\lambda_\mathrm{De}^2 e^2 m_\mathrm{i} \Omega_\mathrm{i}^2 n_0} \frac{d\rho}{d\phi} \right) \right]^{-1}, \end{aligned} \tag{4.50}$$

where Eq. (4.47) is substituted. Finally, we obtain the generalized Bohm criterion for a magnetized plasma from $d\rho/d\phi \leq 0$ and Eqs. (4.49) and (4.50);

$$\frac{ZT_\mathrm{e}}{m_\mathrm{i}} \left\langle v_{\|\mathrm{i}}^{-2} \right\rangle \leq \left[1 - \frac{b_z^2 Z e^2}{m_\mathrm{i} \Omega_\mathrm{i}^2 T_\mathrm{e}} \left(\frac{d\phi}{dx} \right)^2 \right]^{-1}. \tag{4.51}$$

This expression coincides with the generalized Bohm criterion for unmagnetized sheath if the magnetic field is normal to the wall, i.e. $b_z = 0$. When the electric field is negligible, the present expression is reduced to $(ZT_\mathrm{e}/m_\mathrm{i}) \left\langle v_{\|\mathrm{i}}^{-2} \right\rangle \leq 1$, which is the same form as that of zero magnetic field except that the average is taken for the gyrocenter distribution function and the velocity in the average integral is replaced with the parallel velocity. The presence of the electric field makes the right hand side large and then the potential derivative of the charge density becomes small. It means a earlier increase of the charge density and a formation of the magnetic presheath in front of the Debye sheath.

4.4 Numerical solutions and PIC simulation results

In this section, we show the solutions of the model equation obtained in the preceding sections. We have developed a numerical code to solve the model equations and also a full-kinetic PIC simulation code to confirm the validity of our modeling. The results of

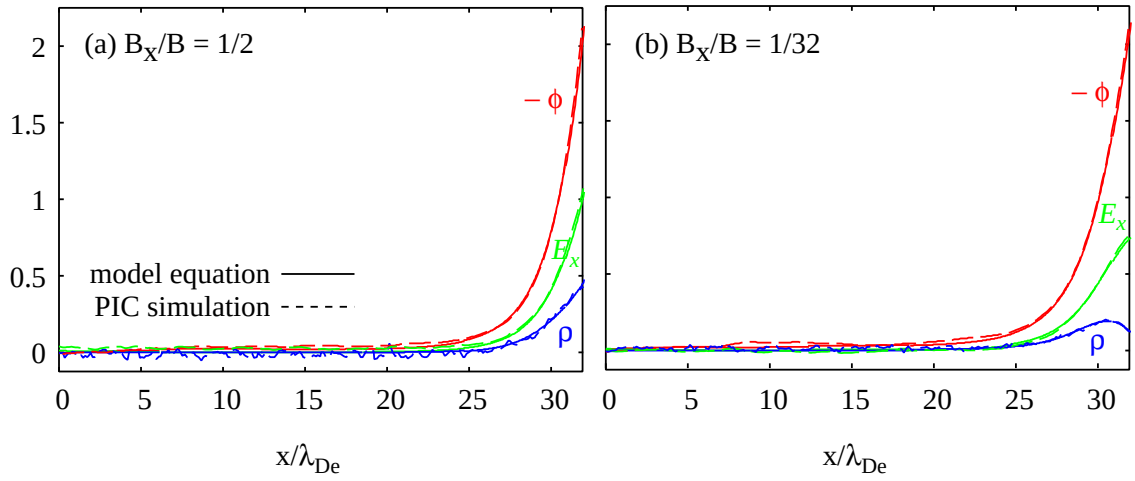

Figure 4.8: Numerical solutions of the model equations (solid curves) and PIC simulation results (dotted curves) for (a) $B_x/B = 1/2$ and (b) $B_x/B = 1/32$. The other plasma parameters are $\mu = 1836$, $Z = 1$, $M_e = 0$, $M_i = 2$ and $C = 0.1$. Three curves in each figure represent the potential, electric field and charge density. These quantities are normalized and plotted as absolute values.

the magnetized case are presented and the dependence of the wall electric field on the magnitude and the direction of the magnetic field are studied.

We use the parameters $\tau = T_i/T_e = 1$, $\mu = m_i/m_e = 1836$ and $Z = 1$ for an unmagnetized plasma and solve Eqs. (4.9) – (4.13) to obtain the density profiles for the parallel drifting velocities $M_e = \bar{v}_e/\sqrt{T_e/m_i} = 0$ and $M_i = \bar{v}_i/\sqrt{T_e/m_i} = 2$ and the ion cut-off velocity $C = v_{ci}\sqrt{m_i/T_e} = 0.1$. The generalized Bohm criterion for a magnetized plasma is satisfied, $(ZT_e/m_i)\left\langle v_{\|i}^{-2}\right\rangle \simeq 0.96$, and the wall potential is $e\Phi/T_e \simeq -2.13$ and the effective temperature ratio is $T_i^*/T_e^* \simeq 0.97$. The magnetic field is assumed to be strong enough to satisfy the gyrokinetic ordering, $v_\perp/\Omega \lesssim L_\phi$. Fig. 4.8 (a) and (b) represent the profiles of the potential, electric field and charge density in the magnetic field characterized by $\rho_i = \sqrt{T_i/m_i}/\Omega_i = \lambda_{De}$ and $B_x/B = 1/2$ (a) and $B_x/B = 1/32$ (b). The angles of the magnetic field are $\varphi = 60^\circ$ and $\varphi = 1.8^\circ$, respectively. Three quantities shown in the figures are normalized and plotted as absolute values. The sold and dotted curves correspond to the solution of the model equations (4.35) – (4.38) and (4.14) and full-kinetic PIC simulation results and they agree quite well each other.

Distinctive differences related to the magnetic field angle are observed on the electric field and charge density profiles near the wall. They decrease when the magnetic field becomes parallel to the wall. The electric field profiles obtained from the model equations with $M_i = 2$ and $\rho_i = \lambda_{De}$ are compared in Fig. 4.9. The solid, dotted and dashed curves correspond to $B_x/B = 1$, $1/2$ and $1/32$, respectively. The decrease of the electric field

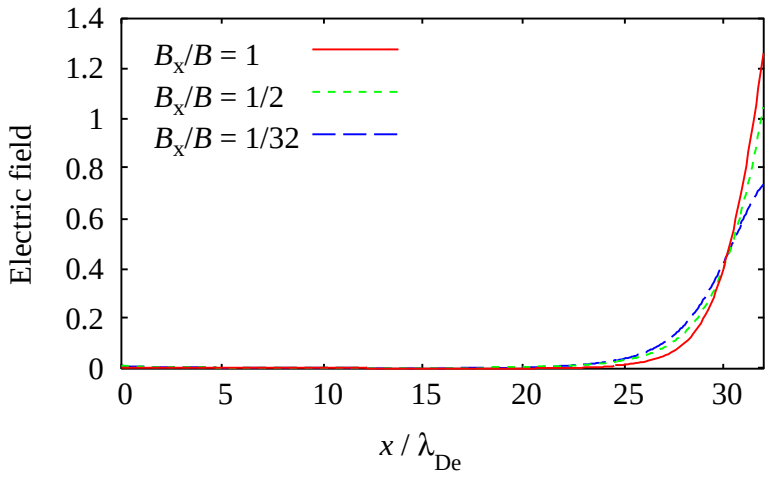

Figure 4.9: Electric field profiles obtained from the model equations for $B_x/B = 1$, $1/2$ and $1/32$. Plasma parameters are $\mu = 1836$, $Z = 1$, $\nu = 1$, $M_e = 0$, $M_i = 2$ and $\rho_i = \lambda_{De}$.

occurs within about $2\lambda_{De}$ from the wall. The length of the sheath layer increases a little for small B_x/B. In order to see the dependence of the reduction of the electric field on the magnetic field angle, we plot the electric field on the wall as a function of B_x/B in Fig. 4.10 for three cases, $\rho_i/\lambda_{De} = 0.5$, 1, and 2. The solid and dotted curves correspond to the results of the model equation and PIC simulation, respectively.

The relative standard deviations of the PIC simulation results are about 1%. Although the numerical solutions of the model equations are slightly larger than those of the PIC simulation in the case of $\rho_i = 0.5\lambda_{De}$ and λ_{De}, the both results show good agreement and give the same dependences on B_x/B. In the case of $\rho_i/\lambda_{De} = 2$, however, the solution of the model equations gives smaller value than the PIC simulation result at $0.2 < B_x/B < 1$. From these results we conclude that our magnetized sheath model equation is valid for the strong magnetic field, $\rho_i/\lambda_{De} \lesssim 1$. The reason of the existence of the lower limit in the magnetic field strength is the gyrokinetic ordering, $v_\perp/\Omega \lesssim L_\phi$. Away from the wall, the scale length of the potential profile increases proportional to the thermal Larmor radius and is much larger than the Debye length, however in the vicinity of the wall, the potential scale length is still dominated by the Debye length and violates the ordering.

In Fig. 4.10, we can observe that the wall electric field decreases almost linearly with respect to $1 - B_x/B$ for $B_x/B > 0.5$ and parabolically for $B_x/B < 0.5$. This different characteristics can be understood as follows. The steep decrease near $B_x/B = 0$ is cause by the particle loss due to the absorption of particles in gyration which is introduced in this work as the factor f_{loss}. When the magnetic field is nearly parallel to the wall, $B_x/B \simeq 0$, the normal velocity of a gyrocenter is considerably small and thus particles strikes the wall mainly because of the perpendicular gyrating motion. The loss of ion due to the gyration

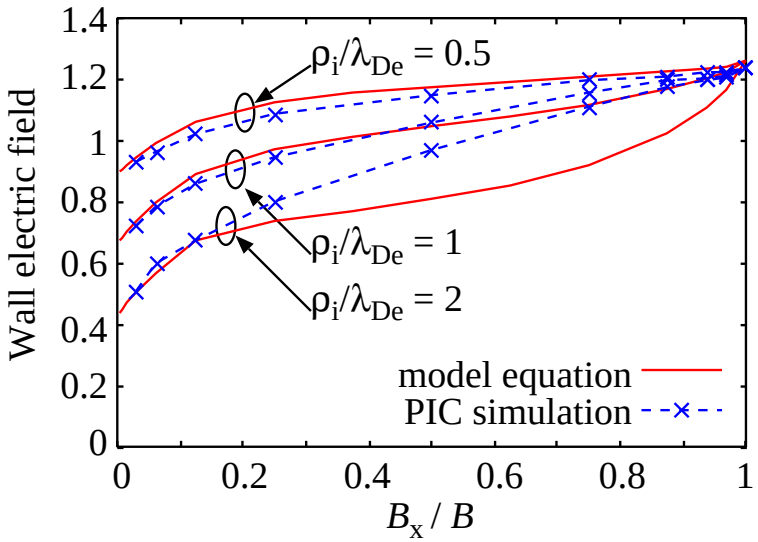

Figure 4.10: Wall electric field as a function of B_x/B. The PIC simulation is performed for $\rho_i/\lambda_{De} = 0.5$, 1 and 2 and for $B_x/B = 1/4$, $1/16$ and $1/64$.

causes the reduction of the charge density and consequently the wall electric field.

On the other hand, when the magnetic field crosses the wall at nearly right angle, $B_x/B \simeq 1$, almost all the particle loss is caused by the parallel motion. The fact that the process of the particle loss is same as the unmagnetized sheath implies the existence of other cause of the reduction. A possible candidate for the reduction is the polarization density due to the perpendicular electric field. An approximate form of the polarization density is usually expressed as a divergence of the guiding-center density multiplied by the polarization shift length $Ze\nabla_\perp\phi/m_i\Omega_i^2$;

$$n_p = \nabla_\perp \cdot \left(n \frac{Ze\nabla_\perp \phi}{m_i \Omega_i^2} \right). \tag{4.52}$$

We note that this polarization density term does not appears in the ion density equation (4.36) because our definition of the gyrocenter includes the polarization shift and thus the gyrocenter density includes the polarization density.

We solved three types of equation to identify the effects of the particle loss factor and the polarization density on the wall electric field. The first equations are the original ones, the second are modified to involve no polarization effect and the last are without the loss factor, i.e. $f_{loss} = 0$. The three curves in Fig. 4.11, solid, dotted and dashed curves, correspond to the solutions of the three types of equations, respectively. The wall electric field without the polarization does not change so much for $B_x/B > 0.5$ and have the same dependence for $B_x/B < 0.5$ as the original solutions. On the other hand, the solutions without the particle loss factor has same dependence for $B_x/B > 0.5$ as the original ones

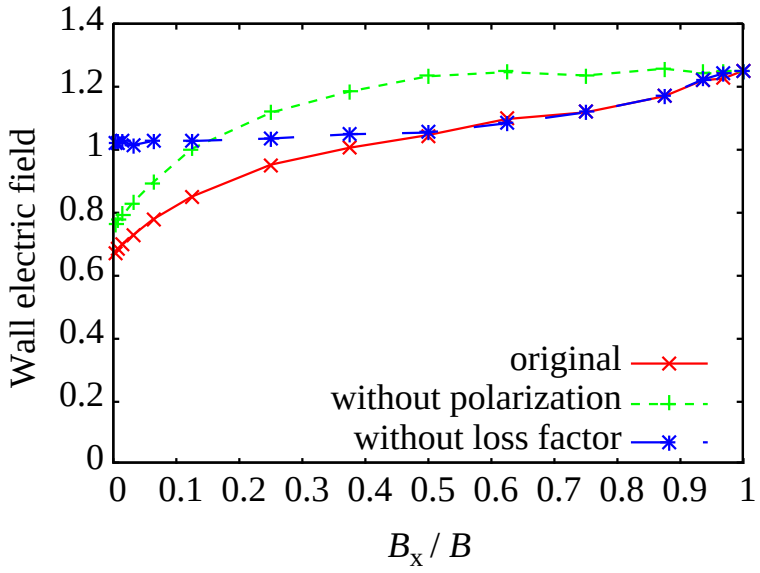

Figure 4.11: Comparison of the wall electric field between the original solution (solid curve), without the polarization effect (dotted curve) and without the particle loss factor (dashed curve).

and becomes nearly constant for $B_x/B < 0.5$. From these considerations, we can conclude that the wall loss of the particle reduces the charge density and the electric field near the wall for $B_x/B < 0.5$, and the polarization effect reduces them in all parameter region $0 < B_x/B < 1$ but the amount of the reduction becomes constant as B_x/B approaches zero.

4.5 Conclusions

The kinetic equations for an electrostatic potential in a sheath layer were derived from the collisionless Vlasov equation. We obtained two set of equations for the unmagnetized and strongly magnetized plasma sheaths. In the derivation for the unmagnetized plasma, we assumed that the plasma source which had the fixed velocity distribution at on end, $x = 0$, and the absorbing wall at the other end, $x = L$. In the sheath layer, $0 < x < L$, no source and no particle collision exist. Ions and electrons are generated at the source boundary and also removed when they move across the boundary toward $x < 0$. We adopted the shifted Maxwellian with a truncation for the ion source velocity distribution. The cut-off velocity was determined to satisfy the generalized Bohm criterion at the source boundary.

In the presence of an uniform magnetic field, the gyrokinetic treatment of magnetized electrons and ions was applied to the plasma sheath problem for the first time. In order to

deal with a strong electric field, we adopted the gyrokinetic theory on a moving frame with the $\mathbf{E}\times\mathbf{B}$ drift velocity [40]. We obtained a potential equations in the sheath layer from the gyrokinetic collisionless Vlasov equation. They have similar forms to the unmagnetized equations, but there are three different points. The first is the B_x/B factors in the flux equations (4.37) and (4.38), which represent the normal velocity component to the wall. The second is the polarization effect in the energy conservation equation (4.33) and the ion density equation (4.36). The last is the particle loss factor $f_{\rm loss}$, which determines the loss rate of the particles due to the gyration near the wall.

The condition for the stable sheath formation in a magnetic field was derived from our sheath model under the assumption of $v_\perp/\Omega \ll L$. If the electric field at the sheath edge is ignorable, the result (4.51) is quite similar to the generalized Bohm criterion without a magnetic field [53] except that the gyrocenter distribution function is used instead of that for actual particles and the parallel velocity should be used instead to the normal velocity to the wall. When an electric field is presence, a term related to the polarization becomes considerable in the criterion and implies the existence of the magnetic presheath.

From the comparison between the numerical solution of our model equation and the results of the full-kinetic particle simulation for various values of B_x/B and $\rho_{\rm i}/\lambda_{\rm De}$, we confirmed that the model provides accurate solutions for the strongly magnetized plasma, i.e. $\rho_{\rm i}/\lambda_{\rm De} \lesssim 1$. In a weaker magnetic field, the solution of the model equation gives smaller electric field for $0.2 < B_x/B < 1$, because the ion Larmor radius becomes larger beyond the gyrokinetic ordering, $v_\perp/\Omega \lesssim L_\phi$.

We also investigated the dependence of the wall electric field on the angle of the magnetic field, B_x/B. It was found that the particle loss due to the gyration and the polarization effect reduce the charge density and the electric field near the wall. The effect of the particle loss is observed for $B_x/B < 0.5$ and becomes larger as B_x/B approaches to 0. On the other hand, the polarization effect always exists except $B_x/B \sim 1$. It increases with the decrease of B_x/B, and is saturated for $B_x/B < 0.5$. The magnitude of these effects on the wall electric field are the same order in the case of $\rho_{\rm i} = \lambda_{\rm De}$.

Our work is based on the assumption of strong magnetization, $\rho_{\rm i} \lesssim \lambda_{\rm De}$. This assumption is not always applicable to the edge plasma in fusion devices. Further investigation for weakly magnetized plasmas, $\rho_{\rm i} \gtrsim \lambda_{\rm De}$ or $\rho_{\rm e} \sim \lambda_{\rm De}$, is required. In order to overcome the lower limit of the magnetic field strength in this model, we are preparing a more exact gyrokinetic formulation without Taylor expansions of ϕ which relies on the ordering $v_\perp/\Omega \lesssim L_\phi$. Also the effects of the particle collision and atomic processes need to be taken into account, because they play a role of additional source and sink and alter the potential profile.

Chapter 5

Analysis of incident angle distribution of ions in a magnetized sheath

5.1 Introduction

When a plasma is facing an electrically floating wall, negative charges accumulate on the surface and a large positive electric field is created in a thin layer, namely a sheath. The electrons are repelled by the electric field and the ions are accelerated toward the wall. If a magnetic field is not present, the width of sheath layer is typically a few Debye length and the wall potential is around twice of the electron temperature.

When a magnetic field is applied to the plasma, the property of the sheath layer changes according to the magnitude and the direction of the field. When the magnetic field is oblique to the wall, an additional ion flux due to the polarization drift creates a quasineutral region in front of the sheath, namely magnetic presheath [56]. The width of the magnetic presheath region is difficult to define exactly, but it was predicted by the fluid study [56] and confirmed by the kinetic simulation [55] that the scale length is proportional to the ion thermal Larmor radius. The influences of the magnetic field are observed also on physical quantities near the wall. The electric field and the charge density in the vicinity of the wall become smaller as the magnetic field decreases. These reductions are significant when the ion thermal Larmor radius becomes longer than the Debye length [55, 63]. Since the wall electric field is a key parameter for the release of dust particles [45], understanding the physics in the sheath layer is an important issue for fusion devices. The incident angle distribution of the particles to the wall is also essential for obtaining the production rate of secondary electrons and the sputtering at the surface [46, 47, 65].

In this work, We analyze the incident angle distribution to the wall in a magnetized plasma by using a gyrokinetic model equation based on Ref. [63] and a full-kinetic

particle-in-cell (PIC) simulation [64]. The model equation is valid for strongly magnetized plasmas, i.e. the ion thermal Larmor radius is comparable or less than the Debye length. We make a comparison between the numerical solution of the model equation and the simulation results. The dependence of the incident angle distributions on the magnitude and the direction of the magnetic field is studied.

This chapter is organized as follows. First, we briefly review the model equations to describe the potential profile in the sheath layer and introduce the incident angle distributions to the wall in Sec. 5.2. In Sec. 5.3, the numerical solutions of the model equation and the results of PIC simulations are compared with each other for a strongly magnetized plasma. The dependence of the incident angle on the magnetic fields is studied by using the PIC simulation. Finally, conclusions are given in Sec. 5.4.

5.2 Kinetic modeling of a sheath layer

We assume an one-dimensional plasma which has a source boundary at one end and an electrically floating wall at the other end. The source boundary provides new particles to compensate the loss of particles at the wall. The effects of collisions and particle generations in the sheath layer are neglected. The system length along the x direction is denoted by L and a perfectly absorbing wall is placed at $x = L$. The potential and density profiles are uniform along y and z directions and monotonically decrease along x direction. The magnetic field $\mathbf{B} \equiv B(\cos\varphi\hat{\mathbf{x}} + \sin\varphi\hat{\mathbf{z}})$ is uniform and has no y component. The angle of the magnetic field with the surface normal is denoted by φ. A plasma source consists of electrons and ions of one species filling the region $x < 0$ and flows into the region $0 < x < L$. The electrostatic potential ϕ is measured from the value at the source end, $x = 0$.

Since a sheath layer has a strong electric field, the usual magnetic moment, $mv_\perp^2/2B$, is not an invariant, but a generalized magnetic moment introduced by Littlejohn [17] has been proved to be a new adiabatic invariant when the ion Larmor radius is comparable or smaller than the scale length of the potential. By using this invariance, the dimension of the velocity space is virtually reduced to one ($v_\parallel$) from three ($v_\parallel$, $v_\perp$ and the gyrophase θ). When the Larmor radius is much larger than the characteristic length, however, the particle motion becomes quite complicated and the velocity space must be treated as three dimensional. The analysis for the parameter $\rho_{\mathrm{ti}}/\lambda_{\mathrm{De}} \gg 1$ requires the complete integrals along the particle trajectory [57] or full-kinetic particle-in-cell (PIC) simulation technics [55,56,58,60]. Here, the Debye length, the thermal ion Larmor radius and the ion cyclotron frequency are denoted by $\lambda_{\mathrm{De}} \equiv \sqrt{n_0 e^2/\epsilon_0 T_{\mathrm{e}}}$, $\rho_{\mathrm{ti}} \equiv \sqrt{T_{\mathrm{i}}/m_{\mathrm{i}}}/\Omega_{\mathrm{i}}$ and $\Omega_{\mathrm{i}} = q_{\mathrm{i}}B/m_{\mathrm{i}}$, respectively.

The model equations describing the potential profile in the sheath layer are derived with three steps. The first is to define the gyrocenter coordinates and introduce the 'gyro-particle' distribution. The motion of a charged particle is described as the superposition of a simple gyration, drift motions and a parallel motion in the gyrocenter coordinate system. The gyration is decomposed from the other components and represented by the time evolution of the gyrophase. The second is to rewrite the energy conservation in terms of the gyrocenter coordinate variables. The third is to express the particle density in terms of the 'gyro-particle' distribution function and integrate the Poisson equation to obtain the potential profile. The details of these procedures and the validity of the model are discussed in [63].

The definitions of the gyrocenter coordinates $(\mathbf{X}, \Theta, \bar{\mu}, v_\parallel)$, gyrocenter position, gyrophase, modified magnetic moment and parallel velocity, are given as follows;

$$\mathbf{v} \equiv \mathbf{D} + v_\parallel \hat{\mathbf{b}}(\mathbf{X}) + V_\perp \hat{\mathbf{c}}(\mathbf{X}), \tag{5.1}$$

$$\mathbf{D} \equiv \frac{\hat{\mathbf{b}}(\mathbf{X}) \times \nabla\phi(\mathbf{X})}{B(\mathbf{X})}, \tag{5.2}$$

$$\mathbf{x} \equiv \mathbf{X} + \frac{mV_\perp}{ZeB(\mathbf{X})}\hat{\mathbf{a}}(\mathbf{X}), \tag{5.3}$$

$$\bar{\mu} \equiv \frac{mV_\perp^2}{2B(\mathbf{X})}, \tag{5.4}$$

where the ion charge is denoted by Ze. The vector $\mathbf{D}$ represents the velocity of the reference frame. The modified magnetic moment $\bar{\mu}$ is defined on the moving frame. The three orthonormal vectors $\hat{\mathbf{a}}$, $\hat{\mathbf{b}}$ and $\hat{\mathbf{c}}$ are defined in terms of the base direction vector $\hat{\mathbf{u}}$ as $\hat{\mathbf{b}} = \mathbf{B}/B$, $\hat{\mathbf{c}}(\Theta) = \hat{\mathbf{u}}\cos\Theta - (\hat{\mathbf{b}} \times \hat{\mathbf{u}})\sin\Theta$ and $\hat{\mathbf{a}} = \hat{\mathbf{b}} \times \hat{\mathbf{c}}$. Since the y direction can be used for the base direction in the magnetic geometry used here, we use $\hat{\mathbf{u}} \equiv \hat{\mathbf{y}}$ in the following discussions. A particle velocity is measured on the moving frame to cancel the potential perturbation caused by the gyration of the particle. In the case of an uniform magnetic field, the energy conservation law is rewritten in terms of the gyrocenter coordinate variables as

$$\frac{m}{2}v_\parallel^2 + B\bar{\mu} + \frac{m}{2B^2}|\nabla_\perp\phi|^2 + Ze\phi + \frac{\bar{\mu}}{2\Omega}\nabla_\perp^2\phi = \text{const.} \tag{5.5}$$

The motion of the charged particle can be determined from this energy equation.

The parallel velocity distribution function at the source boundary, $x = 0$, is assumed to be a shifted Maxwellian which is characterized by a thermal velocity v_{ts} and a parallel drifting velocity $\bar{v}_{\text{s}}$; $f_{0s}(v_\parallel, v_\perp) = (n_0/\sqrt{(2\pi)^3}v_{\text{ts}}^3)\exp(-(v_\parallel - \bar{v}_{\text{s}})^2/2v_{\text{ts}}^2 - v_\perp^2/2v_{\text{ts}}^2)$. Since the plasma can be described by the one dimensional collisionless Vlasov equation $df_{\text{s}}/dt = 0$,

the distribution function f_s is written in terms of the source distribution function $f_{0\mathrm{s}}$ as

$$f_\mathrm{s} = f_{0\mathrm{s}}\left(\sqrt{v_\parallel^2 + \frac{2Ze}{m}\left(\phi + \frac{1}{2B\Omega}|\nabla_\perp\phi|^2 + \frac{\bar{\mu}}{2\Omega}\nabla_\perp^2\phi\right)}, v_\perp(\bar{\mu})\right), \tag{5.6}$$

where the gyrokinetic energy conservation law (5.5) is used. The distribution function f is a function of $\mathbf{X}$, $\bar{\mu}$ and $v_\parallel$. In order to simplify the formula, we introduce dimensionless parameters $\mu \equiv m_\mathrm{i}/m_\mathrm{e}$, $\tau \equiv T_\mathrm{i}/T_\mathrm{e}$, $\psi \equiv -e\phi/T_\mathrm{e}$, $M_\mathrm{e} \equiv \bar{v}_\mathrm{e}\sqrt{m_\mathrm{i}/T_\mathrm{e}} = \sqrt{\mu}\bar{v}_\mathrm{e}/v_\mathrm{te}$ and $M_\mathrm{i} \equiv \bar{v}_\mathrm{i}\sqrt{m_\mathrm{i}/T_\mathrm{e}} = \sqrt{\tau}\bar{v}_\mathrm{i}/v_\mathrm{ti}$, where M_e and M_i represent the ratios of the drifting velocities $\bar{v}_\mathrm{s}$ to the cold-ion sound velocity $\sqrt{T_\mathrm{e}/m_\mathrm{i}}$. We note that the normalized potential ψ has opposite sign to ϕ, thus $0 \le \psi \le \Psi \equiv -e\Phi/T_\mathrm{e}$. By using these parameters and the source distribution function $f_{0\mathrm{s}}$, the densities are obtained as

$$\frac{n_\mathrm{e}}{n_0} = \int_{-\sqrt{2(\Psi-\psi)}}^{\infty} d\hat{v}_\parallel \frac{\nu_\mathrm{e}}{\sqrt{2\pi}} \exp\left[-\frac{1}{2}\left(\sqrt{\hat{v}_\parallel^2 + 2\psi} - \frac{M_\mathrm{e}}{\sqrt{\mu}}\right)^2\right], \tag{5.7}$$

$$\frac{n_\mathrm{i}}{n_0} = \int_0^\infty d\hat{V}_\perp \hat{V}_\perp \int_0^{2\pi} d\theta \int_{\sqrt{2Z_\mathrm{i}\psi_\mathrm{g}}}^\infty d\bar{v}_\parallel \frac{\nu_\mathrm{i} f_\Theta}{(2\pi\tau)^{3/2}} \exp\left[-\frac{1}{2\tau}\left(\sqrt{\hat{v}_\parallel^2 - 2Z_\mathrm{i}\psi_\mathrm{g}} - M_\mathrm{i}\right)^2 - \frac{\hat{V}_\perp^2}{2\tau}\right], \tag{5.8}$$

where the normalized coefficients are denoted by ν_e and ν_i. The gyrophase measured on the stationary frame θ and that on the moving frame Θ are related with the equation $v_\perp\hat{\mathbf{c}}(\theta) = \mathbf{D} + V_\perp\hat{\mathbf{c}}(\Theta)$. This relation can be rewritten as $v_\perp\cos\theta = -(d\phi/dx)\sin\varphi + V_\perp\cos\Theta$ by using $\mathbf{D} = -(d\phi/dx)\sin\varphi\hat{\mathbf{y}}$ and $\hat{\mathbf{u}} = \hat{\mathbf{y}}$.

The wall potential Ψ is determined from the flux balance between electrons and ions. The gyrokinetic modified potential ψ_g is given by

$$\psi_\mathrm{g} = \psi + \frac{\rho_\mathrm{ti}^2}{2\lambda_\mathrm{De}^2}\left(\frac{\hat{V}_\perp^2}{2}\nabla_\perp^2\psi - \frac{Z}{\tau}|\nabla_\perp\psi|^2\right). \tag{5.9}$$

The particle loss factor f_Θ represents Θ-dependent component of the distribution function and takes the value either zero or one. The physical meaning if the factor is intuitively represented in Fig. 5.1. This factor is determined by whether the particle has crossed the boundary $x = L$ in the past or not. If the particle crossed the boundary at some time in the past, the particle has been lost and thus $f_\Theta = 0$. The trajectory denoted by the dashed curve in the figure might be possible without the wall, but here it cannot be realized because the particle is absorbed before reaching there. We use the same algorithm for this calculation as in Ref. [63]. The Θ-dependent component of the electron and small terms such as $\rho_\mathrm{te}/\lambda_\mathrm{De} \ll 1$ are neglected.

In order to obtain the incident angle distribution of ions, we calculate the angle from the velocity space coordinates $(\theta, v_\perp, v_\parallel)$ and the distribution function obtained above. The

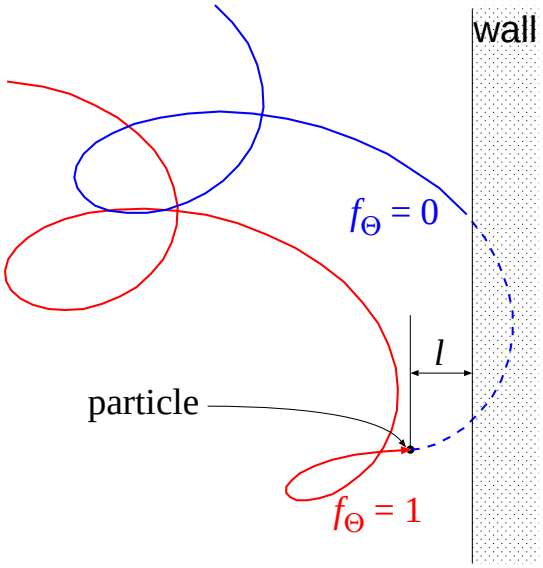

Figure 5.1: Meaning of the particle loss factor f_Θ. The particle can not have the orbit denoted by the dashed curve.

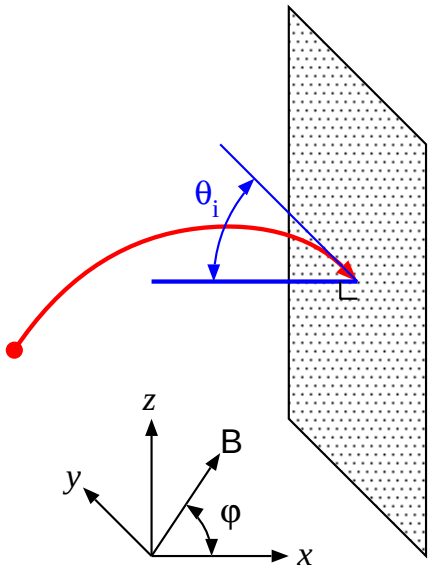

Figure 5.2: Definition of the incident angle θ_i. It is measured from the normal direction to the wall.

incident angle denoted by θ_i is defined by the angle between the velocity and the normal direction of the wall as in Fig. 5.2. Since the velocity can be rewritten into three components as $\mathbf{v} = v_\parallel \hat{\mathbf{b}} + v_\perp \hat{\mathbf{c}}(\theta) = (v_\parallel \cos\varphi + v_\perp \sin\theta \sin\varphi)\,\hat{\mathbf{x}} + v_\perp \cos\theta \hat{\mathbf{y}} + (v_\parallel \sin\varphi - v_\perp \sin\theta \cos\varphi)\,\hat{\mathbf{z}}$, the incident angle is obtained as $\cos\theta_i = \mathbf{v}\cdot\hat{\mathbf{x}}/|\mathbf{v}| = (v_\parallel \cos\varphi + v_\perp \sin\theta \sin\varphi) \,/\, \sqrt{v_\parallel^2 + v_\perp^2}$. A flux for a certain θ_i and energy can be calculated by integrating the velocity distribution function for the fixed θ_i and energy.

5.3 Results and discussion

We employ two numerical codes to obtain the potential profiles in the sheath layer and the incident angle distributions for the same plasma parameters. One is a numerical solver of the model equation given in Sec. 5.2, and the other is a PIC simulation code. The former integrates the Poisson equation, $\nabla^2\psi/\lambda_{De}^2 = Zn_i/n_0 - n_e/n_0$, with Eqs. (5.7) and (5.8) from $x = 0$ toward $x = L$ by Runge-Kutta method of the second order. The spatial step size used here is $\lambda_{De}/16$. This integral requires the boundary value $d\phi/dx|_{x=0} = -E_0 < 0$ and the system length L. Although the parameter L is given beforehand, the source electric field E_0 must be calculated so that the solution of the potential satisfies other constraints such as the system length and the flux balance at the wall. We employ the shooting method to figure out the boundary value E_0.

The latter is a full-kinetic particle code which calculates the trajectories of electrons

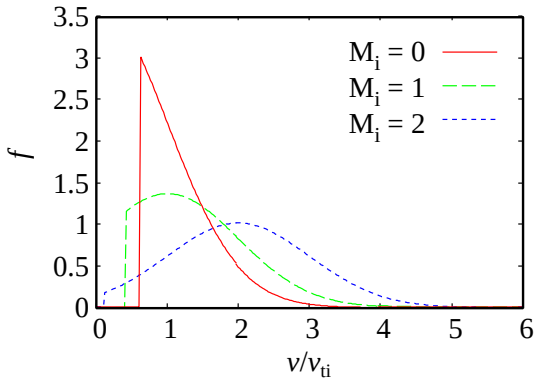

Figure 5.3: Ion velocity distribution functions for $M_\mathrm{i} = 0$, 1 and 2. The velocity cut-off is introduced to fulfill the generalized Bohm criterion.

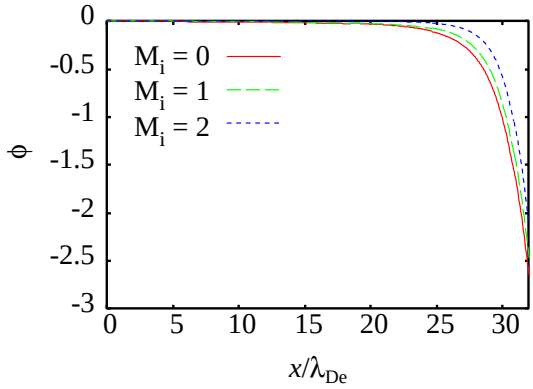

Figure 5.4: Potential profiles for $M_\mathrm{i} = 0$, 1 and 2. The differences in the distribution functions causes the different ion fluxes and potential profiles.

and ions from the Newton's equation of motion;

$$m_\mathrm{s}\frac{d^2\mathbf{x}}{dt^2} = q_\mathrm{s}\frac{d\mathbf{x}}{dt}\times\mathbf{B} - q_\mathrm{s}\nabla\phi. \tag{5.10}$$

The time integral is implemented with the Runge-Kutta method of the fourth order and the time step is determined as $2\pi/|\Omega_\mathrm{e}|\Delta t = 20$ to 40 so that the energy of the plasma is conserved. The magnetic field is assumed to be $\mathbf{B} = B(\cos\varphi\hat{\mathbf{x}} + \sin\varphi\hat{\mathbf{z}})$ and the electrostatic potential ϕ is determined by the Poisson equation, $\nabla^2\phi = -(Zen_\mathrm{i} - en_\mathrm{e})/\epsilon_0$. The Poisson equation is solved by using the finite difference method with the boundary conditions

$$\phi(0) = 0, \quad \left.\frac{d\phi}{dx}\right|_{x=L} = -E_L. \tag{5.11}$$

The wall electric field E_L is determined by the Gauss' theorem. The spatial step size is $\lambda_\mathrm{De}/8$. The number of particles is about a thousand per Debye length, or a hundred per grid. We use the parameters $\tau = T_\mathrm{i}/T_\mathrm{e} = 1$, $\mu = m_\mathrm{i}/m_\mathrm{e} = 1836$, $Z = 1$, $M_\mathrm{e} = 0$ and $M_\mathrm{i} = 2$. In order to realize the generalized Bohm criterion [53, 63], a velocity cut-off is introduced in the ion velocity distribution function. The distribution function for $M_\mathrm{i} = 0$, 1 and 2 are shown in Fig. 5.3. The velocity at the cut-off is determined as $v/v_\mathrm{ti} = 0.61$, 0.41 and 0.11 for $M_\mathrm{i} = 0$, 1 and 2, respectively. The corresponding potential profiles are also shown in Fig. 5.4. Since the ion flux depend on the distribution function, a larger M_i causes a smaller wall potential because of the increase of the ion flux.

We made comparisons of the potential, electric field and charge density profiles between the two codes for $v_\mathrm{ti}/\Omega_\mathrm{i}\lambda_\mathrm{De} = 1$ and confirmed that they quantitatively agreed with each other within the relative error of 1%. The differences between the solution of the

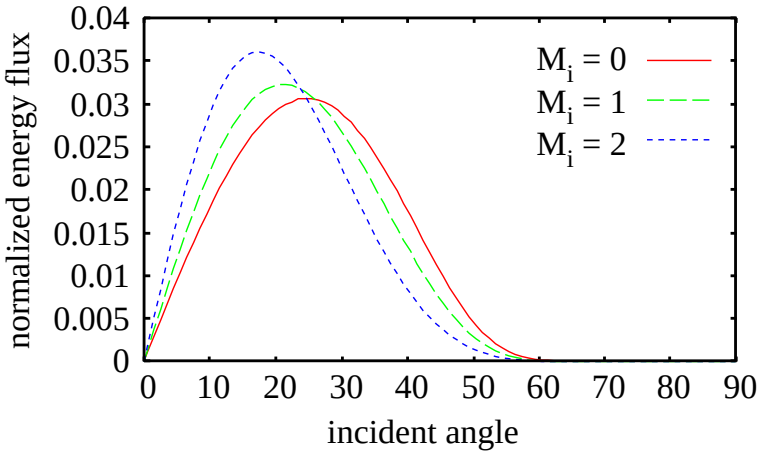

Figure 5.5: Energy flux distribution for $M_\mathrm{i} = 0$, 1 and 2 as a function of the incident angle. The distribution functions given in Fig. 5.3 are employed.

model equation and the PIC simulation results tend to grow for large thermal Larmor radii. When $v_\mathrm{ti}/\Omega_\mathrm{i}\lambda_\mathrm{De} \geq 2$, the relative error exceeds 10%. Therefore, we have to employ the PIC simulation for the case of a weak magnetic field or a dense plasma. The model equation, however, still has benefits compared to the PIC simulation. First, analytic model is suitable to extract fundamental informations such as a stability of the sheath layer and effects of the polarization drift [63]. Second, there is practically no numerical noise in the solution of the model equation, while the statistical process in the PIC simulation causes the noise. The plasma oscillation with a long wave length is also difficult to eliminate in the PIC simulation because of the small dumping rate. The PIC simulation results presented here are time-averaged to reduce the noise and the plasma oscillation.

Before discussing the results for the magnetized plasma, we presents the those of the unmagnetized plasma. The normalized energy flux distribution is shown in Fig. 5.5. The solid, dashed and dotted curves correspond to the parameter $M_\mathrm{i} = 0$, 1 and 2. The each velocity distribution function and potential profile used here are same as in Fig. 5.3 and Fig. 5.4. A shift of the incident angle which yields the maximum energy flux is observed. This tendency is caused by the difference of the normal velocity component for each cases. A large parallel drifting velocity, i.e. $M_\mathrm{i} = 2$, causes a large normal velocity and then the incident angle becomes small.

We make a comparison of the incident angle distribution for $B_x/B = 0$ and $M_\mathrm{i} = 2$ with the approximate form of the angular distribution function obtained by Gottscho [47];

$$f(\theta_\mathrm{i}) \simeq 2\beta\theta_\mathrm{i} \exp\left(-\beta\theta_\mathrm{i}^2\right), \tag{5.12}$$

where the parameter β is given by $\beta = m\overline{v_\parallel^2}/2T_\perp$ for θ_i and the angle θ_i is measured in radian. The quantity $\overline{v_\parallel^2}$ is the average of the square parallel velocity at the wall and

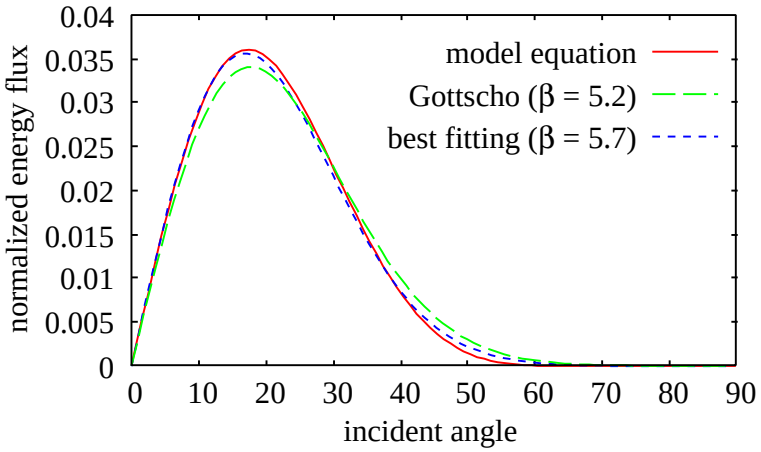

Figure 5.6: Comparisons of the energy flux distributions. The solid, dashed and dotted curves correspond to our model, best fitting function and Gottscho's model.

$T_\perp$ is the perpendicular temperature at the wall. The actual $\overline{v_\parallel^2}$ and $T_\perp$ obtained from the numerical solution yields $\beta = 5.2$. The energy flux distributions at the wall surface, $x = L$, calculated from our model equations and from Gottscho's model are shown in Fig. 5.6. The flux is normalized by the total flux and defined as

$$Q(\theta_{\rm i}) = \int \frac{mv^2}{2}\delta\left(\frac{v_x}{v} - \cos\theta_{\rm i}\right)d^3v \Big/ \int \frac{mv^2}{2}d^3v. \tag{5.13}$$

The flux is normalized so that the total energy flux is unity. We found the parameter β providing the best fitting curve as $\beta = 5.7$, which is also shown in Fig. 5.6 as a dotted curve. The mean square root of the residual is about 1%. Thus, we have confirmed that the Gottscho model practically gives an accurate distribution function for the plasma with a normal magnetic field to the wall.

We show the energy flux distribution for a magnetized plasma in Fig. 5.7 as a function of the incident angle $\theta_{\rm i}$ for $v_{\rm ti}/\Omega_{\rm i} = \lambda_{\rm De}$ and $B_x/B = 1$, $3/4$, $1/4$ and $1/16$. Each magnetic field direction corresponds to the $\theta_{\rm i} = 0°$, $41.4°$, $75.5°$ and $86.4°$. The solid and dashed curves represent the solutions of the model equation and the results of the PIC simulation, respectively. The solid and dashed curves agree well in the whole range of B_x/B and especially good for $B_x/B = 1$ which is equivalent to that of an unmagnetized case. The contour plots of the particle flux are also presented in Fig. 5.8 for four cases; (a) $B_x/B = 1$, (b) $B_x/B = 4/3$, (c) $B_x/B = 1/4$ and (d) $B_x/B = 1/16$. The incident angle for the intermediate magnetic angles, $B_x/B \sim 0.75$, has a broad profile, and the tails reaches the both ends, $\theta_{\rm i} = 0°$ and $90°$. The profile for $B_x/B \sim 0$ are sharply peaked at large incident angle, which means that most particles hit the surface with strongly slanted angles. This tendency is understood as follows. If the magnetic field is nearly parallel to the surface,

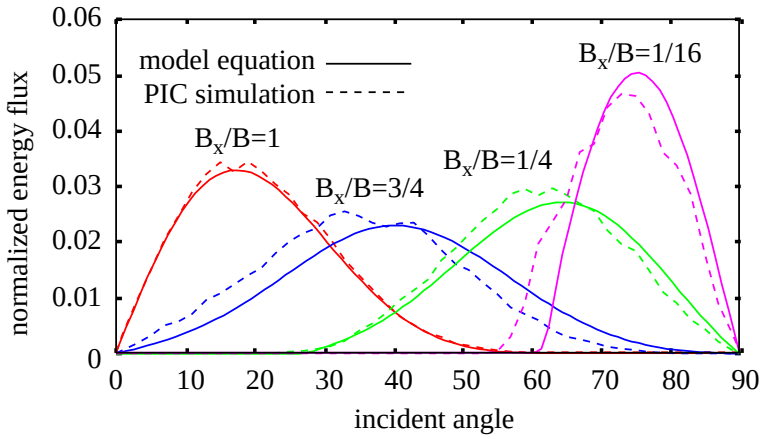

Figure 5.7: Energy flux as functions of the incident angle for $v_{ti}/\Omega_i = \lambda_{De}$ and $B_x/B = 1$, 3/4, 1/4 and 1/16.

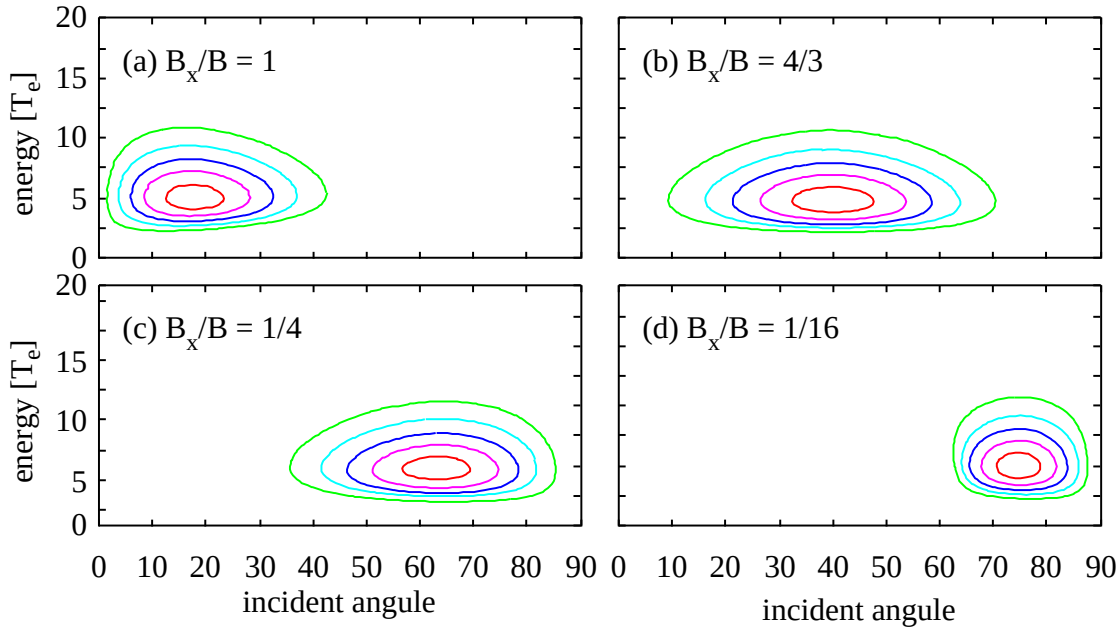

Figure 5.8: Contour plot of the particle flux for the energy and the incident angle. Figure (a), (b), (c) and (d) correspond to the magnetic field of $B_x/B = 1$, 3/4, 1/4 and 1/16, respectively.

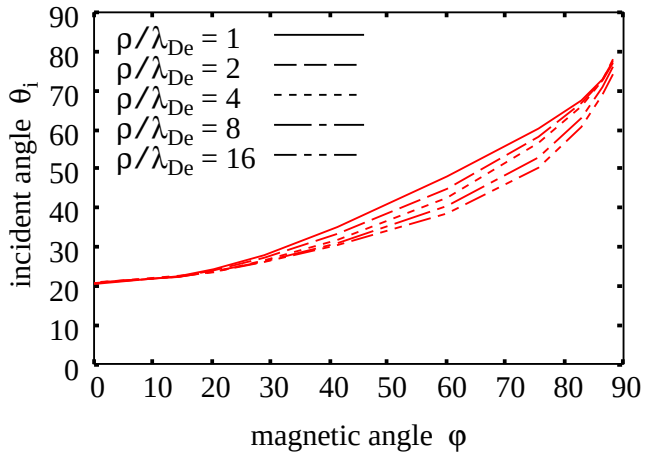

Figure 5.9: Average incident angles obtained from the PIC simulation for $\rho/\lambda_{De} = v_{ti}/\Omega_i\lambda_{De} = 1$, 2, 4, 8 and 16.

the average normal velocity, or normal velocity of the gyrocenter, is much lower than the perpendicular velocity of the gyration. Since a particle is absorbed instantly after a collision with the surface, the circular orbit is scraped off from the edge by the wall. The velocity of the particles in the vicinity of the wall, therefore, have large incident angles.

In order to see the dependence of the incident angles on parameters associated with the magnetic field, we plot the average incident angle as a function of the magnetic field angle φ in Fig. 5.9. The average angles are calculated from the PIC simulation results and weighted by the energy flux. The five curves correspond to the thermal Larmor radii $v_{ti}/\Omega_i\lambda_{De} = 1$, 2, 4, 8 and 16, respectively. We use the system length $L/\lambda_{De} = 32$, 64 and 128 for $v_{ti}/\Omega_i\lambda_{De} = 1$ and 2, $v_{ti}/\Omega_i\lambda_{De} = 4$ and 8, and $v_{ti}/\Omega_i\lambda_{De} = 16$, respectively. When the magnetic field is perpendicular to the wall, $B_x/B = 1$, the perpendicular motion of particles are completely decoupled from the parallel motion and the average incident angles for different $v_{ti}/\Omega_i\lambda_{De}$ coincide to be that of an unmagnetized case. When $\varphi \sim 90°$, θ_i asymptotically approaches to 90°. This behavior is understood as follows. In this case, the normal velocity of particles to the wall is much smaller than the perpendicular velocity. Since particles are immediately absorbed when they hit the wall, almost all the particles remaining in the vicinity of the wall have large incident angles.

A clear dependence of incident angle on the thermal Larmor radii is observed in the range of $30° \lesssim \varphi \lesssim 85°$. The reduction of the incident angles is observed for the weaker magnetic field and especially significant around $\varphi = 70°$. The magnitude of the reduction is logarithmic to the parameter $v_{ti}/\Omega_i\lambda_{De}$ in $1 \le v_{ti}/\Omega_i\lambda_{De} \le 16$. One of the reasons is the increase of the normal velocity due to the polarization drift $(d\mathbf{E}_\perp/dt)/B\Omega = -(v_\parallel/2B\Omega)\partial^2\phi/\partial x^2 \sin 2\varphi\,\hat{\mathbf{x}}$. When the Larmor radius is large compared with the Debye

length, the polarization drift makes the incident angle small. Similar comparisons have been made by DeWald *et al.* [67]. Although they do not specify the absolute value of the ratio $v_{\mathrm{ti}}/\Omega_{\mathrm{i}}\lambda_{\mathrm{De}}$, the dependence of the average angle on the magnetic angle φ and the ratio $v_{\mathrm{ti}}/\Omega_{\mathrm{i}}\lambda_{\mathrm{De}}$ in their paper agree with our results qualitatively.

When the magnetic field becomes normal to the wall, the average incident angle approaches a common value $\theta_{\mathrm{i}} \simeq 21^\circ$. This behavior of the incident angle is consistent with the fact that the parallel and perpendicular motion of particles are completely decoupled if the magnetic field becomes parallel to the normal direction to the wall. Since the perpendicular velocity space is uniform in such case, the plasma becomes equivalent to the unmagnetized one. On the other hand, when the magnetic field becomes perpendicular to the wall, the average incident angle approaches another common value $\theta_{\mathrm{i}} \simeq 90^\circ$. If the magnetic field is nearly parallel to the wall, the averaged normal velocity of a particle, i.e. $v_{\parallel} b_x$, becomes extremely slow and thus the velocity becomes parallel for all the particles hitting the surface.

5.4 Conclusions

The distribution of incident angle when an ion hits the wall in the magnetized plasma was studied by using the model equation and the particle-in-cell (PIC) simulation. The model equation was derived from the gyrokinetic energy conservation law on the moving frame with the $\mathbf{E} \times \mathbf{B}$ drift velocity. The potential profiles and the angular distribution obtained from the model equation and the PIC simulation agreed well with each other in the case of a relatively strong magnetic field, $v_{\mathrm{ti}}/\Omega_{\mathrm{i}}\lambda_{\mathrm{De}} \lesssim 1$. The energy flux distribution for the incident angles becomes broad for intermediate range of B_x/B. On the other hand in the case of magnetic field parallel to the wall, the distribution becomes narrow and has a peak near the region where the perpendicular component of the particle velocity becomes larger than the parallel one.

The average incident angle for various $v_{\mathrm{ti}}/\Omega_{\mathrm{i}}\lambda_{\mathrm{De}}$ was studied by using the PIC simulation. When the magnetic field becomes normal or parallel to the wall, the incident angle approaches the common value $\theta_{\mathrm{i}} = 21^\circ$ or 90°, respectively. The former value corresponds to the unmagnetized one. The dependence on the magnetic field strength is mainly observed when the angle of the magnetic field is in the range $30^\circ \lesssim \varphi \lesssim 85^\circ$. The incident angle decreases as the magnetic field becomes weak.

The range of the parameter $v_{\mathrm{ti}}/\Omega_{\mathrm{i}}\lambda_{\mathrm{De}}$ used in this work does not cover the whole range at the divertor plate in fusion devices. When the magnetic field is weaker so that the thermal electron Larmor radius is comparable or larger than the Debye length, it works as a characteristic length in the potential profile. The incident angle distribution for electron

is also expected to change according to the ratio $v_{te}/|\Omega_e|\lambda_{De}$. The analysis of the incident angle distribution for a wider range of magnetic field strength is a remaining issue. The influence of particle collisions and sources must be evaluated in further studies for more realistic plasmas.

Chapter 6

Conclusions

In the first half of this thesis, the gyrokinetic equations for electromagnetic perturbations were derived by using the modern analytical dynamics and the refined gyrokinetic equations applicable for the plasma with large equilibrium electric fields were also formulated. It was confirmed that the particle dynamics can be more correctly treated for large electric fields. In the latter half, the application of the gyrokinetic equation for the modeling of the sheath plasma in magnetic fields was studied and the dependences of the electric field and incident angle of ions were investigated. The validity of the present model was confirmed by the comparisons with the full-kinetic PIC simulation.

Gyrokinetic equations with the strong electric field

A new comprehensive derivation of the nonlinear gyrokinetic equations is presented in Chap. 2 and its refinement for the strong electric field is presented in Chap. 3.

The objective of Chap. 2 is to obtain the general expressions of the gyrokinetic equations as a preliminary for the succeeding chapters. Employing the 1-form representation of a single particle dynamics and Lie transformation technique, we carried out the standard procedure developed by Littlejohn, Brizard, Qin *et al.* and commonly used in the gyrokinetic analyses. Although there is no significant difference in the essences of their calculations and also ours, they use different ways to represent the gyrocenter coordinate system and the 1-form on it as is described in Sec. 2.2.

We chose a simple and explicit way to obtain the guiding-center 1-form. The guiding-center coordinate is introduced as a usual coordinate transformation used by Littlejohn and Qin instead of a sophisticated but complicated way with the Lie transformation adopted by Brizard. Although our, or Qin's, scheme does not provide the 'best' guiding-center coordinate system, the equations of motion obtained through the Lie transformation employed later are identical with those of Brizard. In order to exclude the arbitrariness

in the definition of the gyrophase, we employed the gyrogauge transformation introduced by Littlejohn. It redefines the base direction by which the gyrophase angle is measured and makes it possible to suppress the physically meaningless terms caused by the arbitrariness.

After the above preliminary transformation, we employed the successive Lie transformations to isolate and decouple the gyrophase dependences in the guiding-center 1-form order by order in Sec. 2.3. While the new coordinate system, or gyrocenter coordinate system, allows a gyrophase dependent perturbation, the equations of motion derived from the gyrocenter 1-form evolves independently of the gyrophase. We obtained a general form of the gyrokinetic 1-form determined by the gauge function and the Lie generator given by ordinary differential equations. Using the Lie generator, we obtained the pullback of the distribution function, i.e. the gyrocenter distribution function expressed by the original particle coordinate variables. The general expression of the charge and current densities to be used in Maxwell's equations were obtained by the pullback technique developed by Brizard and Qin and thus a closed set of the gyrokinetic equations was formulated. In addition to the general expressions of the closed equations, we calculated limiting forms based on the assumptions usually used in the analysis of the micro-instabilities, i.e. the time-scale of the plasma is much more longer than the particle gyration and the dominant motions of the particle are only the parallel and gyrating motions. Finally, we recovered a closed set of the gyrokinetic equations essentially same as those in the previous works by Lee, Dubin, Hahm, Brizard, Qin *et al.*.

In Chap. 3, we have refined gyrokinetic equations applicable to edge plasmas with large flow shears by adopting a modified guiding-center coordinate system as a starting point of the derivation. An attempt to improve the gyrokinetic equation for a strong electric field was originally carried out by Littlejohn and generalized to the plasma with potential perturbations by Brizard, Hahm, Qin *et al.* We adopted the same technique as in their works, i.e. a reference frame moving with an equilibrium drift velocity $\mathbf{D}$ is introduced in the guiding-center coordinate system. Their choice of the reference velocity $\mathbf{D}$ is that of a simple $\mathbf{E} \times \mathbf{B}$ drift for the equilibrium electric field, i.e. $\mathbf{E}_0(\mathbf{X}) \times \mathbf{B}_0 / B_0^2$, measured at the guiding-center position $\mathbf{X}$. Their choice is simple and perfect for the one dimensional potential profile, while it gives less accurate solution for general potential profiles.

Through the investigation of the effects of the reference velocity $\mathbf{D}$ on the zeroth order equations of motion, we obtained a new definition of the velocity in Sec. 3.3 as a ordinary differential equation. The solution of the determining equation of $\mathbf{D}$ was investigated in Sec. 3.4 and a analytical expression of the solution for an special potential profile and a numerical solution for the general profiles were obtained. Through the standard procedure

of derivation of the gyrokinetic equations, the general form of the gyrokinetic 1-form, gauge function and the Lie generators were obtained in Sec. 3.5. Limiting forms for the electrostatic plasma were also obtained.

The validation of the present equations was confirmed numerically in Sec. 3.6. The time-evolution of the particle energy calculated form the solution of the gyrokinetic equations was compared with that directly calculated from the full-kinetic equations, i.e. the usual Newton's equations of motion. From the comparisons of the energy for various values of the electric field, magnetic field, initial velocity and initial position, we confirmed that the refined equations derived here yield more accurate solutions than the previous equations for Qin's simple reference velocity, especially when the the electric field is strong and the curvature of the potential contours is large. The effect of the refinement becomes notable when the $\mathbf{E} \times \mathbf{B}$ drift speed becomes comparable to the thermal velocity.

Kinetic modeling of the sheath layer

The objectives of Chap. 4 and 5 are to understand the physics of the sheath plasma especially the effects of the magnetic fields on the potential profile and particle's incident angle to the wall. To this end, the kinetic equations for an electrostatic potential in a sheath layer were derived from the collisionless Vlasov equation in Chap. 4. In the derivation, we assumed that the plasma source which has the fixed velocity distribution at one end, $x = 0$, and the absorbing wall at the other end, $x = L$. In the sheath layer, $0 < x < L$, no source and no particle collision exist. The fundamental equations were obtained in Sec. 4.2.1 and the stability condition of the sheath formation was also obtained in Sec. 4.2.2. We recovered the generalized Bohm criterion derived by Harrison and Thompson. In addition to that, we obtained a small correction term caused by the presence of the cut-off velocity of electrons.

In the presence of an uniform magnetic field, the gyrokinetic treatment of magnetized electrons and ions was applied to the plasma sheath problem for the first time. In order to describe with the strong electric field in the sheath layer, we adopted the gyrokinetic theory on a reference frame moving with the $\mathbf{E} \times \mathbf{B}$ drift velocity, which was derived in Chap. 4. We obtained potential equations in the sheath layer from the gyrokinetic collisionless Vlasov equation. They are similar to the unmagnetized ones, but they include correction terms caused by the finite Larmor effects, the differences between the parallel and perpendicular motions and the particle dynamics near the wall.

The condition for the stable sheath formation in a magnetic field was also derived under the assumption that $v_\perp/\Omega \ll L$ in Sec. 4.3.3. The result is quite similar to the generalized Bohm criterion without a magnetic field except that the the parallel velocity

should be used in the condition.

In Sec. 4.4, numerical comparisons of the solution obtained from the present model and the results of the full-kinetic particle-in-cell simulation. Here, we adopted a shifted Maxwellian with a truncation for the ion source velocity distribution. The cut-off velocity was determined to satisfy the generalized Bohm criterion at the source boundary. From the comparison of the profiles for various values of B_x/B and ρ_i/λ_{De}, we confirmed that the present model provides accurate solutions for a strongly magnetized plasma, i.e. $\rho_i/\lambda_{De} \lesssim 1$. The dependence of the wall electric field on the angle of the magnetic field, B_x/B, was also investigated. It was found that the particle loss due to the gyration and the polarization effect reduce the charge density and the electric field near the wall. The effect of the particle loss is observed for $B_x/B < 0.5$ and becomes larger as B_x/B approaches to 0. On the other hand, the polarization effect always exists except $B_x/B \sim 1$.

In Chap. 5, distribution of the incident angle of ions when they hit the wall in a magnetized plasma was investigated by using the model equation obtained in Chap. 4 and a full-kinetic PIC simulation. The potential profiles and the angular distribution obtained from the model equation and the PIC simulation agreed well with each other in the case of a relatively strong magnetic field, $v_{ti}/\Omega_i\lambda_{De} \lesssim 1$. The energy flux distribution with respect to an incident angle becomes broad for intermediate range of B_x/B. On the other hand in the case of magnetic field nearly parallel to the wall, the distribution becomes narrow and has a peak near the region where the perpendicular component of the particle velocity becomes larger than the parallel one. The average incident angle for various $v_{ti}/\Omega_i\lambda_{De}$ was studied by using the PIC simulation. In the case of the magnetic field normal to the wall the incident angle approaches the unmagnetized one. On the other hand, in the case of nearly parallel magnetic field, the incident direction approaches parallel to the wall. The dependence on the magnetic field strength is mainly observed when the angle of the magnetic field is in a moderate range. The incident angle decreases as the magnetic field becomes weak.

Future works

The most important issue with regard to the gyrokinetic studies in Chap. 2 and 3 is the rigorous derivation of conserved quantities for the plasma. From the analytic investigation and the numerical verifications in Chap. 3, the improvement of the accuracy for the plasma with large $\mathbf{E}\times\mathbf{B}$ flow shears has been confirmed. The present formulation is, however, based on the single particle 1-form and thus the conserved quantity such as energy and momentum of the many-body system, or plasma, is not obtained here. The existence and the knowledge of the explicit invariant is essential not only for the theoretical com-

pleteness but for the numerical simulation as a tool of validation. The application to the simulation study has been a strong motivation for the development of the gyrokinetic theories and the demand for the global simulation including the edge plasma will become higher. In order to realize efficient and reliable simulation codes, the theoretical assurance of the energy conservation and the determination of its explicit expression may be the most important topic of further study in this field.

Another issue attracting an attention lately is a more rigorous calculation scheme for higher frequency waves. In this thesis, the time-scale of the perturbation potentials is assumed to be much longer than that of the gyration. The determining equation of the gauge function is approximated by using $\partial S/\partial t \sim 0$. Although this reduction yields efficient and sufficiently accurate equations for the low frequency drift waves, it fails in the high frequency range such as ion cyclotron wave. The analytical basis is given by Brizard and Qin and an implementation for a simulation code is also given by Kolesnikov *et al.* [23]. A full-kinetic simulation may be suitable for the ion cyclotron wave in heating processes, but investigation of the such numerical scheme will increase the accuracy even in the case of low frequency wave.

The remaining issue with regard to the sheath modeling in Chap. 4 and 5 is the treatment of a weakly magnetized plasma characterized by the gyroradius longer than the Debye length. The present model equation does not yield accurate solutions in such conditions. One reason is in the incomplete implementation of the pullback expression in the Poisson equation, i.e. the contributions from the Lie generator are ignored here. The use of more rigorous density equation will reduce the limitation on the magnetic field strength, or smallness of the Debye length. It is expected that the generalization of the model for small Debye length reveals the quantitative property of the magnetic presheath.

Another important element in the study of plasma-wall interactions is the collisionality. Although it is ignored here, it should be included when one considers more realistic plasma. With regard to the collisionality and the small Debye length, the investigation of the presheath layer including sources and collisions will be challenging but important application of the sheath modeling.

Appendix A

Modern analytical mechanics

We present a review of the fundamentals of the differential geometry and modern analytical mechanics [68] which is necessary for the derivation of the gyrokinetic equations.

A.1 Fundamental bases of the differential geometry

A.1.1 Vector field

A function on a differentiable manifold $\mathcal{M}$ is defined by a map

$$f : \mathcal{M} \longrightarrow \mathcal{R} : P \in \mathcal{M} \longmapsto f(P) \in \mathcal{R}. \tag{A.1}$$

A curve on a manifold $\mathcal{M}$ is similarly defined by a map

$$c : \mathcal{R} \longrightarrow \mathcal{M} : t \in \mathcal{R} \longmapsto Q = c(t) \in \mathcal{M}. \tag{A.2}$$

An intuitive representation is given in Fig. A.1. From these maps, the directional derivative operator v_Q at the point Q is introduced as

$$v_Q[f] \equiv \frac{df(c(t))}{dt}. \tag{A.3}$$

It operates to an arbitrary function f and is written in a local coordinate q^i as

$$v_Q = \frac{dq^i}{dt}\frac{\partial}{\partial q^i}. \tag{A.4}$$

This differential operator satisfies the following relations;

$$v_Q[af + bg] = av_Q[f] + bv_Q[g], \tag{A.5}$$

$$v_Q[fg] = v_Q[f]g(Q) + f(Q)ua_Q[g]. \tag{A.6}$$

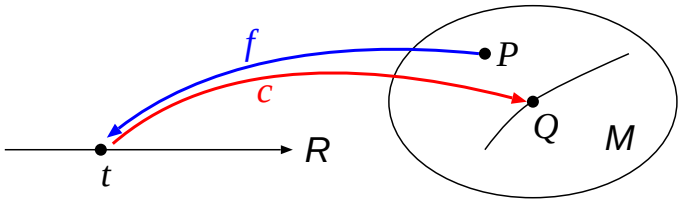

Figure A.1: Function and curve.

A set of these differential operators, therefore, makes a vector space, which is called a tangent space at the point Q on a manifold $\mathcal{M}$ and denoted by $(T\mathcal{M})_Q$. The element of this space, $v_Q \in (T\mathcal{M})_Q$, is called a tangent vector at the point $Q \in \mathcal{M}$. The differential operators,$\partial_i \equiv \partial/\partial q^i$, are the natural bases in the tangent space for the local coordinate system q^i. The union of the tangent space at each point on $\mathcal{M}$,

$$T\mathcal{M} = \bigcup_{Q\in\mathcal{M}} (T\mathcal{M})_Q, \tag{A.7}$$

is the tangent bundle. A vector field is defined as a map from the manifold to the tangent bundle,

$$v : \mathcal{M} \longmapsto T\mathcal{M} : Q \in \mathcal{M} \longmapsto v_Q \in (T\mathcal{M})_Q. \tag{A.8}$$

A trajectory of a point on the manifold carried by the vector field v is called an integral curve. It is given as the solution curve, $c(t) : \mathcal{R} \to \mathcal{M}$, of the differential equation

$$\frac{dc}{dt}(t) = v_{c(t)}. \tag{A.9}$$

It is also expressed in the local coordinate system as $\dot{c}^i = v^i(c)$. A map advancing a point on $\mathcal{M}$ form the initial position Q_0 along the vector field by t is expressed as

$$\varphi_t : \mathcal{M} \longrightarrow \mathcal{M} : Q_0 \longmapsto Q_t = \varphi_t(Q_0). \tag{A.10}$$

The union of the map for each t, $\{\varphi_t \,|\, t \in R\}$ is called a flow. Since it satisfies the following relations

$$\varphi_0 = \mathrm{id} \text{ (identity map)}, \tag{A.11}$$

$$\varphi_{t+s} = \varphi_t \circ \varphi_s, \tag{A.12}$$

$$\varphi_{-t} = (\varphi_t)^{-1}, \tag{A.13}$$

the vector field v makes 1-parameter transformation group and the map φ_t is an element in the group.

A.1.2 One-form

The dual space of the tangential space, $(TM)_Q$, is called a cotangent space and written as $(T^*M)_Q$. As described above, a tangent vector v_Q operates to a function f as $v_Q[f] = v_Q^i \partial_i f$ in a local coordinate system q^i. This relation can be interpreted as the mapping from a tangent vector to a real number;

$$(df)_Q : (T\mathcal{M})_Q \longrightarrow \mathcal{R} : v_Q \longmapsto (df)_Q[v_Q] = v_Q[f] \in \mathcal{R}. \tag{A.14}$$

A set of these maps, makes a vector space, which is called a cotangent space at the point Q on a manifold $\mathcal{M}$ and denoted by $(T^*\mathcal{M})_Q$. If we use the natural bases for a local coordinate system, ∂_i, the dual bases of the cotangent space are dq^i;

$$(dq^i)[\partial_j] = (\partial_j)[q^i] = \frac{\partial q^i}{\partial q^j} = \delta^i_j \tag{A.15}$$

An element in the tangent space, $v_Q = v_Q^i \partial_i$, and an element in the cotangent space, $\gamma_Q = \gamma_{Qi} dq^i$ satisfy the relation

$$\gamma_Q[v_Q] = \gamma_{Qi} v_Q^j (dq^i)[\partial_j] = \gamma_{Qi} v_Q^i. \tag{A.16}$$

The union of the cotangent space at each point on $\mathcal{M}$,

$$T^*\mathcal{M} = \bigcup_{Q \in \mathcal{M}} (T^*\mathcal{M})_Q, \tag{A.17}$$

is the cotangent bundle. A 1-form is defined as a map from the manifold to the cotangent bundle,

$$\gamma : \mathcal{M} \longmapsto T^*\mathcal{M} : Q \in \mathcal{M} \longmapsto v_Q \in (T^*\mathcal{M})_Q. \tag{A.18}$$

A map from a manifold to a real number

$$i_v\gamma : \mathcal{M} \longrightarrow \mathcal{R} : Q \in \mathcal{M} \longmapsto \gamma_Q[v_Q] = \gamma_{Qi} v_Q^i \in \mathcal{R}$$

is called an interior product.

The 1-form corresponds to the total differential of a scalar function. In general, the p+1-form is derived from the p-form by the exterior derivative. The exterior derivative of the 0-form, i.e. scalar function, gives the 1-form;

$$df = \frac{\partial f}{\partial q^i} dq^i. \tag{A.19}$$

The exterior derivative of the 1-form gives the 2-form;

$$d\gamma = d\gamma_i \wedge dq^i = \frac{\partial \gamma_i}{\partial q^j} dq^j \wedge dq^i, \quad dq^i \wedge dq^j = -dq^j \wedge dq^i \tag{A.20}$$

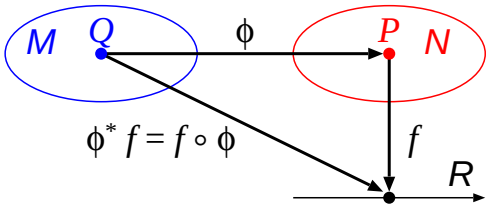

Figure A.2: Function and its pull back.

The interior product of a 2-form ω and a vector field v is given by

$$i_v\omega = i_v(\omega_{ij}dq^i \wedge dq^j) = v^i\omega_{ij}dq^j - v^j\omega_{ij}dq^i = v^j(\omega_{ji} - \omega_{ij})dq^i. \tag{A.21}$$

The exterior derivative in the three dimensional real space (x, y, z) gives the familiar vector equations,

$$df = \nabla f \cdot d\mathbf{r}, \quad d\mathbf{r} = (dx, dy, dz), \tag{A.22}$$

$$d(\mathbf{A} \cdot d\mathbf{r}) = \nabla \times \mathbf{A} \cdot d\mathbf{S}, \quad d\mathbf{S} = (dy \wedge dz, dz \wedge dx, dx \wedge dy), \tag{A.23}$$

$$d(\mathbf{B} \cdot d\mathbf{S}) = \nabla \cdot \mathbf{B}\, dV, \quad dV = dx \wedge dy \wedge dz. \tag{A.24}$$

The identity equation $d(df_n) = 0$ gives the vector identities, $\nabla\times(\nabla f) = \mathbf{0}$ and $\nabla\cdot(\nabla\times\mathbf{A}) = 0$.

A.1.3 Pull back

Suppose there are two manifolds, $\mathcal{M}$ and $\mathcal{N}$ and a map

$$\varphi : M \longrightarrow N : Q \in M \longmapsto P \in N. \tag{A.25}$$

The composed function $f \circ \varphi$ for an arbitrary function $f : \mathcal{N} \mapsto \mathcal{R}$ can be regarded as a function on the manifold $\mathcal{M}$ and written as $\varphi^* f$;

$$(\varphi^* f)(Q) = f \circ \varphi(Q) = f(\varphi(Q)) = f(P) \tag{A.26}$$

This new function is called a pull back. The pull back for the 1-form is given by

$$\varphi_t^*\left(\gamma_i(q)dq^i\right) = \gamma_i(\varphi_t q)d\left(\varphi_t^i q\right) = \gamma_i(\varphi_t q)\frac{\partial\varphi_t^i}{\partial q^j}dq^j. \tag{A.27}$$

An intuitive representation is given in Fig. A.2.

A.1.4 Lie derivative

The Lie derivative generated by a vector field v is formally written as

$$\mathcal{L}_v = \lim_{t\to 0} \frac{\varphi_t^* - \mathrm{id}}{t}, \tag{A.28}$$

where the maps φ^* and id are the pull back of the flow generated by the vector v and the identity map, respectively. The Lie derivative of a function, or 0-form, is given by

$$\begin{aligned}
\mathcal{L}_v f &= \lim_{t\to 0} \frac{\varphi_t^* f(q) - f(q)}{t} \\
&= \lim_{t\to 0} \frac{f(\varphi_t q) - f(q)}{t} \\
&= \lim_{t\to 0} \frac{f(q) + \left(v^i \partial_i f(q)\right) t - f(q)}{t} \\
&= v^i \frac{\partial f}{\partial q^i}.
\end{aligned} \tag{A.29}$$

The Lie derivative of a 1-form is given by

$$\begin{aligned}
\mathcal{L}_v \gamma &= \lim_{t\to 0} \frac{\gamma_i(\varphi_t q)\partial_j \varphi_t^i dq^j - \gamma}{t} \\
&= \gamma_i \frac{\partial v^i}{\partial q^j} dq^j + v^j \frac{\partial \gamma_i}{\partial q^j} dq^i \\
&= \left(\gamma_j \frac{\partial v^j}{\partial q^i} + v^j \frac{\partial \gamma_i}{\partial q^j}\right) dq^i.
\end{aligned} \tag{A.30}$$

These relations can be rewritten without using the local coordinate system as

$$i_v(df) = \mathcal{L}_v f, \tag{A.31}$$

$$\begin{aligned}
i_v(d\gamma) + d(i_v\gamma) &= i_v\left(d\gamma_i \wedge dq^i\right) + d\left(v^i \gamma_i\right) \\
&= \frac{\partial \gamma_i}{\partial q^j}\left(v^j dq^i - v^i dq^j\right) + \left(\frac{\partial v^i}{\partial q^j}\gamma_i + v^i \frac{\partial \gamma_i}{\partial q^j}\right) dq^j \\
&= \mathcal{L}_v \gamma.
\end{aligned} \tag{A.32}$$

A.1.5 Lie transformation

A transport of a point along a vector field v is given by the differential equation

$$\frac{\partial Q}{\partial t} = i_v dQ. \tag{A.33}$$

The flow generated by the vector field is, therefore, written as

$$\varphi_t = \exp(t i_v d). \tag{A.34}$$

This map can be used for the coordinate transformation. The bases of the local coordinate system q^i are transformed to the new bases q^i_t;

$$\varphi_t : q^i \longmapsto q^i_t = \exp(t i_v d)\, q^i. \tag{A.35}$$

If the parameter t is sufficiently small, the transformation is near-identity transformation and thus Taylor expanded as

$$q^i_t = q^i + t v^i + \frac{t^2}{2} i_v (d v^i) + \cdots. \tag{A.36}$$

From the definition, the Lie derivative generated by a vector field v is written as

$$\mathcal{L}_v = \left.\frac{d}{dt}\right|_{t=0} \varphi^*_t, \tag{A.37}$$

where the map φ^*_t is the pull back of the flow. This differential equation yields the pull back of the flow φ_t as an exponential map

$$\varphi^*_t = \exp(t\mathcal{L}_v). \tag{A.38}$$

Therefore, the pull back of 1 1-form $\gamma_t(Q_t)$ is given by

$$\gamma_t(Q_t) = \exp(-t\mathcal{L}_v)\gamma(Q_t) \tag{A.39}$$

$$= \gamma_i(Q_t) dq^i_t - t\mathcal{L}_v\gamma(Q_t) + \frac{t^2}{2}\mathcal{L}^2_v\gamma(Q_t) - \cdots. \tag{A.40}$$

A.2 Mathematical description of the mechanics

A.2.1 Modified Hamilton's principle

Suppose a set of the canonical coordinate variables and the Hamiltonian are given by $\mathbf{q}$, $\mathbf{p}$ and $H(t, \mathbf{q}, \mathbf{p})$. According to the modified Hamilton's principle, the motion generated by the Hamiltonian is determined by the condition that the action integral,

$$I \equiv \int_{t_1}^{t_2} \left(\mathbf{p} \cdot \frac{d\mathbf{q}}{dt} - H \right) dt, \tag{A.41}$$

has an extreme value. The integral can be rewritten as

$$I \equiv \int_{t_1}^{t_2} (\mathbf{p} \cdot d\mathbf{q} - H dt) = \int_{t_1}^{t_2} \gamma_i \frac{dc}{dt} dt = \int_c \gamma_i \, dz^i, \tag{A.42}$$

where the local coordinate system $z^i \equiv (t, \mathbf{q}, \mathbf{p})$ and the 1-form is introduced by

$$\gamma \equiv \mathbf{p} \cdot d\mathbf{q} - H dt, \tag{A.43}$$

or explicitly

$$\gamma_0 = -H(\mathbf{q}, \mathbf{p}), \quad \gamma_{i=1,2,3} = p^i, \quad \gamma_{i=4,5,6} = 0. \tag{A.44}$$

The integral is carried out over the curve c.

The condition for having an extreme value is given by the variational principle,

$$\delta I = \delta \int_c \gamma_i \, dz^i = 0. \tag{A.45}$$

Although the variation of the function γ_i is usually utilized in this calculation, we proceed in a more geometrical expression. The variation of the action integral can be understood as a difference of the integral over a curve c and an infinitesimally deviated curve c'. By construction, the new curve c' has to satisfy the following restrictions;

$$c(t_1) = c'(t_1), \quad c(t_2) = c'(t_2). \tag{A.46}$$

We employ an arbitrary vector field v and a infinitesimally small parameter $\delta\tau$. The curve c' is expressed as

$$c'(t) = c(t) + \delta\tau v. \tag{A.47}$$

The vector field also has the restrictions, $v = 0$ at $t = t_1$ and t_2. The variational principle is rewritten as

$$\delta I = \int_{c+\delta\tau v} \gamma_i \, dz^i - \int_c \gamma_i \, dz^i = \int_c (\varphi^*_{\delta\tau}\gamma - \gamma). \tag{A.48}$$

If we take the limit $\delta\tau \to 0$ in this equation, the right hand side yields the Lie derivative and thus we obtain

$$\lim_{\delta\tau\to 0} \frac{\delta I}{\delta\tau} = \int_c \mathcal{L}_v \gamma = 0. \tag{A.49}$$

Using the relation $\mathcal{L}_v\gamma = i_v d\gamma - d(i_v\gamma)$, the integral is calculated as

$$\int_c i_v d\gamma + \int_c d(i_v\gamma) = \int v^i \left[z^i, z^j\right] \frac{dc}{dt} dt + \left[i_v\gamma\right]_{t_1}^{t_2} = 0, \tag{A.50}$$

where we introduce the Lagrange bracket

$$\left[z^i, z^j\right] \equiv \frac{\partial \gamma_j}{\partial z^i} - \frac{\partial \gamma_i}{\partial z^j}. \tag{A.51}$$

Since Eq. (A.50) has to be valid for any vector field v which vanishes at $t = t_1$ and t_2, it yields the equation of motion,

$$\left[z^i, z^j\right] \frac{dc^j}{dt} = 0, \quad \text{or} \quad i_c d\gamma = 0. \tag{A.52}$$

This equation corresponds to the Euler-Lagrange equation for the Lagrangian.

A.2.2 Fundamental 1 form

A 1-form describing a dynamical system is called a fundamental 1-form. One of the advantages of the 1-form representation of the mechanics is its invariant characteristic in the coordinate transformations. Suppose that a fundamental 1-form is expressed in a coordinate system $q = (q^i)$ as $\gamma = \gamma_i(q)dq^i$ and a new coordinate system $Q = (Q^i)$ is given by $\varphi : q \mapsto Q$. The fundamental 1-form can be expressed also in the coordinate system Q as $\Gamma = \Gamma_i dQ^i$. If the both 1-form represent the same dynamics, they are equivalent, $\Gamma(Q) \equiv \gamma(q)$ or $\Gamma(Q) = \left[\varphi^{-1*}\gamma\right](Q)$. The explicit transformation of the 1-form is as follows;

$$\begin{aligned}\gamma = \gamma_i dq^i &= \gamma_i(\varphi^{-1}Q)d(\varphi^{-1i}Q) \\ &= \varphi^{-1*}\gamma_i \frac{\partial \varphi^{-1i}}{\partial Q^j} dQ^j = \Gamma_j dQ^j. \end{aligned} \tag{A.53}$$

Therefore, the new 1-form is written in terms of the original 1-form as

$$\Gamma_i = \varphi^{-1*}\gamma_j \frac{\partial \varphi^{-1j}}{\partial Q^i}. \tag{A.54}$$

We note that the coordinate transformation here is carried out by the arbitrary map φ and thus there is no restriction in the transformation. On the other hand, the Hamiltonian mechanics requires the recalculation of the Poisson tensor in case of the non-canonical transformation. In the Lagrangian mechanics, only the transformation in the configuration space is available because the coordinate variables for the velocity are automatically determined from those of the position.

A.2.3 Fundamental 1 form of a charged particle

The dynamics of a charged particle is described in the coordinate system $z = (z^0, z^1, \ldots, z^6) = (t, \mathbf{x}, \mathbf{v})$ by the fundamental 1-form

$$\gamma \equiv [m\mathbf{v} + q\mathbf{A}(\mathbf{x})] \cdot d\mathbf{x} - \left[\frac{m}{2}v^2 + q\phi(\mathbf{x})\right] dt. \tag{A.55}$$

The equations of motion are given by the Euler-Lagrange equations;

$$i_{\dot{z}} d\gamma = 0, \quad \text{or} \quad \omega_{ij}\frac{dz^j}{dt} = \left(\frac{\partial \gamma_i}{\partial z^0} - \frac{\partial \gamma_0}{\partial z^i}\right)\dot{z}^0 \ \text{ for } \forall i, \tag{A.56}$$

where the zeroth coordinate variable z^0 represents the time, or $z^0 = t$. The tensor $\overleftrightarrow{\omega}$ introduced here is the Lagrange tensor,

$$\omega_{ij} \equiv \left[z^i, z^j\right] = \left(\frac{\partial \gamma_j}{\partial z^i} - \frac{\partial \gamma_i}{\partial z^j}\right). \tag{A.57}$$

The Poisson tensor $\overleftrightarrow{\sigma}$ is introduced as an inverse matrix of the Lagrange tensor; $\sigma^{ij}\omega_{jk} \equiv \delta^i_j$. Using this relation, the equations of motion are written as the Hamilton equations;

$$\frac{dz^i}{dt} = \sigma^{ij}\left(\frac{\partial \gamma_j}{\partial t} - \frac{\partial \gamma_t}{\partial z^j}\right). \tag{A.58}$$

In the familiar coordinate system $(\mathbf{x}, \mathbf{v})$, the Lagrange and Poisson tensors are given by

$$\omega_{ij} = \begin{pmatrix} -q\mathbf{B}\times\overleftrightarrow{I} & -m\overleftrightarrow{I} \\ m\overleftrightarrow{I} & \overleftrightarrow{0} \end{pmatrix}, \tag{A.59}$$

$$\sigma_{ij} = \begin{pmatrix} \overleftrightarrow{0} & \overleftrightarrow{I}/m \\ -\overleftrightarrow{I}/m & -q\mathbf{B}\times\overleftrightarrow{I}/m^2 \end{pmatrix}. \tag{A.60}$$

where we use the unit tensor $\overleftrightarrow{I} = \delta^{ij}$ and the notation $\epsilon^{ijk}B^k = -\mathbf{B}\times\overleftrightarrow{I}$. Newton's equations of motion are recovered from the Hamilton equations (A.58);

$$\frac{d\mathbf{x}}{dt} = \mathbf{v}, \tag{A.61}$$

$$\frac{d\mathbf{v}}{dt} = \frac{q}{m}\mathbf{v}\times\mathbf{B} - \frac{q}{m}\left(\nabla\phi + \frac{\partial \mathbf{A}}{\partial t}\right). \tag{A.62}$$

Appendix B

Useful formulae

B.1 Vector operations

Levi-Civita symbol ϵ_{ijk} and vector product:

$$\sum_k \epsilon_{ijk}\epsilon_{mnk} = \delta_{im}\delta_{jn} - \delta_{in}\delta_{jm}. \tag{B.1}$$

$$(\mathbf{u}\times\mathbf{v})\times\mathbf{w} = (\mathbf{w}\cdot\mathbf{u})\mathbf{v} - (\mathbf{v}\cdot\mathbf{w})\mathbf{u}. \tag{B.2}$$

$$\mathbf{u}\times(\mathbf{v}\times\mathbf{w}) = (\mathbf{w}\cdot\mathbf{u})\mathbf{v} - (\mathbf{u}\cdot\mathbf{v})\mathbf{w}. \tag{B.3}$$

$$u_i v_j - u_j v_i = \sum_k \epsilon_{ijk}(\mathbf{u}\times\mathbf{v})_k = -(\mathbf{u}\times\mathbf{v})\times\overleftrightarrow{I}. \tag{B.4}$$

$$(\mathbf{u}\times\mathbf{w})\cdot\nabla\times\mathbf{v} = \mathbf{u}\cdot\nabla\mathbf{v}\cdot\mathbf{w} - \mathbf{w}\cdot\nabla\mathbf{v}\cdot\mathbf{u}. \tag{B.5}$$

Orthonormal vectors $\hat{\mathbf{a}}$, $\hat{\mathbf{b}}$ and $\hat{\mathbf{c}}$:

$$\hat{\mathbf{b}}\times = \hat{\mathbf{a}}\hat{\mathbf{c}} - \hat{\mathbf{c}}\hat{\mathbf{a}}. \tag{B.6}$$

$$\hat{\mathbf{b}}\times\hat{\mathbf{b}}\times = -\left(\overleftrightarrow{I} - \hat{\mathbf{b}}\hat{\mathbf{b}}\right)\cdot. \tag{B.7}$$

$$\hat{\mathbf{a}}\cdot\nabla\times\hat{\mathbf{b}} = \left(\hat{\mathbf{b}}\cdot\nabla\hat{\mathbf{b}}\cdot\hat{\mathbf{c}}\right). \tag{B.8}$$

$$\hat{\mathbf{b}}\cdot\nabla\times\hat{\mathbf{b}} = \left(\hat{\mathbf{c}}\cdot\nabla\hat{\mathbf{b}}\cdot\hat{\mathbf{a}}\right) - \left(\hat{\mathbf{a}}\cdot\nabla\hat{\mathbf{b}}\cdot\hat{\mathbf{c}}\right). \tag{B.9}$$

$$\hat{\mathbf{c}}\cdot\nabla\times\hat{\mathbf{b}} = -\left(\hat{\mathbf{b}}\cdot\nabla\hat{\mathbf{b}}\cdot\hat{\mathbf{a}}\right). \tag{B.10}$$

$$\hat{\mathbf{b}}\times(\nabla\times\hat{\mathbf{b}}) = -\hat{\mathbf{b}}\cdot\nabla\hat{\mathbf{b}}. \tag{B.11}$$

$$\nabla\times\hat{\mathbf{b}} = -\hat{\mathbf{c}}\times\nabla\hat{\mathbf{b}}\cdot\hat{\mathbf{c}} - \hat{\mathbf{a}}\times\nabla\hat{\mathbf{b}}\cdot\hat{\mathbf{a}}. \tag{B.12}$$

$$\hat{\mathbf{b}}\cdot\nabla\hat{\mathbf{b}}\times\hat{\mathbf{b}} = \left(\hat{\mathbf{b}}\cdot\nabla\hat{\mathbf{b}}\cdot\hat{\mathbf{a}}\right)\hat{\mathbf{c}} - \left(\hat{\mathbf{b}}\cdot\nabla\hat{\mathbf{b}}\cdot\hat{\mathbf{c}}\right)\hat{\mathbf{a}}. \tag{B.13}$$

$$\left(\hat{\mathbf{b}}\times\nabla\right)\cdot\hat{\mathbf{b}} = -\hat{\mathbf{b}}\cdot\left(\nabla\times\hat{\mathbf{b}}\right). \tag{B.14}$$

B.2 Taylor expansions

$$\mathrm{erf}\,(x) \equiv \frac{2}{\sqrt{\pi}}\int_0^x \exp\left(-x^2\right)dx \tag{B.15}$$

$$\overset{x\ll 1}{\simeq} \frac{2}{\sqrt{\pi}}x - \frac{2}{3\sqrt{\pi}}x^3 + \frac{1}{5\sqrt{\pi}}x^5 + O(x^7) \tag{B.16}$$

$$\overset{x\gg 1}{\simeq} 1 - \frac{\exp\left(-x^2\right)}{\sqrt{\pi}x} + \frac{\exp\left(-x^2\right)}{2\sqrt{\pi}x^3} - \frac{3\exp\left(-x^2\right)}{4\sqrt{\pi}x^5} + O(x^{-7}\mathrm{e}^{-x^2}). \tag{B.17}$$

$$\mathrm{J}_0(z) = 1 - \frac{z^2}{4} + \frac{z^4}{64} + O(z^6). \tag{B.18}$$

$$\mathrm{I}_0(z) = 1 + \frac{z^2}{4} + \frac{z^4}{64} + O(z^6). \tag{B.19}$$

$$\Lambda_0(z) \equiv \mathrm{I}_0(z)\exp(-z) = 1 - z + \frac{3}{4}z^2 - \frac{5}{12}z^3 + O(z^4). \tag{B.20}$$

B.3 Integrals

Error function:

$$\int_0^v dv\,\frac{1}{\sqrt{2\pi}v_\mathrm{t}}\exp\left(-\frac{(v-\overline{v})^2}{2v_\mathrm{t}^2}\right) = \frac{1}{2}\mathrm{erf}\left(\frac{v-\overline{v}}{\sqrt{2}v_\mathrm{ti}}\right) + \frac{1}{2}\mathrm{erf}\left(\frac{\overline{v}}{\sqrt{2}v_\mathrm{t}}\right). \tag{B.21}$$

$$\begin{aligned}\int_0^v dv\,\frac{v}{\sqrt{2\pi}v_\mathrm{t}}\exp\left(-\frac{(v-\overline{v})^2}{2v_\mathrm{t}^2}\right) = {}& \frac{v_\mathrm{t}}{\sqrt{2\pi}}\left(\exp\left(-\frac{\overline{v}^2}{2v_\mathrm{t}^2}\right) - \exp\left(-\frac{(v-\overline{v})^2}{2v_\mathrm{t}^2}\right)\right)\\ &+ \frac{\overline{v}}{2}\left[\mathrm{erf}\left(\frac{\overline{v}}{\sqrt{2}v_\mathrm{t}}\right) + \mathrm{erf}\left(\frac{v-\overline{v}}{\sqrt{2}v_\mathrm{t}}\right)\right].\end{aligned} \tag{B.22}$$

Bessel function:

$$\int_0^{2\pi}\cos n\theta\cos(z\sin\theta)d\theta = [1+(-1)^n]\pi\mathrm{J}_n(z). \tag{B.23}$$

$$\int_0^{2\pi}\sin n\theta\sin(z\sin\theta)d\theta = [1-(-1)^n]\pi\mathrm{J}_n(z). \tag{B.24}$$

$$\int_0^\infty \mathrm{J}_n(\alpha x)\exp(-\beta^2x^2)x\,dx = \frac{\sqrt{\pi}\alpha}{8\beta^3}\exp\left(-\frac{\alpha^2}{8\beta^2}\right)\left[\mathrm{I}_{(n-1)/2}\left(\frac{\alpha^2}{8\beta^2}\right) - \mathrm{I}_{(n+1)/2}\left(\frac{\alpha^2}{8\beta^2}\right)\right]. \tag{B.25}$$

$$\int_0^\infty \mathrm{J}_n(\alpha x)\mathrm{J}_n(\beta x)\exp(-\gamma^2x^2)x\,dx = \frac{1}{2\gamma^2}\exp\left(-\frac{\alpha^2+\beta^2}{4\gamma^2}\right)\mathrm{I}_n\left(\frac{\alpha\beta}{2\gamma^2}\right). \tag{B.26}$$

$$\frac{1}{2\pi}\oint \exp\left(\pm i\rho\mathbf{k}\cdot\hat{\mathbf{a}}\right) = \mathrm{J}_0(k_\perp\rho). \tag{B.27}$$

$$\frac{1}{2\pi}\oint \hat{\mathbf{a}}\exp\left(\pm i\rho\mathbf{k}\cdot\hat{\mathbf{a}}\right) = \pm i\mathbf{k}_\perp\mathrm{J}_1(k_\perp\rho). \tag{B.28}$$

$$\int_0^\infty \frac{1}{2\pi v_t^2} \exp\left(-\frac{v_\perp^2}{2v_t^2}\right) \mathrm{J}_0(k_\perp \rho) 2\pi v_\perp dv_\perp = \exp\left(-\frac{k_\perp^2 \rho_t^2}{2}\right). \tag{B.29}$$

$$\int_0^\infty \frac{1}{2\pi v_t^2} \exp\left(-\frac{v_\perp^2}{2v_t^2}\right) \mathrm{J}_0^2(k_\perp \rho) 2\pi v_\perp dv_\perp = \mathrm{I}_0\left(k_\perp^2 \rho_t^2\right) \exp\left(-k_\perp^2 \rho_t^2\right). \tag{B.30}$$

Bibliography

[1] Hasegawa and Mima, Phys. Fluids, **21**, 87 (1978)

[2] P. H. Rutherford and E. A. Frieman, Phys. Fluids, **11**, 569 (1968)

[3] J. B. Taylor and R. J. Hastie, Plasma Phys., **10**, 479 (1968)

[4] W. W. Lee, Phys. Fluid, **26**, 556 (1983)

[5] W. W. Lee, John A. Krommes, Carl R. Oberman, and Ralph A. Smith, Phys. Fluid, **27**, 2652 (1984)

[6] Robert G. Littlejohn, J. Math. Phys., **23**, 742 (1982)

[7] Robert G. Littlejohn, J. Plasma Phys., **29**, 111 (1983)

[8] S. E. Parker, H. E. Mynick, M. Artun, J. C. Cummings, V. Decyk, J. V. Kepner, W. W. Lee and W. M. Tang, Phys. Plasmas, **3**, 1959 (1996)

[9] Z. Lin, T. S. Hahm, W. W. Lee, W. M. Tang, R. B. White, Science, **281**, 1835 (1998)

[10] G. Furnish, W. Horton, Y. Kishimoto, M. LeBrun and T. Tajima, Phys. Plasmas, **6**, 1227 (1999)

[11] T. M. Antonsen, Jr. and B. Lane, Phys. Fluids, **23**, 1205 (1980)

[12] P. J. Catto, W. M. Tang, and D. E. Baldwin, Plasma Phys., **23**, 639 (1981)

[13] E. A. Frieman and L. Chen, Phys. Fluids, **25**, 502 (1982)

[14] Daniel H. E. Dubin, John A. Krommes, C. Oberman and W. W. Lee, Phys. Fluids, **26**, 3524 (1983)

[15] T. S. Hahm, W. W. Lee and A. Brizard, Phys. Fluids, **31**, 1940 (1988)

[16] Rober. G. Littlejohn, Phys. Fluids, **24**, 1730 (1981)

[17] Robert G. Littlejohn, Phys. Fluids, **24**, 1730 (1981)

[18] Alain Jean Brizard, Ph. D. thesis, Princeton University, 1990

[19] Hong Qin, Ph. D. thesis, Princeton University, 1998

[20] H. Qin and W. M. Tang, Phys. Plasmas, **11**, 1052 (2004)

[21] John R. Cary and Robrty G. Littlejohn, Ann. Phys., **151**, 1 (1983)

[22] H. Qin, W. M. Tang and W. W. Lee, Phys. Plasmas, **7**, 4433 (2000)

[23] R. A. Kolesnikov, W. W. Lee, H. Qin and E. Startsev, Phys. Plasmas, **14**, 072506 (2007)

[24] Alfredo Baños, Jr., J. Plasma Physics, **1**, 305 (1965)

[25] H. Sugama, Phys. Plasmas, **7**, 466 (2000)

[26] Alain J. Brizard, Phys. Rev. Lett., **84**, 5768 (2000)

[27] Alain J. Brizard, Phys. Plasmas, **7**, 4816 (2000)

[28] H. Qin, Fields Ins. Commun., **46**, 171 (2005)

[29] H. Qin, R. H. Cohen, W. M. Nevins and X. Q. Xu, Phys. Plasmas, **14**, 056110 (2007)

[30] Bruce I. Cohen, Timothy J. Williams, Andris M. Dimits and Jack A. Byers, Phys. Fluids B, **8**, 2968 (1993)

[31] G. Rewoldt, M. A. Beer, M. S. Chance, T. S. Hahm, Z. Lin and W. M. Tang, **5**, 1815 (1998)

[32] M. Maccio, J. Vaclavik and L. Villard, Phys. Plasmas, **8**, 895 (2001)

[33] J. E. Kinsey, R. E. Waltz and J. Candy, **12**, 062302 (2005)

[34] B Scott, Plasma Phys. Control. Fusion, **48**, A387 (2006)

[35] J. A. Heikkinen, S. Henriksson, S. Janhunen, T. P. Kiviniemi and F. Ogando, Contrib. Plasma Phys., **46**, 490 (2006)

[36] X. Q. Xu, Z. Xiong, M. R. Dorr, J. A. Hittinger, K. Bodi, J. Candy, B. I. Cohen, R. H. Cohen, P. Colella, G. D. Kerbel, S. Krasheninnikov, W. M. Nevins, H. Qin, T. D. Rognlien, P. B. Snyder and M. V. Umansky, Nucl. Fusion, **47**, 809 (2007)

[37] A. J. Brizard and T. S. Hahm, Rev. Mod. Phys., **79**, 421 (2007)

[38] Alain J. Brizard, Phys. Plasmas, **2**, 459 (1995)

[39] T. S. Hahm, Phys. Plasmas, **3**, 4658 (1996)

[40] H. Qin, Contrib. Plasma Phys., **46**, 477 (2006)

[41] H. Sugama and W. Horton, Phys. Plasmas, **5**, 2560 (1998)

[42] Robert G. Litlejohn, Phys. Rev. A, **38**, 6034 (1988)

[43] T. S. Hahm, Phys. Fluids, **31**, 2670 (1988)

[44] Yasuhiro Idomura, Tomo-Hiko Wakanabe and Hideo Sugama, C. R. Physique, **7**, 650 (2006)

[45] Roman D. Smirnov, Ph. D. thesis, The Graduate University for Advanced Studies, Japan, 2006

[46] R. Chodura, J. Nucl. Mater., **11–12** 420 (1982)

[47] Richard A. Gottscho, J. Vac. Sci. Technol. B, **11** 1884 (1993)

[48] G. Kawamura and A. Fukuyama, submitted to Contrib. Plasma Phys.

[49] T. E. Sheridan, Phys. Plasmas, **8**, 4240 (2001)

[50] E. Tskhakaya, B. Eliasson, P. K. Shukla and S. Kuhn, Phys. Plasmas, **11**, 3945 (2004)

[51] K-U Riemann, J. Phys. D, **36**, 2811 (2003)

[52] K.-U. Riemann, Phys. Plasmas, **13**, 063508 (2006)

[53] E. R. Harrison and W. B. Thompson, Proc. Phys. Soc., **74**, 145 (1959)

[54] D Tskhakaya and S Kuhn, Plasma Phys. Control. Fusion, **47**, A327 (2005)

[55] J. P. Gunn, Phys. Plasmas, **4**, 4435 (1997)

[56] R. Chodura, Phys. Fluid, **25**, 1628 (1982)

[57] U. Daybelge, Phys. Fluid, **24**, 1190 (1981)

[58] S. Devaux and G. Manfredi, Phys. Plasmas, **13**, 083504 (2006)

[59] A. B. DeWald,A. W. Bailey and J. N. Brooks, Phys. Fluids, **30**, 267 (1987)

[60] Devendra Sharma, Phys. Plasmas, **12**, 103506 (2005)

[61] R. J. Procassini, C.K. Birdsall and E.C. Morse, Phys. Fluids B, **2**, 3191 (1990)

[62] T. Lunt, N. Ezumi, W. Bohmeyer, G. Fussmann, J. Nucl. Mater., **337**, 201 (2004)

[63] G. Kawamura and A. Fukuyama, Phys. Plasmas, **14** 083502 (2007)

[64] C. K. Birdsall and A. B. Langdon, *Plasma Physics via Computer Simulation*, (Institute of Physics Publishing, Bristol and Philadelphia, 1991)

[65] E. S. Aydil, B. O. M. Quiniou, J. T. C. Lee, J. A. Gregus and R. A. Gottcho, Mater. Sci. Semicond. Process., **1** 75 (1998)

[66] D. Bohm, *The Characteristics of Electrical Discharges in Magnetic Fields*, edited by A. Guthrie and R. K. Wakerling (McGraw-Hill, New York, 1949), Chapter 3

[67] A. B. Dewald, A. W. Bailey and J. N. Brooks, Phys. Fluids. **30** 267 (1987)

[68] Yamamoto and Nakamura, *Kaisekirikigaku I and II*, Asakura-syoten, Tokyo, 1998 (in Japanese)

Acknowledgments

First of all, I would like to express deep gratitude to my supervisor Professor Atsushi Fukuyama for his continuous support and advice throughout the six years in Kyoto University. I would like to thank him especially for giving me the freedom to work on the subjects of my interest and guiding my work regardless of his workload. I would like thank to Associate Professor Sadayoshi Murakami for his support over five years. I am also grateful to all the members of the laboratory, especially Dr. Morihisa Uchida, Dr. Taku Akutsu, Dr. Mitsuru Honda for their helpful advice.

I am indebted to Dr. Hideo Sugama, Dr. Tomohiko Watanabe and Dr. Yukihiro Tomita of National Institute for Fusion Science, Dr. Tomonori Takizuka and Dr. Yasuhiro Idomura of Japan Atomic Energy Agency, Dr. David Tskhakaya in University of Innsbruck, Dr. Masatoshi Yagi of Kyusyu University, Dr. Yasuaki Kishimoto of Kyoto University, and Dr. Taik Soo Hahm in Princeton University for their helpful comments and suggestions.

I also wish to thank Mr. Kazuhiro Miki and Mr. Kenji Imadera of Kyoto University and Mr. Motoki nakata of the Graduate University for Advanced Studies (Sokendai) for fruitful discussions.

Finally, I would like to thank my parents, Kazuyuki and Takako Kawamura, for their continuous support and encouragement throughout my life.